REACTIONS OF HEME CATALYSTS AT NANOCRYSTALLINE TiO_2 THIN FILM INTERFACES WITH ORGANOHALIDE POLLUTANTS

by

Tamae Ito

A dissertation submitted to The Johns Hopkins University in conformity with the requirements for the degree of Doctor of Philosophy

Baltimore, Maryland
October, 2006

Abstract

Organohalide compounds are one of major pollutants on Environmental Protection Agency's (EPA) contaminants candidate list (www.epa.gov.safewater). Chapter 1 represents the overview of environmental detoxification of groundwater contaminants, electron transfer mechanisms, and the advantages of surface modified nanocrystalline TiO_2 thin films. Chapter 2 describes the enhanced reactivity of heme/TiO_2 compared to heme in fluid solutions. The photoreduction of organohalides, CCl_4, CBr_4, and $CHCl_3$ and chloroacetanilides alachlor (2-chloro-2',6'-diethyl-*N*-(methoxymethyl)acetanilide) and propachlor (2-chloro-*N*-isopropylacetanilide) by iron(II) protoporphyrin IX chloride (heme) in fluid solution and anchored to a mesoporous nanocrystalline (anatase) TiO_2 thin film immersed in solution is reported. The hemes were reacted with organic halides in the dark. Second-order kinetic rate constants of heme/TiO_2 were quantified and were found to be larger than the corresponding rate constants for heme in fluid solution. Chapter 3 explains that the synergy effect of heme/TiO_2 is partially due to the negative shifts in the formal reduction potentials of the catalysts upon surface binding. The spectroscopic and redox properties of iron(III) protoporphyrin chloride (hemin) and cobalt(III) *meso*-tetra(4-carboxyphenyl) porphyrin chloride (CoTCP) were quantified in fluid solution and when anchored to mesoporous nanocrystalline TiO_2 thin films. In acetonitrile and dimethyl sulfoxide electrolytes, TiO_2 binding was found to induce a substantial negative shift in the $M^{III/II}$ formal reduction potentials. In DMSO electrolyte, the $Co^{III/II}$ and $Fe^{III/II}$ potentials were -559 and -727 mV versus ferrocenium/ferrocene (Fc^+/Fc) and shifted to -782 and -1063 mV, respectively, after surface binding. For TiO_2

pretreated with aqueous solutions from pH 4-9, the $Co^{III/II}$ potential showed a -66 mV/pH unit change, while the $Fe^{III/II}$ potential of hemin changed by -40 mV/pH from pH 1 to 14. Spectroelectrochemical data gave isosbestic, reversible spectral changes in the visible region assigned to $M^{III/II}$ redox chemistry with λ_{iso} = 410, 460, 530, 545, 568, and 593 nm for CoTCP/TiO_2 and λ_{iso} = 408, 441, 500, 576, and 643 nm for hemin/TiO_2. In aqueous solution, the CoTCP reduction potentials were also found to be pH dependent upon surface binding, with CoTCP = -583 mV and CoTCP/TiO_2 = -685 mV versus Fc^+/Fc at pH 6. For CoTCP/TiO_2, the aqueous pH dependence of the potentials was -52 mV/pH. In Chapter 4, photodriven multi-electron transfer (MET) processes are described. Hemin (iron protoporphyrin IX) has been anchored to ~15 nm TiO_2 nanocrystallites (anatase) in ~8 μm thick mesoporous thin films. Band gap excitation of these materials in methanol or aqueous (pH 4 or 8) solutions leads to the reduction of hemin to heme ($Fe^{III} \rightarrow Fe^{II}$) and the production of $TiO_2(e^-)$, heme/$TiO_2(e^-)$. The mechanisms and second-order rate constants for the reduction of bromobenzene, chlorobenzene, dichlorobenzene, and trichloroethylene were quantified. In all cases, the concentration of $TiO_2(e^-)$ was found to decrease to near zero before the hemes were oxidized to hemin. Comparative studies with $TiO_2(e^-)$ that were not functionalized with hemes indicate that organohalide reduction is mediated by the hemes. Reactions of 6-bromo-1-hexene with heme/$TiO_2(e^-)$ demonstrate multi-electron transfer reactivity and show that heme/$TiO_2(e^-)$ nanocrystallites deliver two electrons to RX within 4.5 μs. In Chapter 5, the reactions of heme/TiO_2 catalysts in aqueous solution, including reaction orders, MET processes, heme mediated mechanisms, and reaction products, were examined. Hemin was found to bind to mesoporous nanocrystalline (anatase) TiO_2 thin films from DMSO solution, $K_{eq} = 10^5$

M^{-1} at 298 K. The reactions of heme/TiO_2 with CCl_4, $CHCl_3$, propachlor, and trichloroethylene were investigated in methanol, and pH 4 and 8 aqueous solution. The reactions were found to be first-order in heme/TiO_2 and in organohalide. Second-order rate constants measured in aqueous solution increased in the order CCl_4 > propachlor > trichloroethylene > $CHCl_3$. The $Fe^{III/II}$ formal reduction potentials of heme/TiO_2 were estimated by cyclic voltammetry and found to be –340 mV at pH 4 and –600 mV at pH 8 versus Ag/AgCl. Reactions with CCl_4 and $CHCl_3$ were faster at pH 8 than pH 4 (k_{obs} = 14.1 ± 0.7 and 0.63 ± 0.03 M^{-1} s^{-1} at pH 4 *vs.* k = 69 ± 3 and 1.33 ± 0.07 M^{-1} s^{-1} at pH 8, respectively), which was attributed to the more negative formal $Fe^{III/II}$ reduction potential at higher pH. The rate constants for propachlor reduction were similar at both pHs. Experiments were also performed with excess electrons trapped in TiO_2, $TiO_2(e^-)$, and heme/$TiO_2(e^-)$. The reaction of CCl_4 was 20 times faster with heme/$TiO_2(e^-)$ compared to $TiO_2(e^-)$ alone. In the case of trichloroethylene, no reaction was observed for $TiO_2(e^-)$, but rapid reactivity was observed for heme/$TiO_2(e^-)$, k_{obs} = 1.0 x 10^{-3} s^{-1} suggestive of a multi-electron transfer reaction mechanism. Dechlorinated products of propachlor and CCl_4 were identified by GC/MS analysis. Chapter 6 describes the effects of axial ligand on the reactivity of heme catalysts. The reactivity of heme complexes anchored to nanocrystalline mesoporous TiO_2 thin films, Fe^{II}/TiO_2 and bis(pyr)Fe^{II}/TiO_2, toward organohalides pollutants was investigated in pH 4 aqueous solution. Pyridine were found to bind to iron center of the porphyrins with binding constants of 9.3 ± 0.4 x 10^{-4} M^{-2}. Spectroscopic data gave isosbestic points at λ_{iso} = 392, 456, and 570 nm upon addition of pyridine to Fe^{II}/TiO_2. Pyridine axial ligation affected the redox properties of iron porphyrin, the estimated $Fe^{III/II}/TiO_2$ and (pyr)$Fe^{III/II}/TiO_2$ formal reduction potentials

were E° = -900 mV and -160 mV versus ferrocene/ferrocenium (Fc^{+}/Fc) in pH 4. The reaction rates of Fe^{II}/TiO_2 with halomethanes were consistently faster than bis(pyr)Fe^{II}/TiO_2 complexes, partly due to the more negative reduction potentials of $Fe^{III/II}/TiO_2$. Multi electron transfer (MET) reactions of bis(pyr)$Fe^{II}/TiO_2(e^{-})$ with CCl_4 in MeOH formed no carbene adducts, suggestive of the outer sphere electron transfer mechanism when two pyridine axial ligands were present. The detection of tetrachloroethylene as a product of multi-electron transfer supported two-electron reduction of CCl_4. The linear free energy relationships for the second-order rate constants, *k*, versus thermodynamics of the reactions, ΔG, indicated the correlation between the reaction rates and the reduction potentials of $Fe^{III/II}$ and organohalides.

Advisor/Readers: **Gerald J. Meyer**, Kenneth D. Karlin, and Howard D. Fairbrother

Acknowledgements

First, I would like to thank Professor Gerald J. Meyer for his guidance and support in past four years. His broad knowledge and passion for science helped my thesis work and I learned a great deal. He has always cared about the environment and had desire to make it better. It was encouraging to discuss about current environmental issues with him and gave me more desire to work on the environment. I am deeply grateful for his help in improving my English skills in writing and giving oral presentations.

I would also like to thank Professor Kenneth D. Karlin, and Professor Howard D. Fairbrother for being on my thesis committee. I appreciate their valuable guidance on science as well as friendly conversations.

I would like to thank Dr. Sherine O. Obare for her advice and expertise. It was exciting and enjoyable to work and discuss about the research with her in my first and second year of graduate school. Many thanks for former and present Meyer group members, Dr. Jovan Giaimo, Dr. Georg Hasselmann, Dr. David Watson, Dr. Brian Bergeron, Dr. Paul Hoertz, Dr. Nira Birenbaum, Dr. Feng Liu, Dr. Andras Marton, Gerard Higins, Rachael Carlisle, Diane Wong, Chris Clark, Jon Stromberg, Amanda Fond, Aaron Staniszewski, Hailong Xia, Josh Wnuk, James Gardner, Amanda Morris, Shane Ardo, Wei Chen, Ramya Srinivasan, and Rob Freundlich.

Lastly, I would like to thank my father, Mikio Ito, my sister, Misa Saito, my fiancé, Bob Heilen, and all of my relatives for their precious love and supports. I am also thankful to Migiwa Tanaka and all of my good friends for their amazing friendship. It has been an inspiring time in my life. Without any of these, I would not be able to accomplish the thesis work.

Table of Contents

Abstract……..…... **ii**
Acknowledgements…….…... **vi**
Table of Contents……...…..... **vii**
List of Tables……...……...…..... **x**
List of Figures……...…...….... **xi**
List of Schemes……...……...…. **xv**

Chapter 1: Introduction to Remediation of Organohalides Pollutants-Overview **1**
1.1 Organohalides in groundwater……... 1
1.2 Environmental remediation of groundwater contaminants: Inorganic materials…….. 5
1.2.1 Fe^0 remediation……... 5
1.2.2 TiO_2 remediation …… 6
1.2.3 Molecular catalysts……... 11
1.3 Electron transfer mechanisms for reduction of organic compounds…….. 14
1.3.1 Stepwise and dissociative electron transfer mechanisms ……..... 14
1.3.2 Inner- and outer-sphere electron transfer …… 20
1.4 Surface modified nanocrystalline (anatase) TiO_2 thin films……. 22
1.4.1 Characteristic of mesoporous nanocrystalline TiO_2 thin films…….. 22
1.4.2 Functionalizing FeP/TiO_2 ……. 25
1.4.3 Advantages of molecular catalysts/TiO_2 system…… 27
1.5 Conclusions…… 30
1.6 References …… 30

Chapter 2: Oxidation of heme by Organic Halides at Nanocrystalline TiO_2 Interfaces **41**
2.1 Introduction…… 41
2.2 Experimental Section……... 42
2.3 Results……... 44
2.4 Discussion…….. 49
2.5 Conclusions…… 51
2.6 References……. 52

Chapter 3: Controlling Reduction Potentials of Semiconductor-Supported Molecular Catalysts for Environmental Remediation of Organohalide Pollutants **55**
3.1 Introduction…… 55

3.2 Experimental Section…… 58
3.3 Results…… 60
3.4 Discussion……... 72
3.5 Conclusions…… 76
3.6 References……... 77

Chapter 4: Multi-Electron Transfer from Heme-Functionalized Nanocrystalline TiO_2 to Organohalide Pollutants **82**
4.1 Introduction……. 82
4.2 Experimental Section…… 83
4.3 Results…… 85
4.4 Discussion…….. 93
4.5 Conclusions…… 97
4.6 References…….. 97

Chapter 5: Heme Mediated Reduction of Organohalide Pollutants at Nanocrystalline TiO_2 Thin Film Interfaces **100**
5.1 Introduction……. 100
5.2 Experimental Section…… 102
5.3 Results…… 107
5.4 Discussion……... 125
5.5 Conclusions……. 133
5.6 Acknowledgements……... 133
5.7 References……... 134

Chapter 6: Effects of Axial Ligands on Heme/TiO_2 Reactivity: One- and Multi-Electron Reduction of Organohalide Pollutants **139**
6.1 Introduction……. 139
6.2 Experimental Section…… 141
6.3 Results…… 145
6.4 Discussion……... 163
6.5 Conclusions……. 170
6.7 References……... 170

Appendix 1: Mass Spectra Methods and Data for Organohalides and Products in Water **177**
A1.1 Analytical method…….. 177

A1.2 GC/MS spectra of substrate: propachlor and CCl_4 178
A1.3 Products observed from the reactions of propachlor and CCl_4 179

Appendix 2: Cyclic Voltammetry of Molecular Catalysts, TiO_2 Thin Films, and Heme-Functionarized TiO_2 **181**
A2.1 Experimental protocol..... 181
A2.2 Cyclic Voltammetry of catalysts 183

Curriculum Vita..... **186**

List of Tables

Table 1-1. EPA National Primary Drinking Water Standard…….3
Table 1-2. Environmental half-lives of halogenated compounds in aqueous solution at 20 °C……..…….....4
Table 1-3. One- and two-electron reduction potentials of organohalide pollutants……...9
Table 1-4. Reduction potentials for dissociative and stepwise electron transfer……..16
Table 1-5. Biotransformations of RX by microorganisms in anaerobic conditions…….18
Table 2-1. Rate constants for RX reduction by heme in fluid solution and on TiO_2 surface. All measurements were made at room temperature in DMSO. The errors represent standard deviations from multiple trials…….…….……48
Table 3-1. Spectroscopic and Redox Properties of Catalysts in DMSO at roomtemperature……61
Table 4-1. Rate constants for Organohalid Reduction by $TiO_2(e^-)$ and heme/$TiO_2(e^-)$ in Methanol……88
Table 5-1. Second-order rate constants for reduction of organohalides reactions by heme/TiO_2 at room temperature……...116
Table 6-1. Spectroscopic and redox properties of heme complexes in pH 4 and MeOH at room temperature…….148
Table 6-2. Second-order rate constants and ΔG for bis(pyr)$Fe^{II}P/TiO_2$ and $Fe^{II}P/TiO_2$ reactions with halomethanes……..……158
Table A.2.1. Redox properties of catalysts in solution and on TiO_2 thin films……..182

List of Figures

Figure 1-1. Nernstian behavior of TiO_2 conduction band edge, E_{CB}, with pH……10
Figure 1-2. Structure of iron (II) protoporphyrin IX (heme)……...13
Figure 1-3. SEM image of a mesoporous nanocrystalline TiO_2 thin films……...24
Figure 1-4. Proposed binding modes of carboxylic acid molecules with TiO_2. In a) a carboxylate linkage is shown which is expected in basic conditions, and in b) a carboxylic acid linkage is shown which is expected in acidic conditions……..…26
Figure 1.5. A proposed mechanism for electron transfer from the conduction band of TiO_2 to molecular catalysts, $M^{III/II}$. The process was initiated by band gap illumination of TiO_2……...29
Figure 2-1. Steady-state actinometry measurement of hemin in DMSO solution. The photochemical quantum yield was $2.3 \pm 0.6 \times 10^{-6}$……...45
Figure 2-2. UV-visible absorbance spectra of (a) hemin (Fe(III)) on TiO_2 surface (-) and (b) after 15 min of irradiation, producing heme, Fe(II) (- - -). Spectra (c) was obtained after adding RX to the heme/TiO_2 (···). The inset shows time-resolved absorption changes monitored at 400 nm and at 420 nm following the addition of RX. Note that the S/N ratio is significantly low at $\lambda < 400$ nm because of the fundamental TiO_2 absorption……..47
Figure 2-3. The structures of a) propachlor (2-chloro-*N*-isopropylacetanilide) and b) alachlor (2-chloro-2'5=6'-diethyl-*N*-(methozymethyl)acetanilide)……..….48
Figure 2-4. Schematic representation of the proposed mechanism for hemin photoreduction on TiO_2……..50
Figure 3-1. Iron (III) protoporphyrin chloride (hemin). Cobalt (III) meso-tetra (4-carboxyphehyl) porphyrin chloride (CoTCP)……...….57
Figure 3-2. Representative spectroelectrochemical data of molecular catalysts bound to TiO_2. The left-hand side (a) shows hemin reduction in a 50:50 CH_3CN/DMSO electrolyte. The Soret band shifts from 400 nm (Fe^{III}) to 420 nm with negative applied potential. The potentials applied were -250, -350, -400, -500, -550, -600, -650, -700, and -900 mV vs Ag/AgCl. The inset shows expanded absorption spectra from 450 to 700 nm. The arrow shows the direction of absorption change upon applying negative potential. (b) A plot of Fe^{III}/Fe^{II} concentrations vs. applied potential……...64
Figure 3-3. Panel (a) shows the absorption spectra of $Co^{III/II}$TCP/TiO_2 reduction in the CH_3CN electrolyte at the applied potential. Soret bands shift from 420 nm (Co^{III}) to -400 nm with negative applied potential. The applied potentials were -100, -150, -200, -250, -270, -300, -400, and -600 mV vs Ag/AgCl. The inset shows expanded absorption spectra from 450 to 650 nm. The arrow shows the direction of absorption change upon applying negative potential. (b) A plot of Co^{III}/Co^{II} concentrations vs. applied potential……..65
Figure 3-4. (a) The UV-visible absorbance spectra of (1) — hemin (2) –■– heme, and (3) –o – the spectra recorded 2days after the addition of $CHCl_3$ in DMSO electrolyte. (b) The UV-visible absorbance spectra of (1) –■– hemin/TiO_2, (2) — heme/TiO_2, and (3) – o – the spectra obserbed in 30min after the addition of $CHCl_3$

in DMSO electrolyte……..67
Figure 3-5. Formal $Fe^{III/II}$ reduction potential (E°) vs Ag/AgCl of (a) hemin/TiO_2 in a 50:50 CH_3CN/DMSO electrolyte as a function of the pH surface pretreatment of TiO_2. The best-fit line has a slope of 40 mV per pH unit. (b) CoTCP/TiO_2 in a CH_3CN electrolyte as a function of the pH surface pretreatment of the TiO_2. The inset shows a linear fit to the data from pH 4 to 9 with a slope of 66 mV per pH unit……68
Figure 3-6. Representative spectroelectrochemical data of CoTCP/TiO_2 in pH 8 aqueous electrolyte as a function of applied potential (V_{appl} = -50, -100, -150, -200, and -270 mV). The inset shows formal potentials of CoTCP/TiO_2 in aqueous solution as a function of pH. The best-fit line has a slope of 52 mV per pH unit……70
Figure 3-7. Reaction of heme/TiO_2 with 0.2 mM CCl_4 in aqueous solutions at pH 4 and 8. Panel a shows the absorption changes after the addition of CCl_4 at 575 nm (Fe^{II} Q-band) and at 360 nm (Fe^{III} Soret band) in pH 4. Panel b shows first-order kinetic analysis of data in panel a and corresponding data (not shown) at pH 8. Panel c shows the UV-vis spectra of (i) -■- hemin/TiO_2, (ii) -·- heme/TiO_2, and (iii) -△- the final product after the reaction of heme/TiO_2 with CCl_4 in pH 8 aqueous solution. The inset shows an expanded scale in the Q-band region……....71
Figure 3-8. Interfacial energetics at catalyst/TiO_2 interfaces at pH = 6. The conduction band edge position was taken from refs *23* and *51*. The CoTCP data were measured herein. [a]Hemin/TiO_2 could not be measured in water, so the potential difference between $Co^{III/II}$ and $Fe^{III/II}$ in DMSO was assumed to be the same in water. While data are shown for pH = 6, the conduction band edge and the $M^{III/II}$ potentials show nearly Nernstian pH dependences, so the relative energetics are approximately correct at any pH……....74
Figure 4-1. UV-visible absorbance spectra of hemin/TiO_2 (—), after photolysis: heme/$TiO_2(e^-)$ (—), and after addition of (a)1,2-dichlorobenzene and (b) trichloroethylene to yield hemin/TiO_2 (—). The inset shows time-resolved concentration changes upon addition of RX. The first vertical line indicates the time of RX injection (75 s), and the second line corresponds to the time when >90% of the $TiO_2(e^-)$ was consumed and heme oxidation begins……...…87
Figure 4-2 Absorbance at 1000 nm of heme/$TiO_2(e^-)$ (· · ·) and $TiO_2(e^-)$ (-) as a function of time. The arrow indicates the point at which 1,2-dichlorobenzene was added to the external methanol solution……..…89
Figure 4-3. UV-vis absorption spectra of TCE reaction with a) $TiO_2(e^-)$ that shows no reactivity for 3 hours after addition of TCE and b) heme/$TiO_2(e^-)$ that shows the competion of the reaction in 1 hour after the addition of TCE. UV-visible absorbance spectra of hemin/TiO_2 (—), after photolysis, heme/$TiO_2(e^-)$ (—), after addition of TCE to yield heme/TiO_2 (—), and the completion of the reaction to yield hemin/TiO_2 (—)……....90
Figure 4-4. The possible electron transfer processes of heme/$TiO_2(e^-)$ reaction with organohalide pollutants……96
Figure 5-1. Iron (II) protoporphyrin IX (heme)……106
Figure 5-2. Equilibrium binding of hemin to nanocrystalline TiO_2 thin films in DMSO at room temperature, where θ in the fractional surface coverage. The inset shows a double-reciprocal plot of the data from which an equilibrium constant was abstracted, K = 1 x 10^5 M^{-1}……...109
Figure 5-3. a) UV-visible absorbance spectrum of hemin/TiO_2 (—), heme/TiO_2

(—), and the final product after addition of TCE (—) in MeOH. b) The spectral changes observed after addition of 1.6 x 10^{-4} M TCE to heme/TiO_2 in MeOH and c) pH 4 aqueous solution. The arrows show the direction of absorption change after TCE addition……110
Figure 5-4. Cyclic voltammetry of hemin/TiO_2 in aqueous solution in a) pH 4 KNO_3/H_2O and b) pH 8 $NaOH/H_2O$ electrolytes. The half-wave potentials were taken as the formal reduction potentials, and were estimated to be –340 mV and –600 mV vs. Ag/AgCl in pH 4 and 8, respectively……...112
Figure 5-5. a) Plots of heme/TiO_2 (-●-) and hemin/ TiO_2 (—) surface concentrations after the addition of 2.9 x 10^{-4} M CCl_4 in pH 8 aqueous solution. The surface concentrations were determined by standard addition of the observed spectra for 350 – 800 nm. b) Experimental and calculated data are shown before the addition of CCl_4 (Fe^{II}), 200 sec after the addition of CCl_4, and after the reaction was complete (Fe^{III}). The times these spectra were recorded are indicated with arrows in a). The Q-band region is expanded in the inset of b)……....114
Figure 5-6. The observed rate constant for reduction of 4.5 x10^{-4} M CCl_4 in pH 8 aqueous solution as a function of the heme surface coverage……115
Figure 5-7. Plots of the observed rate constants vs the indicated RX concentration in a) MeOH and b) in pH 8 acetate aqueous solution. The inset of b) shows and expanded plot for propachlor and TCE……..…117
Figure 5-8. The durability of heme/TiO_2 thin films was determined with 2.9 x 10^{-4} M CCl_4 at pH 8. After 31 cycles of washing, photoreduction, and CCl_4 reactions, the material was no longer redox active……..…..118
Figure 5-9. a) The UV-visible absorption spectra observed after bandgap excitation of a TiO_2 thin film immersed in pH 4 H_2O. b) UV-visible absorption spectrum of (—) hemin/TiO_2, the spectrum after ultra band gap illumination assigned to (—) heme/$TiO_2(e^-)$, and the final spectrum (—) after addition of CCl_4 into the external pH 4 solution. The final CCl_4 concentration was 1.4 x 10^{-4} M. The inset shows time resolved concentration observed after the addition of CCl_4. The arrow indicates the time of CCl_4 injection (120 s)……..120
Figure 5-10. a) The absorption at 800 nm of a $TiO_2(e^-)$ and a heme/$TiO_2(e^-)$ thin film recorded as a function of time. The arrow indicates the time at which CCl_4 was injected (60 s) into the external pH 8 aqueous solution. The CCl_4 concentration was 4.5 x10^{-4} M. b) Natural log plots of the data in a) from which observed rate constants were abstracted, k_{obs} = 2.4 x 10^{-3} s^{-1} for $TiO_2(e^-)$ and k_{obs} = 2.5 x 10^{-2} s^{-1} for heme/$TiO_2(e^-)$. c) Plot of the observed rate constants for CCl_4 reduction as a function of $TiO_2(e^-)$……..122
Figure 5-11. a) The UV-vis absorption spectrum of hemin/TiO_2 (—), the spectrum after ultra band gap illumination assigned to heme/$TiO_2(e^-)$ (—), and the final spectrum (—) after addition of TCE into the external pH 8 aqueous solution. The final TCE concentration was 2.5 x 10^{-4} M. b) Natural log plots of data from reactions of $TiO_2(e^-)$ (□) and heme/$TiO_2(e^-)$ (o). $TiO_2(e^-)$ shows no reactivity with TCE. The reaction of heme/$TiO_2(e^-)$ with TCE from which an observed rate constant was abstracted, k_{obs} = 1.0 x 10^{-3} s^{-1}……...123
Figure 6-1. a) UV-visible absorbance spectrum of bis(pyr)Fe^{II}P/TiO_2 in pyridine (—) and pH 4 acetic acid aqueous solution(—). b) UV-visible absorbance spectrum of ferric forms of heme complexes, Fe^{III}P/TiO_2 (—) and bis(pyr)Fe^{III}P/TiO_2 (—) in

pH 4 acetic acid aqueous solution. c) UV-visible absorbance spectrum of ferrous forms of heme complexes, $Fe^{II}P/TiO_2$ (—) and bis(pyr)$Fe^{II}P/TiO_2$ (—) in pH 4 acetic acid aqueous solution……..……....147
Fig 6-2. a) The spectral changes observed after addition of 1.1 x 10^{-2} M pyridine to $Fe^{II}P/TiO_2$ in pH 4 aqueous solution. The arrows show the direction of absorption change after the addition. The inset shows the UV-visible absorbance spectrum of the final bis(pyr)$Fe^{II}P/TiO_2$ spectrum from a. (—) and bis(pyr)$Fe^{II}P/TiO_2$ prepared for RX reactions (—). b) The plot of log $(A-A_0)/(A_\infty-A)$ vs. log [pyr]. The binding constant of pyridine to $Fe^{II}P/TiO_2$ estimated from the intercept of the fitted line was $\beta_2 = 9.3 \pm 0.4 \times 10^4$ M^{-2}……..……152
Figure 6-3. The spectroelectrochemical data of bis(pyr)FeP/TiO_2 in pH 4 acetic acid/KNO_3 electrolyte. The Soret band shifts from 398 nm (Fe^{III}) to 414 nm (Fe^{II}) with negative applied potential. The arrow shows the direction of absorption change upon applying negative potential. Isosbestic points were observed at λ_{iso} = 398, 452, 474, 576, and 654 nm. The inset shows the plot of % concentration of Fe^{III} and Fe^{II} vs. applied potential. The formal reduction potential of bis(pyr)FeP/TiO_2 in pH 4 was -160 mV vs. $Fc^{+/0}$…….…...154
Figure 6-4. The RX reactions of bis(pyr)$Fe^{II}P/TiO_2$ in pH 4 acetic acid solution. a)UV-visible absorbance spectra of bis(pyr)$Fe^{III}P/TiO_2$ (—), bis(pyr)$Fe^{II}P/TiO_2$ (—), and the final product after addition of 5.83 x 10^{-4} M CCl_4 (—). b) The spectral changes observed after addition of 5.83 x 10^{-4} M CCl_4 to bis(pyr)$Fe^{II}P/TiO_2$ in pH 4. The arrows show the direction of absorption change after the addition. c) The plot of bis(pyr)$Fe^{III}P/TiO_2$ (—) and bis(pyr)$Fe^{II}P/TiO_2$ (—) monitored by the Soret bands at 398 nm and 414 nm. d) Plots of the observed rate constants vs. the indicated RX concentration in pH 4……..…....157
Figure 6-5. The UV-vis absorption specta of a) bis(pyr)$Fe^{III}P/TiO_2$ (—), bis(pyr)$Fe^{II}P/TiO_2(e^-)$ (—) after ultra band gap illumination, and the final spectrum after addition of CCl_4 assigned to bis(pyr)$Fe^{III}P/TiO_2$ (—) in MeOH, and b) $Fe^{III}P/TiO_2$ (—), $Fe^{II}P/TiO_2(e^-)$(—) after ultra band gap illumination, and the final spectrum after addition of assigned to carbene adduct, $(CCl_2)Fe^{II}P/TiO_2$ (—) in MeOH……..…....160
Figure 6-6. Thermondynamic correlation of second-order reaction constants vs. ΔG calculated from the difference between $Fe^{III/II}$ formal reduction potentials and one-electron reduction potentials of halomethanes. The reactions for a) bis(pyr)$Fe^{II}P/TiO_2$, R^2 = 0.85, and b) $Fe^{II}P/TiO_2$, R^2 = 0.97, in pH 4 acetic acid aqueous solution……..162
Figure A1-1. Mass spectrum of propachlor and CCl_4 in pentane. The retention time for propachlor and CCl_4 were R.T. = 20.4 and 4.0 min……..178
Figure A.1-2. GC/MS spectra of the products formed after the reactions of heme/$TiO_2(e^-)$ by electrocatalysis in pH 8 aqueous solution. a) shows the product observed from the reactions with propachlor, assigned to be deschloropropachlor (mz = 177, R.T. = 17 min). This product was also detected in the photocatalytic reactions. b) shows the main product observed from the reactions with CCl_4, assigned to be chloroform (m/z = 118, R.T. = 3.6). This product was also observed from the photocatalytic reactions. C) shows the product observed from the reactions with CCl_4, assigned to be tetrachloroethylene (m/z = 164, R.T. = 8.3). This product was not detected in the photocatalytic reactions……...180
Figure A.2-1. Cyclic voltammetry of a) hemin and b) CoTCP in 0.1 M

TBAH/DMSO electrolyte vs. Ag/AgCl. The concentration of molecular catalysts was 0.01 M and the scan rate was 100 mV/sec……....183
Figure A.2-2. Cyclic voltammetry of hemin (—), TiO_2 (—), and hemin/TiO_2 (—) in 0.1 M TBAH/DMSO electrolyte vs. Ag/AgCl. The scan rate was 100 mV/sec……..…184
Figure A.2-3. Cyclic voltammetry of FTO (—), bis(pyr)$Fe^{III/II}$ (—),and bis(pyr)$Fe^{II/II}$/TiO_2 (—) in 0.1 M TBAH/Pyridine electrolyte vs. Ag/AgCl. The scan rate was 100 mV/sec…….……...185

List of Schemes

Scheme 4-1. The electron transfer pathways of the radical clock, 6-bromo-1-hexene that yields a) 1-hexene as a product of two-electron transfer process and b) 1-methylcyclopentane as a product of two single electron transfer processes…..……..…92

Chapter 1. Introduction

1.1 Organohalides in Groundwater

The sustainability of a drinking water is a serious environmental concern (1-5). According to the Eurochloro Organization, 80% of diseases could come from what we drink (1). The World Health Organization (WHO) also reported that diseases associated with dirty water cause 25,000 deaths per day (2). Even though three-quarters of the Earth's surface is water, only ~1% is available for drinking (1). Hence, maintaining clean drinking water is a worldwide necessity and organohalide pollutants and their toxicological properties have become a global concern in last few decades.

Organohalide pollutants present in wastewater and groundwater are a major environmental issue because of their impacts on human health (2-6). In fact, about 44% of pollutants on the Environmental Protection Agency's contaminants candidate list are organohalides (5). Due to their wide spread use in the pharmaceutical and chemical industries, organohalide chemicals (RX) continue to be introduced and found in a wide range of environments. It has been estimated that about 85 % of all medicines either contain chlorine or use chlorine as part of the manufacturing processes (1). Organohalides are also commonly used as pesticides, such as dichloro-diphenyl-trichloroethane (DDT), adrin, heptachlor, and chlordane, some were banned in the 1970s because of their persistence in the environment and toxicity to non-target species as well as humans. Exposure to pesticides has been statistically linked to poor semen quality, nervous and blood system problems, as well as carcinogenicity (5). They have been

known to affect organs, such as the liver and kidney, and increase the risk of cancer (Table 1-1).

Organohalides including pesticides, that have been banned, are frequently found as contaminants throughout the world in the air, water, soil, food, and even in humans (7-10). Unfortunately, when organohalides enter the environment, they can cause damage for decades. Table 1-2 gives the time required for half-life the pollutant to react in water at 20 °C. Many organohalide pollutants have long half-lifes (Table 1-2), CCl_4 is 7000 years, for example (11). Therefore, many organohalides are inert in the environment. They are also widely distributed at the μg RX per 1 L H_2O level in rain water, water supplies, and oceans (12, 13). Concentrations of chlorinated hydrocarbons in the food chain have also been reported (14). In 1975, 33 μg/L chloroform and 5 μg/L carbon tetrachloride were found in cheshire cheese, for example.

New methods for remediation of organohalide (RX) pollutants are important for maintenance of underground aquifers and groundwater resources. It is a major environmental challenge to remove or detoxify pollutants present in the environment. Establishment of an effective detoxification technology for decreasing the high concentration of pollutants found in the environment is extremely important. Accordingly, the removal of organohalide contaminants either in *situ* or above ground treatment is an active research area (1-6, 11). Thus, many processes and technologies have been proposed over the years to clean up polluted water (5, 15).

Table 1-1. EPA National Primary Drinking Water Standard (1d).

Contaminant	**MCLG (mg/L)**	**MCL (mg/L)**	**Potential Health Effect**	**Common Source**
Bromate	Zero	0.010	Increased risk of cancer	Byproduct of drinking water disinfection
Haloacetic- acids	N/a	0.06	Increased risk of cancer	Byproduct of drinking water disinfection
Total Trihalo-methanes	None N/a	0.10 0.080	Liver, kidney or central nervous system Increased risk of cancer	Byproduct of drinking water disinfection
Chlorine (as Cl_2)	4.0	4.0	Eye/nose irritation Stomach discomfort	Water additive used to control microbes
Alachlor	Zero	0.002	Nervous system or blood problems Increased risk of cancer	Added to water during sewage and wastewater treatment
Carbon- tetrachloride	Zero	0.005	Liver problems Increased risk of cancer	Discharge from chemical plants and other industrial activities
Dichloro-ethane	Zero	0.005	Liver problems Increased risk of cancer	Discharge from drug and chemical factories
1,2-Dichloro- ethane	Zero	0.005	Increased risk of cancer	Discharge from industrial chemical factories
Chloro-benzenes O-Dichloro-benzene	0.1 0.6	0.1 0.6	Liver or kidney problems Liver, kidney, or circulatory system problem	Discharge from chemical and agricultural chemical factories
1,1,2-Trichloroethane	0.003	0.005	Liver, nervous system, or circulatory problems	Discharge from industrial chemical factories

MCLG: Maximum Contaminant Level Goal, MCL: Maximum Contaminant Level, n/a: Individual MCLGs for individual contaminants.

Table 1-2 Environmental half-lives of halogenated compounds in aqueous solution at 20 °C.

Compound	Half-life (yrs)	Reference
Dichloromethane	704	*J. Phys. Chem. Ref. Data* **1978**, *7*, 383-415
Chloroform	3500	*J. Phys. Chem. Ref. Data* **1978**, *7*, 383-415
Carbontetrachloride	7000	*J. Phys. Chem. Ref. Data* **1978**, *7*, 383-415
Bromoform	686	*J. Phys. Chem. Ref. Data* **1978**, *7*, 383-415
Bromochloromethane	44	*J. Phys. Chem. Ref. Data* **1978**, *7*, 383-415
Bromodichloromethane	137	*J. Phys. Chem. Ref. Data* **1978**, *7*, 383-415
Dibromochloromethane	274	*J. Phys. Chem. Ref. Data* **1978**, *7*, 383-415
Trichloroethene	2.5	*Proc.R.Soc.London Ser. B.* **1975**, *189*, 305-32
Tetrachloroethene	6	*Proc.R.Soc.London Ser. B.* **1975**, *189*, 305-32

1.2 Environmental remediation of groundwater contaminants: inorganic materials

Catalytic dehalogenation of organohalide pollutants with inorganic materials has been studied to a large extent (15-26). The common approaches reported in the literature include the use of 1) zero-valent iron (Fe^0), 2) semiconductor nanoparticles such as TiO_2, and 3) molecular catalysts. The degradation of some organohalide pollutants by these inorganic solids and molecules, and their influence on the environment are discussed below.

1.2.1 Fe^0 remediation

Zero-valent iron (Fe^0) has been extensively used for the remediation of organohalide pollutants in groundwater (15-18). In the environment, iron acts as an electron donor and reduces RX pollutants. For example, Pearson et. al., reported methylamine as a product of the reactions of halonitromethanes with Fe^0(18). Similarly, Eykholt and Davenport detected chloride and dechlorinated acetanilides after reactions with chloroacetanilide herbicides (19).

Fe^0 is not a common component in the natural environment and it is a challenge to maintain the reactive redox state at the iron surface. In addition, the Fe^0 catalysts sometimes generate a distribution of products that can be more toxic than the original organohalides. For example, the reaction of iron powders with highly

chlorinated hydrocarbons such as tetrachloroethene (PCE) and trichloroethene (TCE) has been observed to produce *cis*-1,2-dichloroethene (DCE) and vinyl chloride (VC) (21, 22). According to the U.S. Environmental Protection Agency, a drinking water limit for vinyl chloride is 0.002 mg/L, which are in fact, more toxic to humans than TCE that has a drinking water limit of 0.005 mg/L (1e, 22).

Iron particles have been found to be more reactive when coated with other metallic particles. This may be because the supporting metals prevent the oxidation of reactive iron surface sites (23-25). Wang and Zhang found that the reactions of TCE with Pd/Fe nano-particles reacted 6.8 times faster compared to Fe nanoparticles alone under the same conditions (23). Moreover, the products of the reactions with Pd/Fe yielded no DCE and VC whereas these toxic products were detected when only iron powders were reacted. Further studies are required to determine the mechanistic details and to establish a technique for organohalide remediation.

In most Fe^0 reactions with organohalide pollutants, inner sphere surface mediated electron transfer processes have been proposed (19, 20). However, the chemical nature of the reactive surface states remains unknown.

1.2.2 TiO_2 remediation

Semiconductor nanomaterials are of growing interests in many fields of study. Some potential advantages of nanostructured semiconductor materials for detoxification of organohalide pollutants include 1) an enormous surface area for pollutant or catalysts activation, 2) redox and optical properties that can often be

systematically tuned with particle size and/or shape (26-28) and 3) surfaces that are easily functionalized for enhanced reactivity with organohalide pollutants (29, 30). Advantages of surface modification are discussed in section 1.4. A disadvantage of TiO_2 is that ultraviolet irradiation is required and this may limit some applications.

The TiO_2 semiconductor is a popular photocatalyst that has been extensively studied for oxidative and reductive remediation of organic contaminants in aqueous solution (31-37). The conduction band electron (e_{CB}^-) and the valence band hole (h_{VB}^+) produced after photo-excitation of TiO_2 are known to react with a wide range of environmental pollutants (31-37). Conduction band electrons react with variety of organohalides (such as PCBs, halogenated alkanes, and pesticides) through reductivedehalogenation pathways (31, 32). A proposed reductive dehalogenation mechanism that could be initiated by band gap illumination of TiO_2 is shown in Equations 1a-1c (38, 39).

$$TiO_2 + h\nu \rightarrow e_{CB}^- + h_{VB}^+ \qquad (1\text{-a})$$

$$RX + TiO_2(e^-) \rightarrow R\bullet + X^- \qquad (1\text{-b})$$

$$\text{or} \qquad RX + 2\ TiO_2(e^-) \rightarrow R^- + X^- \qquad (1\text{-c})$$

Photoreductive degradation of organohalide pollutants may occur by either one- or multi- electron transfer processes. These processes have previously been inferred by analysis of the organohalide pollutants (31, 32). For example, Choi and Hoffmann observed reaction products after the photoreduction of TiO_2 in the presence of CCl_4 that strongly suggested both one- and two-electron transfer

intermediates were present (31). They concluded that the two-electron transfer reduction of CCl_4 was thermodynamically more favorable compared to the one-electron transfer pathway.

The potential of the TiO_2 conduction band edge is known to follow a Nernstian shift with pH, i.e. 59 mV/pH (44-46), Figure 1-1. This behavior results in conduction band electrons that are stronger reductants at higher pHs. In fact, increased rate constants for RX photoreductions with TiO_2 at higher pH have been reported (31, 32).

Multi-electron transfer reduction of organohalide pollutants is one active area of research (31, 40-43). It has theoretically been predicted that two-electron transfer reduction potentials of many organohalide compounds (Equation 1c) are more positive than the one-electron transfer reduction potentials (Equation 1b) (40-42). Therefore, the two electron transfer pathways can occur at potentials where competitive O_2 or proton reduction are minimal. The one- and two-electron transfer reduction potentials for selected organohalides are shown in Table 1-3. We reported a 75 ~ 150 fold increase in the rate constants for aryl halides reduction when multiple electrons were present on heme functionalized TiO_2 nanoparticles (43). Details of this study are presented in Chapter 4.

Table 1-3: One- and two-electron reduction potentials of organohalide pollutants (40).

Organohalide	1 e^- reduction (V) *	2 e^- reduction (V) *
CBr_4	+0.397	+0.659
CCl_4	+0.085	+0.673
$CHBr_3$	+0.035	+0.629
$CHCl_2Br$	-0.066	+0.599
$CHCl_3$	-0.145	+0.560
CH_2Cl_2	-0.428	+0.494
TCE**	-0.674	+0.537

* Reduction potentials vs. NHE (40).

** The one- and two-electron reduction potentials are dependent on the products formed. The values given are for cis-dichloroethylene radical, •CCl=CHCl (one-electron reducton) and cis-dichloroethylene, ClHC=CHCl (two-electron reduction).

Figure 1-1: Nernstian behavior of TiO_2 conduction band edge, E_{CB}, with pH.

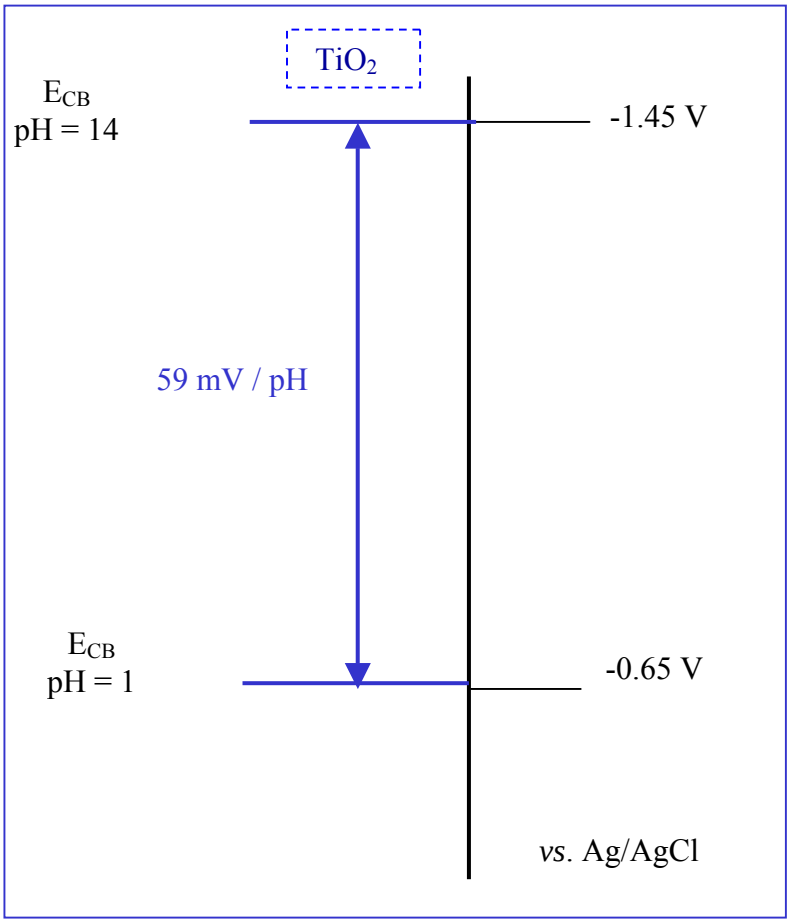

Schmelling and co-workers demonstrated the CdS deposited on TiO_2 nanoparticles and showed enhanced reactivity of 2,4,6-trinitrotoluene (TNT) in alcoholic aqueous solution (47). They proposed that electron transfer from CdS to TiO_2 enhanced the lifetime of the valence band hole in CdS resulting in more efficient methanol oxidation. Thus the effects of the band edges can enhance the lifetime of photo-generated charges in the semiconductor that may lead to RX detoxification. Similarly, deposition of metallic particles on TiO_2 has also been shown to improve the quantum yields of some catalytic reactions (48- 49).

1.2.3 Molecular catalysts

Organohalides can react with a variety of transition metal macrocycles, such as Fe^{II}, Fe^{I}, Co^{I} and Ni^{I} metallo porphyrins (50-68). The reaction mechanisms for organohalide reductions with macrocycles are thought to include both inner- or outer-sphere electron transfer mechanisms (50-68). Similar reactions are thought to occur in living organisms (69-76), but the detailed mechanisms remain clear.

Investigation of heme catalysts and halogenated compounds *in vitro* may be useful models of biological RX transformations. Heme is the main focus of the catalysis aspects of this thesis work, Fig 1-2. The heme catalysts in cytochrome P-450 is thought to mediate both oxidation and reduction of organohalide pollutants (11, 55, 62, 63, 69-83). In fact, practical applications of proteins for the biodegradation of RX in a natural environment had been proposed (73, 78). In my thesis work, a heme catalyst was employed to understand fundamental redox

reactions and electron transfer mechanisms with organohalide pollutants under mild conditions.

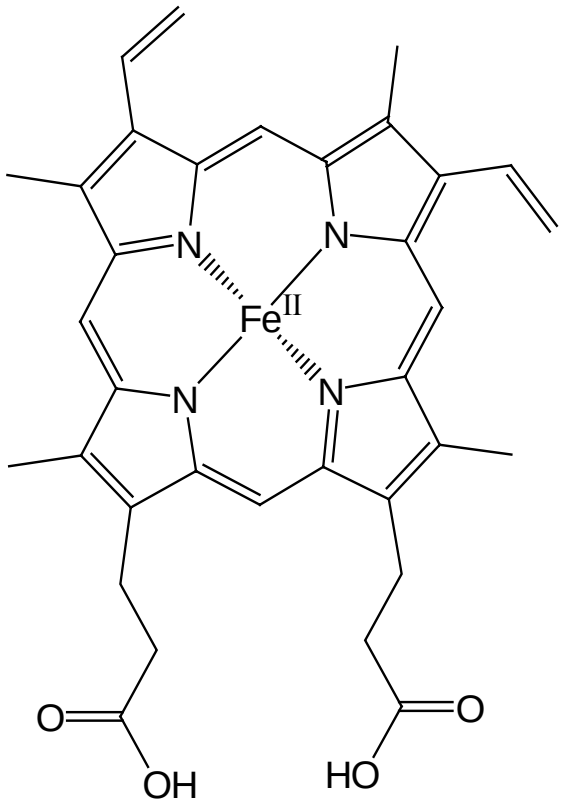

Figure 1-2: Structure of iron (II) protoporphyrin IX (heme)

1.3 Electron transfer mechanisms for reduction of organic compound

Electron transfer chemistry of organohalide pollutants is of considerable interest to environmental scientists (50, 52, 58, 84, 85). While the reduction of organic contaminants has been studied to a large extent, detailed molecular level descriptions of electron transfer mechanisms are lacking. A full understanding of electron transfer mechanisms allows one to predict and control organohalide redox reactions. We begin by discussing stepwise and dissociative transfer reactions.

1.3.1 Stepwise and dissociative electron transfer mechanisms

Under anaerobic conditions, two electron transfer mechanisms for the reduction of organohalides have been reported: stepwise and dissociative mechanisms (86, 87).

1) Stepwise mechanism

$$RX + e^- \rightarrow RX^- \qquad (1\text{-d})$$

$$RX^- \rightarrow R^\bullet + X^- \qquad (1\text{-e})$$

2) Dissociative mechanism

$$RX + e^- \rightarrow R^\bullet + X^- \qquad (1\text{-f})$$

In the stepwise electron transfer mechanism, a reduced organohalide (RX^-) intermediate is present, (40, 86). While in the dissociative mechanism, electron

transfer and C-X bond cleavage occur in a concerted process. The dissociative mechanism is generally thought to be irreversible (40) and was predicted to be more favorable than the stepwise mechanism for some organohalides, such as PCE, TCE, and some halomethanes (86, 87). Constentin and co-workers found more negative reduction potentials for the stepwise pathway (Equation 1-d) compared to the dissociative pathway (Equation 1-f) for perchloroethylene (PCE), $E°(C_2Cl_4/C_2Cl_4^-)$ = -1.71 V and $E°(C_2Cl_4/C_2Cl_3^{\bullet}+Cl^-)$ = -1.33 V *vs.* NHE, respectively. In general, the dissociative electron transfer process was energetically more favorable than the stepwise process.

In principle, a stepwise process may occur when RX^- is a stable species (40, 88, 89). For example, Burrow et. al. found that the stability of RX^- anions increased when F was substituted for Cl (88). The stepwise process may also become more favorable than the dissociative process depending on the environment of the reaction (88-89).

Table 1-4: Reduction potentials for dissociative and stepwise electron transfer

	Compound		E° (V)	vs.	Solvent	Reference
Dissociated	Carbontetrachloride	$CCl_4/{}^{\bullet}CCl_3$, Cl^-	~ +0.25	NHE	water	42
		${}^{\bullet}CCl_3/{:}CCl_2$, Cl^-	~ +0.8	NHE	water	42
	Dichloroethylene	$ClHC{=}CHCl/\ {}^{\bullet}CH{=}CHCl$, Cl^-	-1.96	SCE	DMF	79
	Trichloroethylene	$ClHC{=}CCl_2/\ ClHC{=}CCl^{\bullet}$, Cl^-	-1.728	SCE	DMF	79
	Tetrachloroehtylene	$Cl_2C{=}CCl_2/\ Cl_2C{=}CCl^{\bullet}$, Cl^-	-1.60	SCE	DMF	79
Stepwise	Dichloroethylene	$ClHC{=}CHCl/\ ClHC{=}CHCl^{\bullet-}$	-2.33	SCE	DMF	79
	Trichloroethylene	$ClHC{=}CCl_2/\ ClHC{=}CCl_2^{\bullet-}$	-2.21	SCE	DMF	79
	Tetrachloroehtylene	$Cl_2C{=}CCl_2/\ Cl_2C{=}CCl^{\bullet-}$	-1.98	SCE	DMF	79

In the dissociative electron transfer mechanisms, the alkyl radical can undergo several reactions, such as scavenging a hydrogen atom, Equation 1-g (90), or dimerization of the radicals, Equation 1-i (90). In addition, the alkyl radical may undergo a second dissociative electron transfer reaction, Equation 1-h (32, 91). For example, in case of CCl_4:

$$CCl_4 + e^- \rightarrow {}^{\bullet}CCl_3 + Cl^- \begin{cases} {}^{\bullet}CCl_3 + {}^{\bullet}H \rightarrow HCCl_3 & \text{(1-g)} \\ {}^{\bullet}CCl_3 + e^- \rightarrow [{:}CCl_2] + Cl^- & \text{(1-h)} \\ 2\ {}^{\bullet}CCl_3 \rightarrow Cl_3C\text{-}CCl_3 & \text{(1-i)} \end{cases}$$

This shows that a single electron transfer reaction can lead to a distribution of products. The relative concentration of these products (i.e. $HCCl_3$, [**:**CCl_2], and Cl_3C-CCl_3) depend on a variety of factors such as the availability of H atoms, the CCl_4 concentrtation, the concentration of the reducing equivalent, and the thermodynamic driving force. Products consistent with these reduction mechanisms have been observed in mammalian systems and microorganisms (11, 73, 90, 91). Examples of biotransformations of halogenated compounds by microorganisms are shown in Table 1-5 (11, 92).

Table 1-5: Biotransformations of RX by microorganisms in anaerobic conditions (11).

RX	System*	Product
Carbon tetrachloride	Mixed culture Methanogenic culture	Carbon dioxide
	Mixed culture	Chloroform
	Soil / aquifer	Chloroform
Chloroform	Mixed culture methanogenic culture	Carbon dioxide
1,1-Dichloroethane	Mixed culture	Chloroethane
	Methanogenic culture	Carbon dioxide
1,1,1-Trichloroethane	Mixed culture Methanogenic culture Soil / aquifer	1,1-Dichloroethane
1,1,2,2-Tetrachloroethane	Mixed culture Methanogenic culture Soil / aquifer	1,1,2-Trichloroethane
Chloroethene	Mixed culture Methanogenic culture	Carbon dioxide
Trichloroethene	Mixed culture Methanogenic culture Soil / aquifer	Dichloroethene
Tetrachloroethene	Mixed culture Methanogenic culture	Trichloroehene

*Methanogenic culture; Xanthobacter, monooxygenase, Mycobacterium, or Pseudomonas.
Mixed culture; mixture of microorganisms used in methanogenic culture.

An issue that arises relevant to the alkyl radical is whether it is more easily reduced than the parent organohalides (42, 87). Balko and Tratnyek calculated the formal reduction potential of $^{\bullet}CCl_3$, $E°(^{\bullet}CCl_3/{:}CCl_2, Cl^-) = +0.8$ vs. NHE, Equation 1-h, that was more positive than that of $E°(CCl_4/^{\bullet}CCl_3, Cl^-) = +0.25$ vs. NHE, Equation 1-f (42). In other words, the second electron transfer was more favorable than the first electron transfer. Costentin et. al. also reported that the formal reduction potentials of vinyl radicals formed from reduction of tetra-, tri-, and dichloroethylene were more positive than the reduction potentials of the parent olefins (87).

Most reductive RX reactions with nickel (57-60), iron (55, 60-64), chromium (65- 66), and cobalt (67-68, 86) transition metal porphyrins were proposed to occur by a dissociative electron transfer mechanism to yield a halide, an alkyl radical, and an oxidized transition metal compound (11).

$$M^{red} + RX \rightarrow M^{ox} + R^{\bullet} + X^- \qquad (1\text{-j})$$

Electron transfer processes are often thought to be the rate-limiting step in RX reduction mechanisms (87, 93). Therefore, one might anticipate that the rate constants for the reactions would correlate with the Gibbs free energy change (determined from standard reduction potentials) in a Marcus fashion (87). Indeed, the recent studies reported for organohalides reactions has shown that the rate constants correlates with the reduction potentials of catalysts (56, 85).

1.3.2 Inner- and outer-sphere electron transfer

The classical studies of the late Henry Taube established that redox reactions in fluid solution occur by two different mechanisms: inner- and outer-sphere. In an outer sphere mechanism, the coordination sphere of the electron donor and acceptor remain constant throughout the redox reaction. In an inner sphere mechanism, a ligand bridges the donor and accepter during the electron transfer event. There has been much discussion of whether environmental RX redox reactions occur by inner sphere mechanisms (32, 50, 56, 58, 60, 62). Some two-electron transfer reaction products derived from organohalide pollutants have been observed and it was suggested to undergo inner sphere electron transfer (50, 58, 62). With TiO_2 or Fe^0 catalysts, the mechanisms issue is very difficult to address as the reactive sites where a ligand might bridge have not been identified.

A possible evidence for inner-sphere electron transfer may be an observation of metal-carbenes in the reductions of CCl_4 and DDT (94-96). UV-visible spectral studies of inner-sphere electron transfer of heme catalysts with CCl_4 and DDT and the formation of carbene adducts have been established in the past 30 years (94, 95). In 1977, Mansuy et. al. demonstrated formation of carbene products in the reactions of Fe porphyrins and DDT in the presence of Fe^0 or other reductants. Recently, similar carbene formation with a heme catalyst anchored to TiO_2 was reported in MeOH (96). This produces some evidence for an inner-sphere electron transfer mechanism. However, one cannot fully rule out the possibility that the carbene is formed by an outer sphere mechanism which then coordinates to the iron center.

Some additional evidence suggests an outer-sphere electron transfer mechanism for the reduction of RX (56, 60). Perlinger et. al. utilized outer-sphere $Co^{II}W_{12}O_{40}^{7-}$ electron transfer to reduce organohalides (56). The $Co^{II}W_{12}O_{40}^{7-}$ complex is known to be an outer-sphere one-electron transfer reagent. They tabulated rate constants for the reduction of a variety of organohalides and constructed these with the rate constants measured for iron porphyrins, FeP. A log k_{FeP} vs. log k_{CoW} plot was linear with the slope of 1, which suggested that the iron porphyrin also reacted by an outer-sphere electron transfer mechanism.

Inner-sphere electron transfer mechanisms require the availability of an open coordination site. Therefore, organohalide reductions by hemes may depend on the axial ligands coordinated to the iron. Studies of this type are presented in Chapter 6. A good example of this is the reaction of heme/TiO_2 with CCl_4 in MeOH. A two-electron reduction of heme catalysts anchored to TiO_2 particle, heme/$TiO_2(e^-)$, reacted with CCl_4 to produce carbene adducts (96). However, when axial ligand were replaced by pyridines, carbene-heme formation was not observed under the same experimental conditions.

1.4 Surface modified nanocrystalline TiO_2 thin films

In this thesis work, heme catalysts were anchored to mesoporous nanocrystalline (anatase) TiO_2 thin films. There are several potential advantages of nanocrystalline mesoporous TiO_2 thin films over the colloidal suspensions that have previously been used for environmental studies (31-37). The most obvious is that the nanocrystalline thin films can be introduced into and removed from a wide variety of environments including ground and ocean water. They do not suffer from aggregation or 'salting out' which is common in colloidal suspensions. In addition, the mesoporous structure allows facile diffusion of RX or other pollutants to catalytic sites in the film. Some preparations of the TiO_2 thin films are given below as background.

1.4.1 Characteristic of nanocrystalline mesoporous (anatase) TiO_2 thin films

The TiO_2 films consisting of anatase particles were prepared by the hydrolysis of $Ti(iOPr)_4$ using a sol-gel method (115). The reaction mixture had the consistency and appearance of white glue. Thin films are prepared by depositing a few milliliters of this mixture onto glass slides and spreading the material with a glass test tube. Sintering is then performed in air at 450 $^{\circ}$C for 30 min.

An SEM image of this thin film is shown in Figure 1-3. The films are transparent in the visible region and the anatase particles are ~ 10 –15 nm in diameter. The film has a high surface area such that 800 ± 200 molecules can be anchored to a

nano particle (97). This also provides more active sites to react with organohalide pollutants. The TiO_2 thin films can also be useful for potential practical applications such as solar-energy conversion (98-102), environmental remediation (31, 103, 104), and chemical sensing (105, 106).

Figure 1-3: SEM image of a mesoporous nanocrystalline TiO_2 thin films

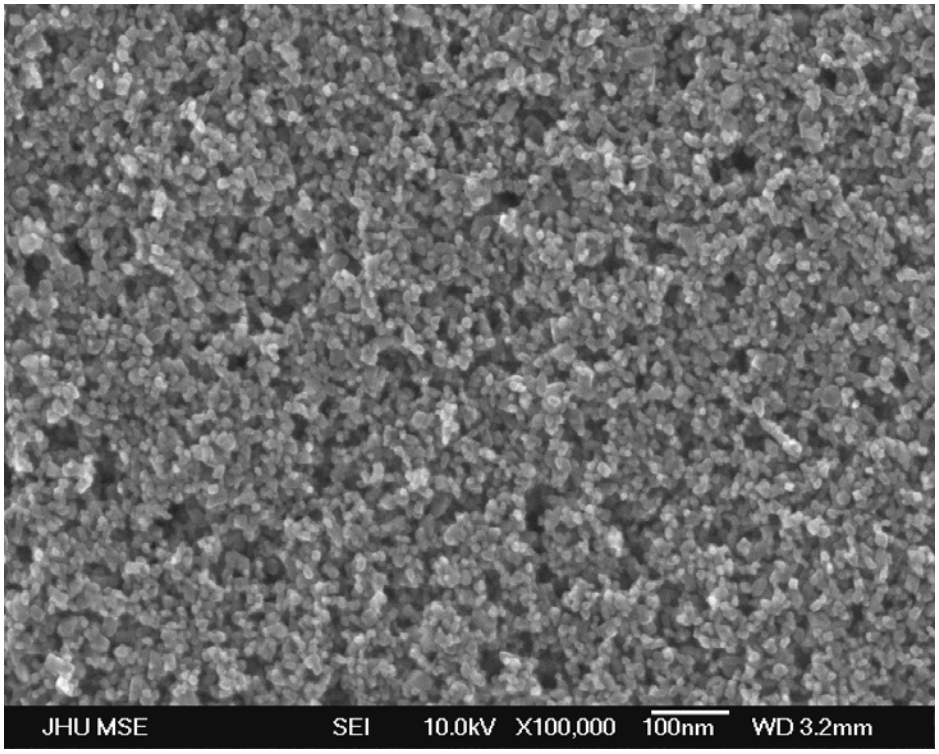

1.4.2 Functionarizing FeP/TiO_2

Molecular catalysts with functional groups, such as $–CO_2H$ or $–PO_3H$, can be used for binding to semiconductor surfaces. It was previously found that the binding mode to the semiconductor surfaces depended on the interfacial pH (107-111). It has been suggested that the TiO_2 surface deprotonates the carboxylic acid or phosphonic acid groups and promotes surface binding. A low energy asymmetric CO_2^- stretch is observed that is consistent with carboxylate binding (111, 112). In acidic conditions, molecules anchor to surface with the uncomplexed carboxylic acid termed a "carboxylic acid" linkage, while in basic conditions, a "carboxylate" linkage have been observed (Fig 1-4). However, the exact nature of surface linkage remains a topic of investigation.

a) Carboxylate linkage

b) Carboxylic acid linkage

Figure 1-4: Proposed binding modes of carboxylic acid molecules with TiO_2. In a) a carboxylate linkage is shown which is expected in basic conditions, and in b) a carboxylic acid linkage is shown which is expected in acidic conditions.

1.4.3 Advantages of molecular catalysts/TiO_2 system

Organohalide dehalogenation by molecular catalysts anchored to semiconductor surfaces has not received much attention (29, 30). An advantage of binding catalysts to transparent semiconductor surfaces (i.e. large band gap) is that the RX redox chemistry can be monitored by electronic spectroscopy in a transmission mode with high signal-to-noise. It is beneficial that the catalysts/TiO_2 can electronically communicate with the outside world and the corresponding redox chemistry can be quantified spectroscopically in a transmission mode. It also has the advantage that the semiconductor can be used to maintain the desired oxidation state of the catalysts with applied potentials or light. This is beneficial because the reduced state of molecular catalysts is often reactive and formed by a strong chemical reducing agents in fluid solution. The introduction of additional chemical agents might complicate the reaction mechanisms. Another advantage of this molecular catalysts/TiO_2 is that it eliminates the use of chemical reducing agents that may cause further pollution in natural water.

The quantum yield for the photoreduction of Co^{III} and Fe^{III} macrocycles can be improved by anchoring molecular catalysts to semiconductor surfaces (29). Steady-state actinometry measurements of hemin/TiO_2 showed that the photochemical quantum yields for the hemin/TiO_2 to heme/TiO_2 were $2.0 \pm 0.3 \times 10^{-3}$ and $1.6 \pm 0.3 \times 10^{-2}$ in acidic water and dimethyl sulfoxide (DMSO), respectively.

The value of the quantum yield for the photoreduction of hemin in DMSO fluid solution was ~10^{-4} (113).

The results above show that TiO_2 conduction band electrons can be used to reduce molecular catalysts. A simplified mechanism for electron transfer from TiO_2 to a molecular catalyst ($M^{III/II}$) is shown in figure 1-5. Here, band gap excitation results in electron-hole pair formation. In the presence of a sacrificial electron donor, the valence band holes are consumed and electrons reduce the metal center. An energetic requirement for this mechanism is that the TiO_2 conduction band be more negative than the formal reduction potential of the catalyst.

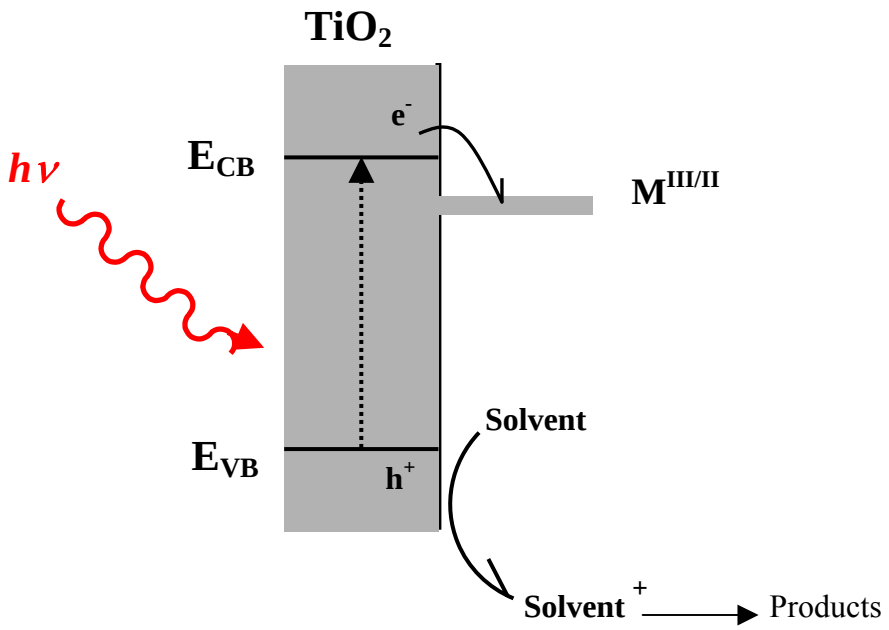

Figure 1.5: A proposed mechanism for electron transfer from the conduction band of TiO_2 to molecular catalysts, $M^{III/II}$. The process was initiated by band gap illumination of TiO_2.

The reactions were usually carried out under anaerobic conditions to avoid a competitive reduction of O_2. Indeed, Choi et. al., showed that the rate of CCl_4 loss at irradiated TiO_2 interfaces was faster when O_2 was absent. This was due to the fact that the reduction of O_2 by $TiO_2(e^-)$ was competitive with CCl_4 reduction (114).

1.5 Conclusions

Understanding dehalogenation processes of organohalide pollutants is an active research area. Heme-functionalized TiO_2 thin films focused in this thesis may be beneficial to optimize the reactivity of the catalysts and study the electron transfer mechanisms. It may also be possible to control the redox properties of molecular catalysts anchored to TiO_2 ($Fe^{III/II}/TiO_2$) and therefore, the reactions of organohalides. The following chapters in this thesis describe the synergystic effects of molecular catalysts/TiO_2 system, effects of $M^{III/II}$ formal reduction potentials, single- and multi-electron transfer mechanisms, kinetics study of the reactions, as well as effects of axial ligation toward reduction of organohalide pollutants.

1.6 References

1 Eurochlor Organization www.eurochlor.org. Accessed Aug 2006.

2 The World Health Organization (WHO) www.who.int/water_sanitation_health. Accessed March 2006.

3 Tesfamichael, A. A., Kaluarachchi, J. J. Uncertainty analysis of pesticide residues in drinking water risk assessment. *Human Ecological Risk Assessment* **2004,** *10*, 1129-1153.

4 Simmons, J. E., Richardson, S. D., Speth, T. F., Miltner, R. J., Rice, G., Schenck, K. M., Hunter, E. S., Teuschler, L. K. Development of a research strategy for integrated technology-based toxicological and chemical evaluation of complex mixtures of drinking water disinfection by products. *Environ. Health. Perspectives* **2002,** *110*, 1013-1024.

5. U.S. Environmental Protection Agency (2000) a) Federal Register, www.epa.gov/safewater/gwr/gwrprop.pdf. b) Drinking water contaminant candidate list. c) Conducting a risk assessment of mixtures of disinfections byproduct of chemical mixtures. Washington, DC. U. S. Environmental Protection Agency. Accessed 2005. d) List of drinking water contaminants and MCLs. http://www.epa.gov/safewater/mcl.html. Accessed Oct 2003. e) National Primary drinking water stantdards, EPA570/9-91-012FS.

6 Duran, N., Esposite, E. Potential applications of oxidative enzymes and phenoloxidase-like compounds in wastewater and soil treatment: a review. *Appl. Catal. B: Environ.* **2000,** *28*, 83-99.

7. Kolpin, D. W.; Thurman, E. M.; Goolsby, D. A. Occurrence of Selected Pesticides and Their Metabolites in Near-Surface Aquifers of the Midwestern United States. *Environ. Sci. Technol.* **1996,** *30*, 335-340.

8 Chesters, G., Simsiman, G. V., Levy, J., Alhajjar, B. J., Fathulla, R. N., Harkin, J. M. Environmental fate of alachlor and metolachlor. *Rev. Environ. Contam. Toxicol.* **1989,** *110*,1-74.

9 Munger, R., Isacson, P., Hu, S., Burns, T., Hanson, J., Lynch, C. F., Cherryholmes, K., van Dorpe, P., Hausler, W. J. Intrauterine growth retardation in Iowa communities with herbicide-contaminated drinking water supplies. *Environ. Health. Perspectives* **1997,** *105*, 308-314.

10 Barr, D. B., Barr, J. R., Maggio, V. L., Whitehead, R. D. Jr., Sadowski, M. A., Whyatt, R. M., Needham, L. L. A multi-analyte method for the quantification of contemporary pesticides in human serum and plasma using high-resolution mass spectrometry. *J. Chromatogr. B Analyt. Technol. Biomed. Life Sci.*, **2002,** *778*, 99-111.

11 Vogel, T., M., Criddle, C. S., McCarty, P. L. Transformations of halogenated aliphatic compounds. *Environ. Sci. Technol.* **1987,** *21*; 722-736.

12 Pearson, C. R. Chlorinated C_1 and C_2 hydrocarbons in the marine environment. *Proc. R. Soc. Lond. B* **1975,** *189*, 305-332.

13 Verstraeten, I. M., Thurman, E. M., Lindsey, M. E., Lee E. C., Smith, R. D. Changes in concentrations of triazine and acetamide herbicides by bank filtration, ozonation, and chlorination in a public water supply. *J. Hydrol*. **2002**, *266*, 190-208.

14 McConnell, G., Ferguson, D. M., Pearson, C. R. Chlorinated hydrocarbons and the environment. *Endeavour* **1975**, *34*, 13-18.

15. a) Groundwater Remediation Technology Analysis Center (GWRTAC) www.gwrtac.org. b) Remtech Engineers http://www.remtech-eng.com. c) Biological Remediation and Environmental Remediation for Hydrocarbon Contaminants. http://naturalenviro.com. d) Development in Innovative Groundwater Treatment. http://www.clu-in.org/products/newsltrs/gwc/view.cfm?issue=gwc1201.htm.

15 Matheson, M. J., Tratnyek, P. G. Reductive Dehalogenation of Chlorinated Methanes by Iron Metal. *Environ. Sci. Technol.* **1994,** *28,* 2045-2053.

16 Loch, A. R., Lippa, K. A., Carlson, D. L., Chin, Y. P., Traina, S. J., Roberts, A. L. Nucleophilic Aliphatic Substitution Reactions of Propachlor, Alachlor, and Metolachlor with Bisulfide (HS^-) and Polysulfides (S_n^{2-}). *Environ. Sci. Technol.* **2002,** *36*, 4065-4073.

17 Roberts, A. L., Totten, L. A., Arnold, W. A., Burris, D. R., Campbell, T. J. Reductive Elimination of Chlorinated Ethylenes by Zero-Valent Metals. *Environ. Sci. Technol.* **1996,** *30*, 2654-2659.

18 Pearson, C. R., Hozalski, R. M., Arnold, W. A. Degradation of chloropicrin in the presence of zero-valent iron. *Environ. Toxicol. Chem*. **2005**, *24*, 3037-3042.

19 Eykholt, G. R., Davenport, D. T. Dechlorination of the Chloroacetanilide Herbicides Alachlor and Metolachlor by Iron Metal**.** *Environ. Sci. Technol.* **1998,** *32***,** 1482-1487.

20 Satapanajaru, T., Shea, P. J., Comfort, S. D., Roh, Y. Green Rust and Iron Oxide Formation Influences Metolachlor Dechlorination during Zerovalent Iron Treatment. *Environ. Sci. Technol.* **2003,** *37***,** 5219-5227.

21 Gillham, R. W., O'Hannesin, S. F. Enhanced degradation of halogenated aliphatics by zero-valent iron. *Ground Water* **1994**, *32*, 958-967.

22 Orth, W. S.; Gillham, R. W. Dechlorination of trichloroethene in aqueous solution using Fe^0. *Environ. Sci. Technol.* **1996,** *30***,** 66-71.

23 Wang, C. B., Zhang, W. X. Synthesizing nanoscale iron particles for rapid and complete dechlorination of TCE and PCBs. *Environ. Sci. Technol.* **1997,** *31***,** 2154-2156.

24 Zhang, W., Wang, C. B., Lien, H. L. Treatment of chlorinated organic contaminants with nanoscale bimetallic particles. *Catal. Today* **1998**, *40*, 387-395.

25 Schrick, B., Blough, J. L., Jones, A. D., Mallouk, T. E. Hydrodechlorination of trichloroethylene to hydrocarbons using bimetallic nickel-iron nanoparticles. *Chem. Mater*, **2002**, *14*, 5140-5147.

26 Alivisatos, A. P. Perspectives on the physical chemistry of semiconductor nanocrystals. *J. Phys. Chem*. **1996**, *100*, 13226-13329.

27 Alivisatos, A. P. Semiconductor clusters, nanocrystals, and quantum dots. *Science* **1996**, *217*, 933-937.

28 Zhang, J. Z. Ultrafast studies of electron dynamics in semiconductor and metal collidal nanoparticles: effects of size and surface. *Acc. Chem. Res*. **1997**, *30*, 423-429.

29 Obare, S. O., Ito, T., Balfour, M. H., Meyer, G. J. Ferrous hemin oxidation by organic halides at nanocrystalline TiO_2 interfaces. *Nano Lett*.**2003**, 3, 1151-1153.

30 Obare, S. O., Ito, T., Meyer, G. J. Controlling reduction potentials of semiconductor-supported molecular catalysts for environmental remediation of organohalide pollutants. *Environ. Sci. Technol*. **2005**, *39*, 6266-6272.

31 Choi, W., Hoffmann, M. R. Photoreductive mechanism of CCl_4 degradation on TiO_2 particles and effects of electron donors. *Environ. Sci. Technol*. **1995**, *29*, 1646-1654.

32 Calhoun, R. L., Winkelmann, K., Mills, G. Chain photoreduction of CCl_3F induced by TiO_2 particles. *J. Phys. Chem. B* **2001**, *105*, 9739-9746.

33 Weaver, S., Mills, G. Photoreduction of 1,1,2-trichlorotrifluoroethane initiated by TiO_2 particles. *J. Phys. Chem. B* **1997**; *101*, 3769-3775.

34 Choi, W., Hong, S. J., Chang, Y.-S., Cho, Y. Photocatalytic degradation of polychlorinated dibenzo-*p*-dioxins on TiO_2 film under UV or solar light irradiation. *Environ. Sci. Technol.* **2000,** *34*, 4810-4815.

35 Wong, C. C., Chu, W**.** The Hydrogen peroxide-assisted photocatalytic degradation of alachlor in TiO_2 suspensions. *Environ. Sci. Technol.* **2003**; *37*, 2310-2316.

36 Konstantinou, I. K., Sakellarides, T. M., Sakkas, V. A., Albanis, T. A. Photocatalytic degradation of selected s-triazine herbicides and organophosphorus insecticides over aqueous TiO_2 suspensions. *Environ. Sci. Technol.* **2001**, *35*, 398-405.

37 Kim, S., Park, H., Choi, W. Comparative study of homogeneous and heterogeneous photocatalytic redox reactions: $PW_{12}O_{40}^{3-}$ vs TiO_2. *J. Phys. Chem. B* **2004**, *108*, 6402-6411.

38 Radlowski, C., Sherman, W. V. The γ Radiolysis of 2-propanol. V. Oxidation by carbon tetrachloride. *J. Phys. Chem.* **1970**, *74*, 3043-3047.

39 Warren V. Sherman, Rudolph Evans, Edwin Nesyto, Cecilia Radlowski**.** Mechanism of the radiation-induced dechlorination of 1,1,1-trichloro-2,2-bis(p-chlorophenyl)ethane in alcoholic solution. *J. Phys. Chem.* **1971**, *75*, 2762-2765.

40 Totten, L. A., Roberts, A. L. Calculated one- and two-electron reduction potentials and related molecular descriptors for reduction of alkyl and vinyl halides in water. *Crit. Rev. Environ. Sci. Technol*. **2001**, *31*, 175-221.

41 Craig S. Criddle, C. S., McCarty, P. L. Electrolytic model system for reductive dehalogenation in aqueous environments. *Environ. Sci. Technol.* **1991,** *25*, 973-978.

42 Balko, B. A., Tratnyek, P. G. Photoeffects on the reduction of carbon tetrachloride by zero-valent iron. *J. Phys. Chem. B* **1998,** *102*, 1459-1465.

43 Obare, S. O., Ito, T., Meyer, G. J. Multi-electron transfer from heme-functionalized nanocrystalline TiO_2 to organohalide pollutants. *J. Am. Chem. Soc.* **2006**, *128*, 712-713.

44 Zaban, A., Ferrere, S., Sprague, J., Gregg, B. A. pH-dependent redox potential induced in a sensitizing dye by adsorption onto TiO_2. *J. Phys. Chem. B* **1997**, *101*, 55-57.

45 Qu, P., Thompson, D. W., Meyer, G. J**.** Temperature-dependent electron injection from Ru(II) polypyridyl compounds with low lying ligand field states to titanium dioxide. *Langmuir* **2000**, *16*, 4662-4671.

46 Nelson, B. P., Candal, R., Corn, R. M., Anderson, M. A**.** Control of surface and potentials on nanoporous TiO_2 films by potential-determining and specifically adsorbed ions. *Langmuir* **2000**, *16*, 6094-6101.

47 Obare, S. O., Meyer, G. J. Nanostructured materials for environmental remediation of organic contaminants in water. *J. Environ. Sci.Health A* **2004**, *39*, 2549-2582.

48 Schmelling, D. C., Gray, K. A., Kamat, P. V. Role of reduction in the photocatalytic degradation of TNT. *Environ. Sci. Technol.* **1996**, *30*, 2547-2555.

49 KVinodgopal, K., Kamat, P. V**.** Enhanced rates of photocatalytic degradation of an azo dye using SnO_2/TiO_2 coupled semiconductor thin films. *Environ. Sci. Technol.* **1995**, *29*, 841-845.

50 Krone, U. E., Thauer, R. K., Hogenkamp, H. P. C., Steinbach, K. Reductive formation of carbon monoxide from carbon tetrachloride and Freons 11, 12, and 13 catalyzed by corrinoids. *Biochemistry* **1991,** *30*, 2713-2719.

51 Zhou, D. L., Njue, C. K., Rusling, J. F**.** Covalently Linked Scaffold of Cobalt Corrins on Graphite for Electrochemical Catalysis in Microemulsions**.** *J. Am. Chem. Soc.* **1999**, *121*, 2909-2914.

52 McCauley, K. M.; Wilson, S. R.; van der Donk, W. A**.** Synthesis and characterization of chlorinated alkenylcobaloximes to probe the mechanism of vitamin B_{12}-catalyzed dechlorination of priority pollutants. *Inorg. Chem.* **2002**, *41*, 393-404.

53 Woods, S. L., Trobaugh, D. J., Carter, K. J. Polychlorinated biphenyl reductive dechlorination by vitamin B_{12s}: thermodynamics and regiospecificity. *Environ. Sci. Technol.* **1999,** *33*, 857-863.

54 Brault, D., Neta. P. Reactions of iron porphyrins with trifluoromethyl, trifluoromethylperoxy, and tribromomethylperoxy radicals. *J. Phys. Chem.* **1987**, *91*, 4156-4160.

55 Wade, R. S., Castro, C. E. Oixidation of heme proteins by alkyl halides. *J. Am. Chem. Soc.* **1973,** *95*, 231-234.

56 Perlinger, J. A.; Buschmann, J.; Angst, W.; Schwarzenbach, R. P. Iron porphyrin and mercaptojuglone mediated reduction of polyhalogenated methanes and ethanes in homogeneous aqueous solution. *Environ. Sci. Technol.* **1998**, *32*, 2431-2437.

57 Stolzenberg, A. M., Zhang, Z. F430 model chemistry. An investigation of nickel complexes as catalysts for the reduction of alkyl halides and methyl coenzyme-M by sodium borohydride. *Inorg. Chem*. **1997**, *36*, 593-600.

58 Singh, K., Horng, Y. C., Ragsdale, S. W. Rapid ligand exchange in the MCRred1 form of methyl-coenzyme M reductase. *J. Am. Chem. Soc*. **2003**, *125*, 2436-2443.

59 Neumann, A., Siebert, A., Trescher, T., Reinhardt, S., Wohlfarth, G., Diekert, G. Tetrachloroethene reductive dehalogenase of dehalospirillum multivorans: substrate specificity of the native enzyme and its corrinoid cofactor. *Arch. Microbiol*. **2002**, *177*, 420-426.

60 Bakac, A., Espenson, J. H**.** Kinetics and mechanism of the alkylnickel formation in one-electron reductions of alkyl halides and hydroperoxides by a macrocyclic nickel(I) complex. *J. Am. Chem. Soc.* **1986**, *108*, 713-719.

61 Brault, D. Model studies in cytochrome P-450-mediated toxicity of halogenated compounds: radical processes involving iron porphyrins. *Environ. Health Perspectives* **1985,** *64*, 53-60.

62 Castro., C. E., Wade, R. S., Belser, N. O. Biodehalogenation: reactions of Cytochrome P-450 with polyhalomethanes. *Biochemistry* **1985**, *24*, 204-210.

63 Nassar, A. F., Bobbitt, J. M., Stuart, J. D., and Rusling, J. F. Catalytic reduction of organohalides pollutants by Myoglobin in a biomembrane-like surfactant film. *J. Am. Chem. Soc.* **1995**, *117*, 10986-10993.

64 Castro, C. E. Biodehalogenation. *Environ. Health Perspect*. **1977**, *21*, 279-283.

65 Kochi, J. K., Powers, J. W. Mechanism of reduction of alkyl halides by chromium(II) complexes. Alkylchromium species as intermediates. *J. Am. Chem. Soc.* **1970,** *92*, 137-146.

66 Freedman, D. L., Lehmicke, L., Verce, M. F. Reductive dechlorination of tetrachloroethene following abiotic versus biotic reduction of hexavalent chromium. *Bioremed. J*. **2005**, *9*, 87-97.

67 Follett, A. D., McNeill, K. Evidence for the formation of a cis-dichlorovinyl anion upon reduction of cis-1,2-dichlorovinyl(pyridine)cobaloxime. *Inorg. Chem*. **2006**, *45*, 2727-2732.

68 Halpern, J., Maher, J. P. Kinetics of the reactions of pentacyanocobaltate(II) with organic halides. *J. Am. Chem. Soc.* **1965,** *87*, 5361-5366.

69 Franzen, S., Belyea, J., Gilveey, L. B., Davis, M. F., Chaudhary, C. E., Sit, T. L., Lommel, S. A. Proximal cavity, distal histidine, and substrate hydrogen-bonding mutations modulate the activity of *Amphitrite ornate* dehaloperoxidase. *Biochem*. **2006**, *45*, 9085-9094.

70 Bernhardt, R. Cytochromes P450 as versatile biocatalysts. *J. Biotechnol*. **2006**, *124*, 128-145.

71 Osborne, R. L., Raner, G. M., Hager, L. P., Dawson, J. H. *C. fumago* chloroperoxidase is also a dehaloperoxidase: Oxidative dehalogenation of halophenols. *J. Am. Chem. Soc*. **2006**, *128*, 1036-1037.

72 Nienhaus, K., Deng, P., Belyea, J., Franzen, S., Nienhaus, U. G. Spectroscopic study of substrate binding to the carbonmonoxy form of dehaloperoxidase from *Amphitrite ornate*. *J. Phys. Chem. B* **2006**, *110*, 13264-13276.

73 Sukumaran, S., Atkins, W. M., Shanker, R. Engineering cytochrome P-450s. *Appl. Biochem. Biotechnol*. **2002**, *102-103*, 291-302.

74 Li, S., Wackett, L. P. Reductive dehalogenation by cytochrome P450CAM: Substrate binding and catalysis. *Biochem.* **1993**, *32*, 9355-9361.

75 Castro, C. E., Yokoyama, W., Belser, N.O. Biodehalogenation: Active site versus enzymic and whole cell rates with cytochromes P-450. *Environ. Toxicol. Chem*. **1989**, *8*, 13-18.

76 Ni, S., Fredrickson, J. K., Luying, X. Purification and characterization of a novel 3-chlorobenzoate-reductive dehalogenase from the cytoplasmic membrane of *Desulfomanile tiedjei* DCB-1. *J. Bacteriol*. **1995**, *177*, 5135-5139.

77 Yanagita, K., Sagami, I., Shimizu, T. Distal site and surface mutations of cytochrome P450 1A2 markedly enhance dehalogenation of chlorinated hydrocarbons. *Arch. Biochem. Biophys*. **1997**, *346*, 269-276.

78 Osborne, R. L., Taylor, L. O., Han, K. P., Ely, B., Dawson, J. H. Amphitrite ornate dehaloperoxidase: enhanced activity for the catalytically active globin using MCPBA. *Biochem. Biophys. Res. Comm.* **2004**, *324*, 1194-1198.

79 Manchester, J. I., Ornstein, R. L. Rational approach to iproving reductive catalysis by cytochrome P450cam. *Biochimie* **1996**, *78*, 714-722.

80 Manchester, J. I., Paulsen, M. D., Robert, R., Ornstein, R. L. 1,1,1-trichloroethane-bound cytochrome P450cam dynamics. Does active site water make a difference? *Chem. Phys*. **1996**, *204*, 223-231.

81 Picardal, F. W., Arnold, R. G., Couch, H., Little, A. M., Smith, M. E. Involvement of cytochromes in the anaerobic biotransformation of tetrachloromethane by *Shewanella putrefaciens* 200. *Appl. Environ. Microbiol*. **1993**, *59*, 3763-3770.

82 Chen, X., Hu, N., Zeng, Y., Rusling, J. F., Yang, J. Ordered electrochemically active films of hemoglobin, didodecyldimethylammonium ions, and clay. *Langmuir*, **2000**, *15*, 7022-7030.

83 Larson, R. A., Cervini-Silva, J. Dechlorination of substituted trichloromethanes by and iron(II) porphyrin. *Environ. Toxicol. Chem*. **2000**, *19*, 543-548.

84 Follett, A. D., McNeill, K. Evidence for the formation of a *cis*-dichlorovinyl anion upon reduction of *cis*-1,2-dichlorovinyl(pyridine)cobaloxime. *Inorg. Chem*. **2006**, *45*, 2727-2732.

85 Bylaska, E. J., Dixon, D. A., Felmy, A. R., Tratnyek, P. G. One-electron reduction of substituted chlorinated methanes as determined from ab initio electronic structure theory. *J. Phys. Chem. A.* **2002**, *106*, 11581-11593.

86 Costentin, C., Robert, M., Saveant, J. M. Does catalysis of reductive dechlorination of tetra- and trichloroethylenes by vitamin B_{12} and corrinoid-based dehalogenases follow an electron transfer mechanism? *J. Am. Chem. Soc.* **2005**, *127*, 12154-12155.

87 Costentin, C., Robert, M., Saveant, J. M. Successive removal of chloride ions from organic polychloride pollutants. Mechanisms of reductive electrochemical elimination in aliphatic gem-polychlorides, α,β-polychloroalkenes, and α,β-polychloroalkanes in mildly protic medium *J. Am. Chem. Soc.* **2003**, *125*, 10729-10739

88 Burrow, P. D., Modelli, A., Chiu, N. S. Temporary negative ions in the chloromethanes $CHCl_2F$ and CCl_2F_2: characterization of the σ* orbitals. *J. Chem. Phys*. **1982**, *77*, 2699-2701.

89 Kriegman-King, M. R., Reinhard, M. Transformation of carbon tetrachloride by pyrite in aqueous solution. *Environ. Sci. Technol*. **1994**, *28*, 692-700.

90 Castro, C. E., Kray, W.C. The cleavage of bonds by low valent transition metal ions. The homogeneous reduction of alkyl halides by chromous sulfate. *J. Am. Chem. Soc.* **1963**, *85*, 2768-2773.

91 Wade, R. S., Havlin, R., Castro, C. E. Oxidation of iron(II) porphyrins by organic molecules. *J. Am. Chem. Soc.* **1969**, *91*, 7530-7530.

92 Cline, P. V., Viste, D. R. Migration and degradation patterns of volatile organic compounds. *Waste Manage. Res*. **1985**, *3*, 351-360.

93 Song, H., Carraway, E. R. Reduction of chlorinated ethanes by nanosized zero-valent iron: kinetics, pathways, and effects of reaction conditions. *Environ. Sci. Technol.* **2005,** *39*, 6237-6245.

94 Mansuy, D., Lange, M., Chottard, J. C., Guerin, P., Morliere, P., Brault, D., Rougee, M Reaction of carbon tetrachloride with 5,10,15,20-tetraphenyl-porphinato iron (II) [(TPP)Fe^{II}]: evidence for the formation of the carbene complex [(TPP)$Fe^{II}(CCl_2)$]. *J. Chem. Soc., Chem. Comm*. **1977**, *18*, 648-649.

95 Mansuy, D., Lange, M., Chottard, J. C. Reaction of 2,2-bis(p-chlorophenyl)-1,1,1-trichloroethane (DDT) with iron (II) porphyrins. Isolation of the vinylidene carbene complex, tetraphenylporphyriniron(II) ($C{:}C(p\text{-}Cl\text{-}C_6H_4)_2$). J. Am. Chem. Soc. 1978, 100, 3213-3214.

96 Stromberg, J. R., Wnuk, J. D., Pinlac, R. A. F., Meyer, G. J. Multielectron Transfer at Heme-Functionalized Nanocrystalline TiO_2: Reductive Dechlorination of DDT and CCl_4 Forms Stable Carbene Compounds. Stromberg, J. R., Wnuk, J. D., Pinlac, R. A. F., Meyer, G. J. *Nano Lett.* **2006**, *6*, 1284-1286.

97 Hoertz, P. G., Thompson, D. W., Friedman, L. A.,Meyer, G. J. Ligand-localized electron trapping at sensitized semiconductor interfaces. *J. Am. Chem. Soc*. **2002**, *124*, 9690-9691.

98 O'Regan, B., Gratzel, M. A low-cost, high-efficiency solar cell based on dye-sensitized colloidal TiO_2 films. *Nature* **1991**, *353*, 737-740.

99 Houarner, C., Blart, E., Buvat, P., Odobel, F. Ruthenium bis-terpyridine complexes connected to an oligothiophene unit for dry dye-sensitized solar cells. *Photochem. Photobiol. Sci*. **2005**, *4*, 200-204.

100 Mosurkal, R., Kim, Y G., Kumar, J., Li, L., Walker, J., Samuelson, L. A. Mono- and dinuclear ruthenium complexes for nanocrystalline TiO_2 based dye-sensitized photovoltaics. *J. Macro. Sci*. **2003**, *A40*, 1317-1325.

101 Anpo, M., Takeuchi, M. The design and development of highly reactive titanium oxide photocatalysts operating under visible light irradiation. *J. Catal*. **2003**, *216*, 505-516.

102 Hara, K., Tachibana, Y., Ohga, Y., Shinpo, A., Suga, S., Sayama, K., Sugihara, H., Arakawa, H. Dye-sensitized nanocrystalline TiO2 solar cells based on novel coumarin dyes. *Solar Energy Materials and Solar Cells* **2003**, *77*, 89-103.

103 Wu, J. C. S., Lin, H. M. Photoreduction of CO_2 to methanol via TiO_2 photocatalyst. *Inter. J. Photoenergy* **2005**, *7*, 115-119.

104 Linsebigler, A. L., Lu, G., Yates, J. T. Photocatalysis on TiO_2 surfaces: Principles, mechanisms, and selected results. *Chem. Rev*. **1995**, 95, 735-758.

105 Liu, Y., Jun, L., Wang, M., Li, A., Liu, H., He, P., Yang, X., Li., J. Preparation and properties of nanostructure anatase TiO2 monoliths using 1-butyl-3-methylimidazolium tetrafluoroborate room-temperature ionic liquids as template solvents. *Crystal Growth and Design* **2005**, *5*, 1643-1649.

106 Armstrong, R. A., Armstrong, G., Canales, J., Bruce, P. G. TiO_2-B nanowires. *Angew. Chem. Inter*. **2004**, *43*, 2286-2288.

107 Jean Desilvestro, J., Graetzel, M., Kavan, L., Moser, J., Augustynski, J**.** Highly efficient sensitization of titanium dioxide. *J. Am. Chem. Soc.* **1985**, *107*, 2988-2990.

108 Moser, J., Graetzel, M. Photosensitized electron injection in colloidal semiconductors. *J. Am. Chem. Soc.* **1984**, *106,* 6557-6564.

109 Kalyanasundaram, K., Vlachopoulos, N., Krishnan, V., Monnier, A., Graetzel, M. Sensitization of titanium dioxide in the visible light region using zinc porphyrins. *J. Phys. Chem.* **1987,** *91,* 2342-2347.

110 Dobson, K. D., and McQuillan, A. J. In situ infrared spectroscopic analysis of the adsorption of aromatic carboxylic acids to TiO_2, ZrO_2, Al_2O_3, and Ta_2O_5 from aqueous solutions. *Spectrochem Acta A* **2000**, *56*, 557-565.

111 Strommen, D. P., Mallick, P. K., Danzer, G. D., Lumpkin, R. S., Kincaid, J. R. Normal-coordinate analyses of the ground and 3MLCT excited states of tris(bipyridine)ruthenium(.II). *J. Phys. Chem.* **1990,** *94*, 1357-1366.

112 Finnie, K. S., Bartlett, J. R., Woolfrey, J. L**.** Vibrational spectroscopic study of the coordination of (2,2'-bipyridyl-4,4'-dicarboxylic acid)ruthenium(II) complexes to the surface of nanocrystalline titania. *Langmuir,* **1998**, *14*, 2744-2749.

113 Hendrickson, D. N., Kinnaird, M. G., Suslick, K. S**.** Photochemistry of (5,10,15,20-tetraphenylporphyrinato)iron(III) halide complexes, Fe(TPP)(X). *J. Am. Chem. Soc.* **1987**, *109*, 1243-1244.

114 Cho, Y., Choi, W., Lee, C. H., Hyeon, T., Lee, H. I**.** Visible light-induced degradation of carbon tetrachloride on dye-sensitized TiO_2. *Environ. Sci. Technol.* **2001,** *35,* 966-970.

115. Heimer, T. A.; D'Arcangelis, S. T.; Farzad, F.; Stipkala, J. M.; Meyer, G. J. An acetylacetonate-based semiconductor-sensitizer linkage. *Inorg. Chem.* **1996**, *35*, 5319-5324.

Chapter 2. Oxidation of Heme by Organohalides at Nanocrystalline TiO_2 Interfaces

2.1 Introduction

Organohalide (RX) pollutants can present serious health risks, and their prevalence in groundwater is of considerable environmental concern. Many organohalides were introduced into groundwater decades ago, but others, such as chloroacetanilide herbicides, continue to be introduced today.[1-3] The remediation of organic halide pollutants by inorganic solids and molecular compounds has been reported in the literature.[3-14] Inorganic solids, such as iron particles, are often reactive toward RX, but the reaction chemistry generally leads to distributions of products.[3-6] A potential advantage of molecular compounds is that they can be fine-tuned to react selectively with specific pollutants to yield desired environmentally benign products. However, molecular catalysts are generally active only in highly reduced[7-11] (or oxidized)[12-14] states, and it is unclear how these reactive states can be maintained in the environment. In principle, the oxidation state of molecular catalysts can be controlled electrochemically or photochemically when they are supported on an appropriate inorganic material. If the support material is also catalytic toward RX, one could potentially take advantage of the specificity of molecular catalysts and the redox stability of the solid-state material to produce hybrid molecular-material catalysts that are more active than the individual parts.

In this Chapter, we report the reduction of organohalides by heme (Fe(II)) anchored to nanocrystalline TiO_2 thin films. The ferrous state was generated through band gap illumination of the hemin-modified semiconductor. We indeed find that the reactivity of heme/TiO_2 exceeds that of heme or TiO_2 alone.

2.2 Experimental section

Materials. Organohalides, CCl_4, CBr_4, and $CHCl_3$ and chloroacetanilides alachlor (2-chloro-2',6'-diethyl-*N*-(methoxymethyl)acetanilide) and propachlor (2-chloro-*N*-isopropylacetanilide) were used as received. Titanium(IV) isopropoxide and iron(III) protoporphyrin IX chloride (hemin) were obtained from Aldrich Chemical Co., and L-cysteine was obtained from Avocado Research Chemicals. All solvents were of HPLC grade and were obtained from Fisher Scientific. Deionized water was used for the measurements in aquesou soulutions.

Nanocrystalline TiO_2 film preparation. Transparent TiO_2 films consisting of ~10-nm-diameter TiO_2 anatase particles were prepared by the hydrolysis of $Ti(iOPr)_4$ using a sol-gel technique as described previously in the literature.[15] The TiO_2 particles were cast as mesoporous thin films (~10 μm) onto transparent microscope glass slides and heated at 420 ºC for 30 min. The attachment of hemin to the TiO_2 surface was achieved by soaking the freshly prepared TiO_2 films for 24 h in an 8 μM hemin solution in DMSO at room temperature. The concentration of hemin adsorbed on the TiO_2 surface was typically ~2 μM. Once hemin was anchored to TiO_2

particles, it remained bound strongly. The hemin/TiO_2 films were rinsed with DMSO or pH 4 aqueous solutions prior to the reaction.

Photoreduction of hemin and kinetic measurements of organohalides reactivity. The nanocrystalline thin films, hemin/TiO_2, were placed diagonally in DMSO solution in a standard quartz cuvette. The cuvette was sealed with a rubber septum. The photoreduction from Fe^{III} to Fe^{II} was performed in N_2-saturated solutions with bandgap ($h\nu > 3.2$ eV) excitation of TiO_2. Bandgap excitation generates electron-hole pairs in the TiO_2 nanocrystallites. The conduction band electrons can reduce Fe^{III} to Fe^{II} and the valence-band hole can oxidize solvent or ions. Absorption spectra and steady-state kinetic data were acquired using a Cary 50 UV-visible spectrophotometer. Irradiations of hemin/TiO_2 films was carried out using a 1000-W Xe lamp with a KV 370 filter. In each case, samples were illuminated for 15 min.

A Varian Cary 50 UV-visible spectrophotometer was also used to acquire time-resolved spectra for the reaction of Fe^{II}/TiO_2 with RX. The experiments were performed in the dark to preclude secondary photocatalytic reactions. An aliquot of N_2 saturated RX in DMSO or acidic water was added to Fe^{II}/TiO_2 thin film immersed in the same solvent. The disappearance of Fe^{II} Soret absorbance at 420 nm and the appearance of Fe^{III} Soret at 400 nm were analyzed with a first-order kinetic model, where pseudo-first-order kinetic rate constants, $k_{obs,}$ were obtained.

2.3 Results

The attachment of hemin to the nanocrystalline TiO_2 particles produced a dark-orange film with a UV-visible absorption spectrum that was within experimental error the same as that for free hemin in solution.[16-19] Band gap illumination in nitrogen-saturated DMSO (or H_2O pH 4) generated the absorption spectrum expected for heme (Fe(II)).[19] The Fe(II) oxidation-state assignment was established on the basis of comparisons with the literature and the spectrum of hemin following chemical or photochemical reduction in fluid solution.

Steady-state actinometry measurements were used to calculate photochemical quantum yields of $(2.0 \pm 0.3) \times 10^{-3}$ and $(1.6 \pm 0.3) \times 10^{-2}$ in acidic water and dimethyl sulfoxide (DMSO), respectively (Figure 2-1). The quantum yield is defined as moles of Fe(III) consumed divided by moles of photons absorbed, Equation 2a. The photogenerated heme/TiO_2 (Fe(II)) was stable in the dark for days.

ϕ = [mole of reduced catalyst formed] / [mole of photons absorbed] (2a)

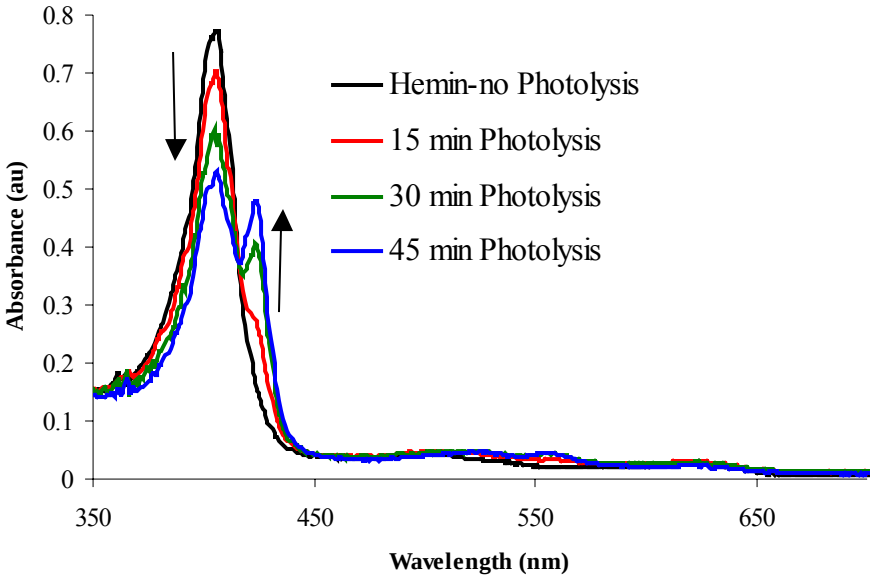

Figure 2-1. Steady-state actinometry measurement of hemin in DMSO solution. The photochemical quantum yield was $2.3 \pm 0.6 \times 10^{-6}$.

The reaction of heme (Fe(II)) with RX pollutants was examined both in solutions and on TiO_2. The addition of RX resulted in an exponetial loss of the heme (Fe(II)) concentration and the formation of hemin (Fe(III)), Figure 2-2. The UV-visible absorbance spectrum of the ferric hemin produced after the addition of RX to ferrous hemin gave a Soret band identical to that of Fe(III) before photoreduction, but differences in the Q-band region were observed.

The reactivity was qualitatively the same for all of the RX compounds in aqueous solution and were quantitatively analyzed in DMSO. Second-order rate constants were abstracted for plots of k_{obs} versus [RX] for each organic halide and are compared to those for ferrous hemin generated by L-cysteine reduction in fluid DMSO solution (Table 2-1). In some cases, such as chloroform or alachlor, no reactivity was observed in solution for days, but the reaction proceeded to completion within minutes on the TiO_2 surface. For the other RX compounds, the kinetic rate constants for the heme/TiO_2 were found to be 1-4 times faster.

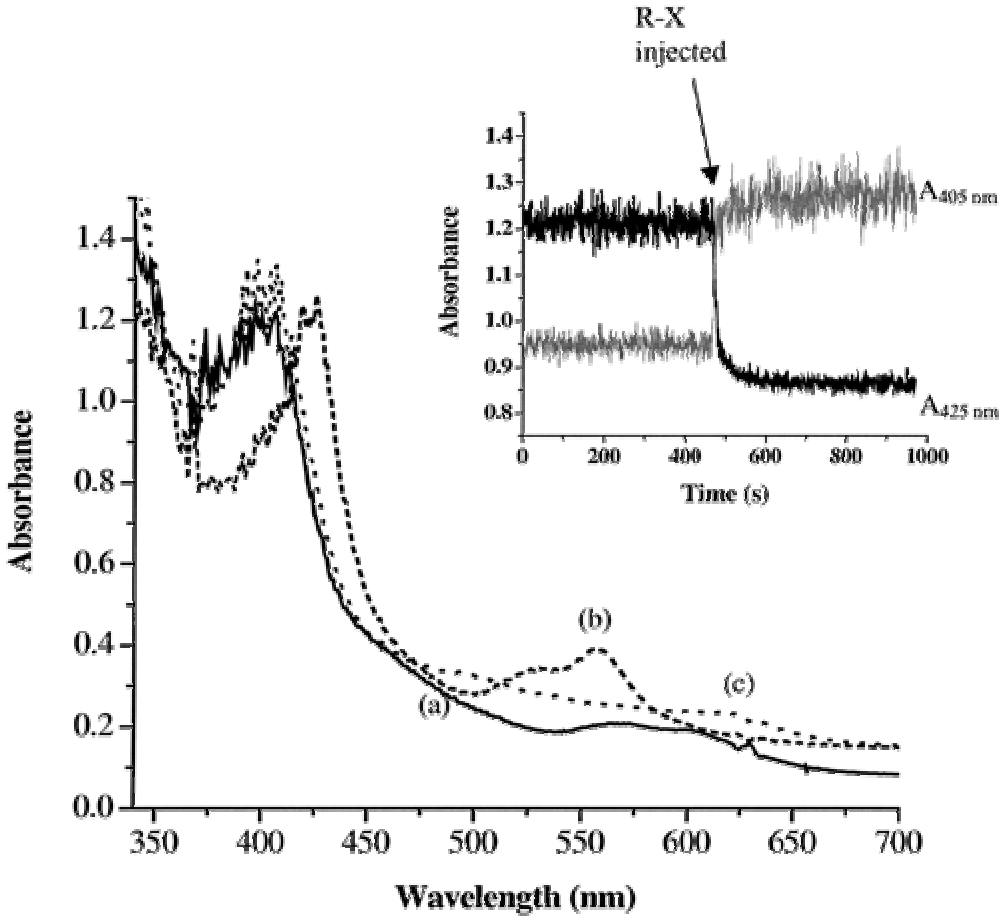

Figure 2-2. UV-visible absorbance spectra of (a) hemin (Fe(III)) on TiO_2 surface (-) and (b) after 15 min of irradiation, producing heme, Fe(II) (- - -). Spectra (c) was obtained after adding RX to the heme/TiO_2 (···). The inset shows time-resolved absorption changes monitored at 400 nm and at 420 nm following the addition of RX. Note that the S/N ratio is significantly low at $\lambda <$ 400 nm because of the fundamental TiO_2 absorption.

Table 2-1. Rate constants for RX reduction by heme in fluid solution and on TiO_2 surface. All measurements were made at room temperature in DMSO. The errors represent standard deviations from multiple trials.

RX	Heme in solution	Heme/TiO_2 (at surface)
	k ($M^{-1}s^{-1}$)	k ($M^{-1}s^{-1}$)
CBr_4	50.31 ± 0.060	64.00 ± 2.000
CCl_4	0.031 ± 0.003	0.060 ± 0.010
$CHCl_3$	> 4 days	0.009 ± 0.002
Propachlor	0.0100 ± 0.0003	0.400 ± 0.007
Alachlor	> 4 days	0.100 ± 0.003

Figure 2-3. The structures of a) propachlor (2-chloro-*N*-isopropylacetanilide) and b) alachlor (2-chloro-2'5=6'-diethyl-*N*-(methozymethyl)acetanilide).

a.

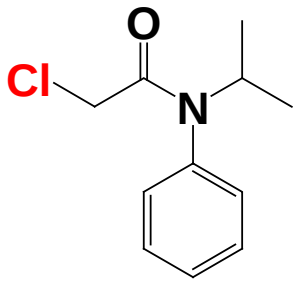

Propachlor

b.

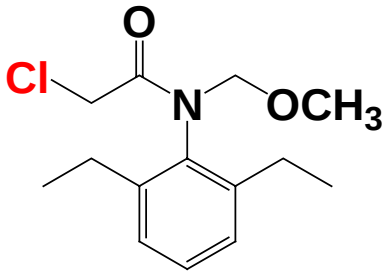

Alachlor

2.4 Discussion

A proposed mechanism for the hemin photoreduction is shown in Figure 2-4. We note that similar mechanisms have been proposed in the literature for molecular compounds on TiO_2 interfaces[20-22] as well as Fe(III)-doped TiO_2.[23,24] Band gap excitation produces an electron-hole pair. The conduction band electron reduces hemin (Fe(III)) to heme (Fe(II)), and the valence-band hole oxidizes solvent. Prolonged irradiation after the ferric hemin was quantitatively reduced to heme did not yield the well-known absorption of reduced TiO_2 in DMSO, and no further absorption changes were observed.[25] This suggests that the heme mediates electron-hole pair recombination in TiO_2.

An alternative mechanism for photoreduction literature that had been proposed in the ligand-to-metal charge transfer involves excitation of ferric porphyrins that induces homolytic cleavage of the Fe-Cl bond, leading to ferrous porphyrins and the $Cl^{\bullet}$ radical.[18,26-29] This mechanism is not favored on the basis of the relatively high quantum yields measured for hemin photoreduction on TiO_2. We and others have found that the photoreduction quantum yields for hemin in fluid solution are more than 2 orders of magnitude smaller.[28,29] In fact, irradiation conditions sufficient to photoreduce all hemin/TiO_2 resulted in no measurable production of heme in DMSO. The quantum yield for hemin photoreduction in DMSO was determined to be $(2.3 \pm 0.6) \times 10^{-6}$.

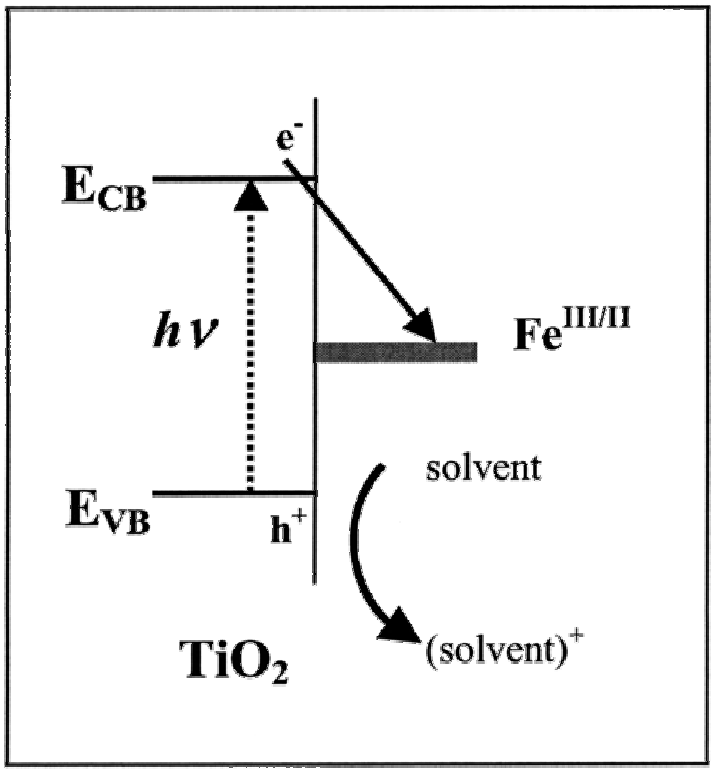

Figure 2-4 Schematic representation of the proposed mechanism for hemin photoreduction on TiO_2.

The reactions were studied in the dark by the addition of RX to the external solvent after the photoreduction of hemin/TiO_2. This was done to eliminate possible contribution from the excited TiO_2 to the observed RX chemistry. The Q-band region after RX addition to heme/TiO_2 was different from that of hemin/TiO_2 before the photoreduction. These new spectral features are not well understood, however, it may be a result of Fe(III) binding to a new axial ligand such as the solvent (DMSO), for example.

The enhanced reactivity of heme catalysts on TiO_2 compared to that in fluid solution was observed for all RX measured in this study. In some cases, such as chloroform and alachlor, the reactivity was greatly increased, Table 2-1. For example, the reaction of chloroform with heme in DMSO solution was spectroscopically not observed for 4 days, but the reaction of heme/TiO_2 with the same concentration of chloroform was completed in 30 min. An explanation of the enhanced reactivity is unknown but may result from shifts in the Fe(III/II) reduction potential upon surface binding and/or the activation of R-X by the dark TiO_2 surface.

2.5 Conclusions

We have shown that hemin (Fe(III)) can be efficiently photoreduced on TiO_2. Band gap illumination also resulted in the reduction of Fe(III) to Fe(II) when the films were immersed in acidic water (pH4). The heme (Fe(II)) anchlored to a mesoporous nanocrystalline (anatase) TiO_2 thin film reacts with organic halide pollutants. The

reactivity is rapid relative to that measured in fluid solution. The enhanced reactivity upon surface binding to TiO_2 is encouraging for future applications and studies. Future studies will focus on understanding these and other molecular details with a wider range of catalysts. We will also identify the RX reaction products. The observation of RX photoreactivity of heme supported on TiO_2 in water is particularly encouraging and suggests that the materials may be suitable for aqueous environmental photocatalysis.

2.6 References

1. Perciasepe, R. *Fed. Regist.* **1998**, *63*, 10273-10287. http://www.epa.gov/safewater/ccl/ccl_fr.pdf (accessed March 2003).

2. *National Primary Drinking Water Standards*; EPA 816-F-01-007; EPA: Washington, DC; http://www.epa.gov/safewater/consumer/mcl.pdf (accessed March 2003).

3. Loch, A. R.; Lippa, K. A.; Carlson, D. L.; Chin, Y. P.; Traina, S. J.; Roberts, A. L. Nucleophilic Aliphatic Substitution Reactions of Propachlor, Alachlor, and Metolachlor with Bisulfide (HS^-) and Polysulfides (S_n^{2-}). *Environ. Sci. Technol.* **2002,** *36*, 4065-4073

4. Yin, H.; Wada, Y.; Kitamura, T.; Yanagida, S. Photoreductive Dehalogenation of Halogenated Benzene Derivatives Using ZnS or CdS Nanocrystallites as Photocatalysts. *Environ. Sci. Technol*. **2001**, *35*, 227.

5. Pecher, K.; Haderlein, S. B.; Schwarzenbach, R. P. Reduction of Polyhalogenated Methanes by Surface-Bound Fe(II) in Aqueous Suspensions of Iron Oxides. *Environ. Sci. Technol*. **2002**, *36*, 1734.

6. Murena, F.; Schioppa, E. Kinetic analysis of catalytic hydrodechlorination process of polychlorinated biphenyls (PCBs). *Appl. Catal., B* **2000**, *27*, 257.

7. Bressan, M.; d'Alessandro, N.; Liberatore, L.; Morvilee, A. Ruthenium-catalyzed oxidative dehalogenation of organics. *Coord. Chem. Rev*. **1999**, *185-6*, 385.

8. Maldotti, A.; Amadelli, R.; Bartocci, C.; Carassiti, V.; Polo, E.; Varani, G. Photochemistry of iron-porphyrin complexes. Biomimetics and catalysis. *Coord. Chem. Rev.* **1993**, *125*, 143.

9. Maldotti, A.; Andreotti, L.; Molinari, A.; Carassiti, V. *J.* Photochemically driven models of oxygenases based on the use of iron porphyrins. *Biol. Inorg. Chem.* **1999**, *4*, 154.

10. Dobson, D. J.; Saini, S. Porphyrin-modified electrodes as biomimetic sensors for the determination of organohalide pollutants in aqueous samples. *Anal*. *Chem*. **1997**, *69*, 3532-3538.

11. Kadish, K. M.; Franzen, M. M.; Han, B. C.; Araullo-McAdams, C.; Sazou, D. Effect of the porphyrin macrocycle on the spectroscopic properties and catalytic activity of electroreduced nickel(II) porphyrins. *Inorg. Chem*. **1992**, *31*, 4399.

12. Sattari, D.; Hill, C. L. Catalytic carbon-halogen bond cleavage chemistry by redox-active polyoxometalates. *J. Am. Chem. Soc*. **1993**, *115*, 4649.

13. Mylonas, A.; Papaconstantinou, E. Photocatalytic degradation of chlorophenols to CO_2 and HCl with polyoxotungstates in aqueous solution. *J. Mol. Catal*. **1994**, *92*, 261.

14. Ozer, R. R.; Ferry, J. L. Photocatalytic oxidation of aqueous 1,2-dichlorobenzene by polyoxometalates supported on the NaY zeolite. *J. Phys. Chem. B* **2002**, *106*, 4336-4342.

15. Heimer, T. A.; D'Arcangelis, S. T.; Farzad, F.; Stipkala, J. M.; Meyer, G. J. An acetylacetonate-based semiconductor-sensitizer linkage. *Inorg. Chem*. **1996**, *35*, 5319-5324.

16. Shantha, P. K.; Saini, G. S. S.; Thanga, H. H.; Verma, A. L. Photoreduction of iron protoporphyrin IX chloride in non-ionic Triton X-100 micelle studied by electronic absorption and resonance Raman spectroscopy. *J. Raman Spectrosc*. **2001**, *32*, 159.

17. Hoshino, M.; Ueda, K.; Takahashi, M.; Yamaji, M.; Hama, Y. Photoreduction of iron(III) tetraphenylporphyrin in ethanol studied by laser flash photolysis: effect of concentration on quantum yields. *J. Chem. Soc., Faraday Trans*. **1992**, *88*, 405.

18. Bartocci, C.; Scandola, F.; Ferri, A.; Carassiti, V. Photoreduction of hemin in alcohol-containing mixed solvents. *J. Am. Chem. Soc*. **1980**, *102*, 7067.

19. Maldotti, A.; Bartocci, C.; Amadelli, R.; Carassiti, V. Photocatalytic reactions in the 2,3,7,8,12,13,17,18-octaethylporphyrinatoiron(III)-ethanol-carbon tetrachloride system. *J. Chem. Soc., Dalton Trans.* **1989**, 1197.

20. Linsebigler, A. L., Lu, G., Yates, J. T. Photocatalysis on TiO_2 surfaces: Principles, mechanisms, and selected results. *Chem. Rev*. **1995**, 95, 735-758.

21. Lewis, N. S. An analysis of charge transfer rate constants for semiconductor/liquid interfaces. *Annu. Rev. Phys. Chem*. **1991**, *42*, 543.

22. *Photocatalysis: Fundamentals and Applications*; Serpone, N., Pelizzetti, E., Eds.; Wiley-Interscience: New York, 1989.

23. Molinari, A.; Amadelli, R.; Antolini, L.; Maldotti, A.; Battioni, P.; Mansuy, D. Phororedox and photocatalytic processes on Fe(III)-porphyrin surface modified nanocrystalline TiO_2. *J. Mol. Catal*. **2000**, *158*, 521.

24. Amadelli, R.; Bregola, M.; Polo, E.; Carassiti, V.; Maldotti, A. Photooxidation of hydrocarbons on porphyrin-modified titanium dioxide powders. *J. Chem. Soc., Chem. Commun*. **1992**, 1355.

25. Qu, P.; Meyer, G. J. Dye sensitization of electrodes. In *Electron Transfer in Chemistry*; Balzani, V., Ed.; John Wiley and Sons: New York 2001; Ch. 2, Part 2, Vol. IV, pp 355-411.

26. Bartocci, C.; Maldotti, A.; Varani, G.; Carassiti, V.; Battioni, P.; Mansuy, D. Iron meso-tetra(2,6-dichlorophenyl)porphyrin as a very efficient catalyst for the photoreduction of carbon tetrachloride by alcohols. *J. Chem. Soc., Chem. Commun.* **1989**, 964.

27. Richman, R. M.; Peterson, M. V. Photodisproportionation of m-oxo-bis[(tetraphenylporphinato)iron(III)]. *J. Am. Chem. Soc.* **1982**, *104*, 5795.

28. Hendrickson, D. N.; Kinnaird, M. G.; Suslick, K. S. Photochemistry of (5,10,15,20-tetraphenylporphyrinato)iron(III) halide complexes, Fe(TPP)(X). *J. Am. Chem. Soc.* **1987**, *109*, 1243-1244.

29. Bizet, C.; Morliere, P.; Brault, D.; Delgado, O.; Bazin, M.; Santus, R. Photoreduction of iron(III) porphyrins. *J. Photochem. Photobiol.* **1981**, *34*, 315

Chapter 3: Controlling Reduction Potentials of Semiconductor-Supported Molecular Catalysts For Environmental Remediation of Organohalide Pollutants

3.1 Introduction

Heterogeneous catalysts, such as zero-valent iron, have widely been used for RX remediation (*1-3*). However, these and other heterogeneous catalysts generally yield a distribution of products, some of which can be more toxic than the initial RX compound. In principle, a homogeneous catalyst can be fine-tuned to selectively react with specific environmental pollutants to yield a desired reaction product (*1-14*). A potentially attractive approach for environmental remediation applications is to anchor molecular catalysts to heterogeneous catalysts supports (*4, 15, 16*). This could provide the specificity of a molecular catalyst with the stability and enhanced reactivity common to heterogeneous catalysts. An early example that utilized this approach was cobalt tetrasulfo-phthalocyanine anchored to colloidal titanium dioxide particles in aqueous solution (*17, 18*). This was found to be an efficient electron-transfer system that photocatalyzed the reduction of dioxygen (*17*) and the oxidation of sulfur dioxide (*18*).

The environmental literature contains additional examples of molecular catalysts incorporated within solid-state materials such as sol-gels, clays, polymers, and insulating metal oxides (*4,15, 16, 19-23*). It is generally found that the interface has a significant

influence on environmental reactivity. In this chapter, we report on the use of mesoporous nanocrystalline (anatase) thin films as solid-state supports for RX catalysts. We find that the semiconducting nature of these films can be utilized to maintain a desired oxidation state for environmental photocatalysis or electrocatalysis. In Chapter 2, we reported enhanced RX reactivity of iron(II) protoporphyrin (IX) (heme) anchored to such films relative to that measured in fluid solution (*24*). While a full explanation for the enhanced reactivity was still lacking, it was suggested that the heterogeneous interface altered the heme reduction potential. Surprisingly little is known about how surface immobilization alters the redox properties of molecular catalysts in the environment. Such an understanding is important because it enables one to predict reactivity and test electron transfer theories (*25*, *26*). Here, we have quantified reduction potentials of iron(III) protoporphyrin chloride (hemin) and cobalt(III) *meso*-tetra(4-carboxyphenyl) porphyrin chloride (CoTCP) catalysts in fluid solution and when attached to nanocrystalline TiO_2. The compounds are shown in Figure 3-1. We find that surface binding and pH control the catalysts' formal reduction potentials and reactivity with CCl_4 and $CHCl_3$.

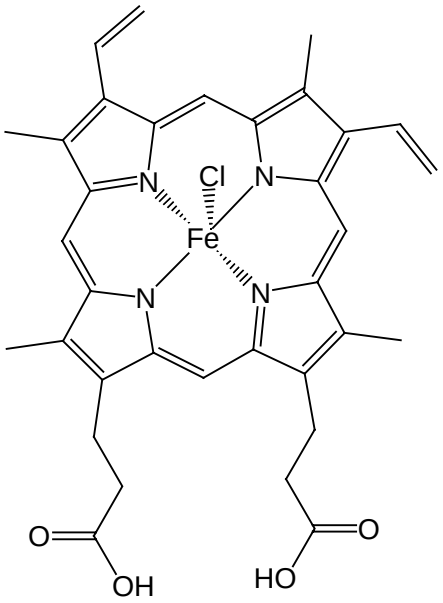

Iron (III) protoporphyrin chloride (hemin)

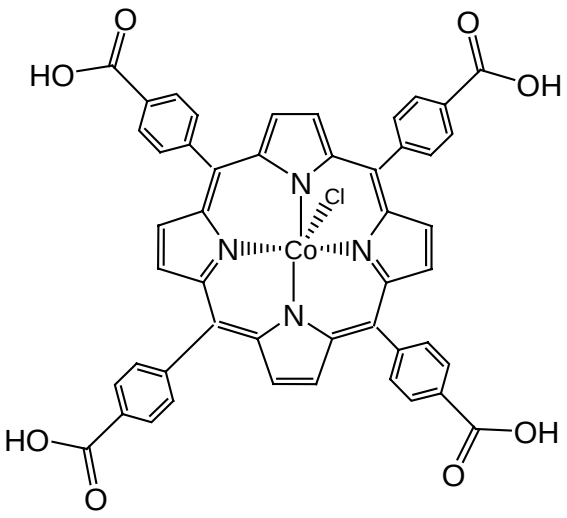

Cobalt (III) meso-tetra(4-carboxyphenyl) porphyrine chloride (CoTCP)

Figure 3-1: Iron (III) protoporphyrin chloride (hemin). Cobalt (III) meso-tetra (4-carboxyphehyl) porphyrin chloride (CoTCP).

3.2 Experimental Section

Materials. HPLC grade acetonitrile (CH_3CN), dimethyl sulfoxide (DMSO), concentrated sulfuric acid, acetic acid, and nitric acid were obtained from Fisher Scientific. Sodium acetate was obtained from J.T. Baker. Titanium (IV) isopropoxide (Aldrich), tetrabutylammonium hexafluorophosphate (TBAH) (Fluka), sodium hydroxide (Aldrich), iron (III) protoporphyrin chloride (Fluka), iron (III) meso-tetraphenyl porphyrin chloride (Frontier Scientific), and cobalt (III) meso-tetra(4-carboxyphenyl) porphyrin chloride (Frontier Scientific), were used as received. L-Cysteine was obtained from Research Chemicals Ltd. Deionized water was used in aqueous measurements and reactions.

Nanocrystalline TiO_2 Film Preparation. Transparent TiO_2 films consisting of ~ 10 nm diameter anatase particles were prepared by the hydrolysis of $Ti(iOPr)_4$ using a sol-gel technique previously described in the literature (*22*). The TiO_2 pastes were cast as mesoporous thin (~10μm) films onto transparent fluorine-doped tin oxide (FTO). Freshly prepared TiO_2 films on FTO were soaked in the aqueous solutions of known pH for at least 2 hrs and then allowed to air-dry for 2 hours. The pH values were measured using an Orion Model 420A pH meter before and after exposure to the metal oxide surface. The films were then soaked in 2-8 μM DMSO solutions of hemin or CoTCP overnight at room temperature. Once compounds were anchored, the catalysts

remained strongly bound to the surface in DMSO/CH_3CN solvent mixtures and aqueous solutions. Some desorption was observed in neat DMSO.

Spectroelectrochemistry/Electrochemistry. The TiO_2 thin films or a transparent FTO electrode were placed diagonally in a standard quartz cuvette. The cuvette was sealed with a rubber septum and then purged with N_2 gas for at least 30 min before applying a potential. A PAR™ Model 173 Potentiostat was used to apply the desired potentials in a standard three-electrode arrangement with a Pt gauze counter electrode and a Ag/AgCl reference electrode. A N_2 atmosphere was kept throughout the measurements. A Cary 50 spectrometer was used to measure absorbance spectra. Each potential was held until the UV-Vis spectrum became time-independent at which the equilibrium was assumed (30 min ~ 5 hours). As electrolytes, tetrabutyl ammonium hexafluorophosphate (TBAH) was used in non-aqueous solutions and KNO_3 was used in aqueous solutions.

Cyclic voltammetry was used to measure formal potentials of the molecular catalysts (50 mM) in 0.1 M TBAH/DMSO solutions. A BAS model CV-50 W potentiostat was used in a standard three-electrode arrangement consisting of a Glassy carbon working electrode, a Pt gauze counter electrode, and Ag/AgCl reference electrode.

Kinetic Analysis of Organohalide Reactivity. A Varian Cary 50 UV-visible spectrophotometer was used to acquire time-resolved spectra for the reaction of heme/TiO_2 with CCl_4. An aliquot of N_2 saturated CCl_4 in H_2O was added to heme/TiO_2

thin film immersed in an aqueous solution. The disappearance of heme Q-band absorbance at 575 nm and the appearance of hemin Soret band at 360 nm were analyzed with a first-order kinetic model. Pseudo-first-order kinetic rate constants, $k_{obs,}$ were obtained by fitting to equation 1.

$$\ln A = \ln A_0 - k_{obs}\, t \qquad (1)$$

3.3 Results

Both hemin and CoTCP bind to nanocrystalline TiO_2 thin films in DMSO. The concentration dependent binding was well described by the Langmuir adsorption isotherm model from which limiting surface coverages and adduct formation constants were abstracted, Table 3-1. The kinetics for binding were not studied in detail. However, equilibrium was achieved within 24 hours. Significantly, iron (III) meso-tetraphenyl porphyrin chloride, which lacks the carboxylic acid functional groups, did not bind to TiO_2 surfaces under these same conditions.

The surface bound complexes were found to be stable in aqueous solutions and DMSO/CH_3CN (v:v 1:1) for periods of days. The frequency of the Soret and lower energy absorption bands were unchanged upon surface binding, although some broadening was observed.

Table 3-1. Spectroscopic and Redox Properties of Catalysts in DMSO at roomtemperature.

Catalyst	Soret λ_{max} (nm) (ε, $M^{-1}cm^{-1}$)	K_{eq} (M^{-1})	Γ_{max} [b] (mol)	$E°$ ($M^{III/II}$) (mV)
Heme	423 (208,000)			
Heme/TiO_2	422			
Hemin	402 (140,000)			-727[a]
Hemin/TiO_2	390	1×10^5	2.0×10^{-8}	-1063 [a]
$Co^{II}TCP$	395 (130,000)			
$Co^{II}TCP/TiO_2$	396			
$Co^{III}TCP$	425 (120,000)			-559[a]
$Co^{III}TCP/TiO_2$	423	1×10^5	1.6×10^{-8}	-782[a]

[a] Formal potentials measured vs ferrocenium/ferrocene ($Fc^{+/0}$).
[b] Limiting surface coverage (mol/cm^2) x surface area of TiO_2 (cm^2).

Formal $M^{III/II}$ reduction potentials (E°) for hemin and CoTCP were measured in fluid solution and when anchored to TiO_2 surfaces (*28-30*). Cyclic voltammetry was used to measure formal potentials in DMSO electrolyte. The $M^{III/II}$ redox chemistry showed equivalent anodic and cathodic peak currents, $i_{pa}/i_{pc} \sim 1$, and a peak-to-peak separation of ~100 mV. Plots of the square root of the peak current versus scan rate were linear as expected for a diffusional process (*28*). Ferrocene added to the electrolyte demonstrated a one-electron process, and all potentials were referenced versus ferrocenium/ferrocene ($Fc^{+/0}$). The $Fe^{III/II}$ and $Co^{III/II}$ formal potentials were measured to be -727 and - 559 mV versus $Fc^{+/0}$ in 0.1 M TBAH/DMSO electrolyte. The cyclic voltammetry of the catalysts bound to TiO_2 was very similar to those previously reported for unfunctionalized TiO_2 thin films (*29*). Superimposed on a background current from reduction of the TiO_2 were peaks attributable to reduction of the molecular catalysts. However, the lack of a corresponding oxidation precluded meaningful estimates of the formal reduction potentials.

Spectroelectrochemistry provided an appropriate method to measure the $M^{III/II}$ potentials of the catalysts bound to TiO_2. The absorption spectra of the reduced and oxidized compounds have previously been reported for hemin/heme related (*30-33*) and Co porphyrin (*34-36*) compounds, and this aided our analysis. The absorption spectra of the molecular catalysts on TiO_2 showed isosbestic changes as they were reduced or oxidized. Upon stepping the applied potential to a new value, the absorption spectra were recorded every few minutes until the steady-state concentrations did not change as a function of time. For hemin, isosbestic points were observed at λ_{iso} = 408, 441, 500, 576, and 643 nm and at λ_{iso} = 410, 460, 530, 545, 568, and 593 nm for CoTCP (Figure

3-2). The formal reduction potential corresponded to the equilibrium potential where the concentration of reduced and oxidized compounds was equal (*28*) (i.e., see Figure 3-2). When the bias was removed under anoxic conditions, the concentrations of the catalysts in the two oxidation states did not change. The reduction potentials of the compounds in DMSO electrolyte and when anchored to TiO_2 are given in Table 3-1.

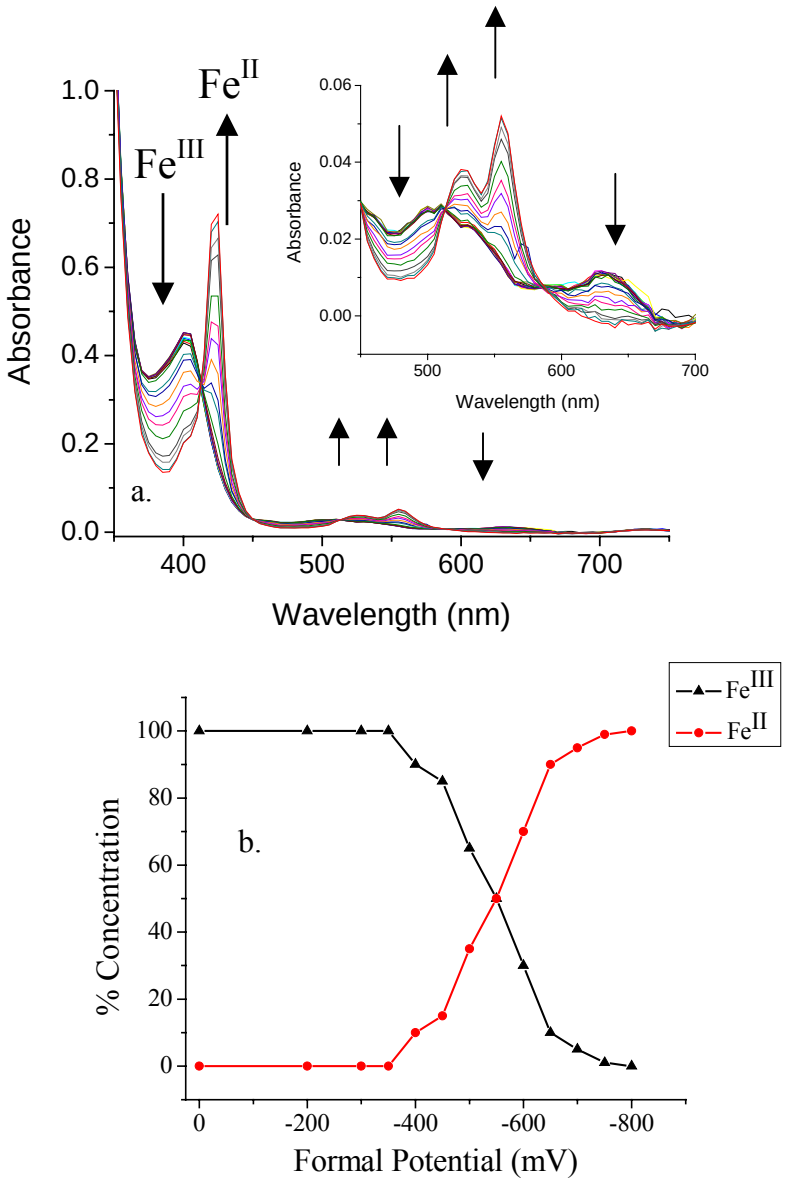

Figure 3-2. Representative spectroelectrochemical data of molecular catalysts bound to TiO_2. The left-hand side (a) shows hemin reduction in a 50:50 CH_3CN/DMSO electrolyte. The Soret band shifts from 400 nm (Fe^{III}) to 420 nm with negative applied potential. The potentials applied were -250, -350, -400, -500, -550, -600, -650, -700, and -900 mV vs Ag/AgCl. The inset shows expanded absorption spectra from 450 to 700 nm. The arrow shows the direction of absorption change upon applying negative potential. (b) A plot of Fe^{III}/Fe^{II} concentrations vs. applied potential.

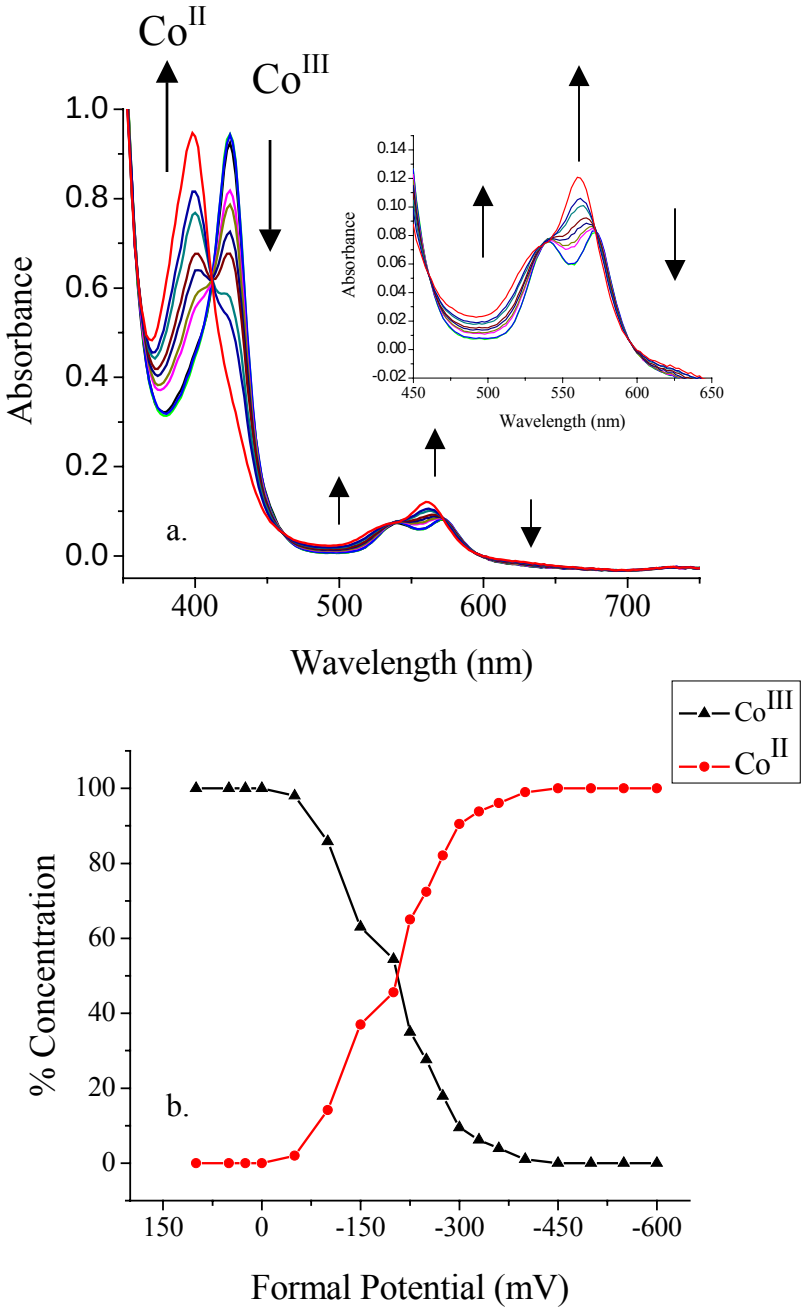

Figure 3-3. Panel (a) shows the absorption spectra of $Co^{III/II}TCP/TiO_2$ reduction in the CH_3CN electrolyte at the applied potential. Soret bands shift from 420 nm (Co^{III}) to 400 nm with negative applied potential. The applied potentials were -100, -150, -200, -250, -270, -300, -400, and -600 mV vs Ag/AgCl. The inset shows expanded absorption spectra from 450 to 650 nm. The arrow shows the direction of absorption change upon applying negative potential. (b) A plot of Co^{III}/Co^{II} concentrations vs. applied potential.

Figure 3-4 shows visible absorbance spectra of hemin in the ferric and ferrous Fe^{II} state (called heme) (*37*). Upon the addition of excess $CHCl_3$ to the heme solution, no change in absorbance was measured after 2 days. Figure 3-4b shows visible absorption data for the same reaction, except with hemin and heme bound to the TiO_2 surface. Upon addition of $CHCl_3$ to heme/TiO_2, the absorption spectra expected for hemin/TiO_2 were observed immediately and were complete within 30 min. In the case of CCl_4, the rate constants for heme and heme/TiO_2 were 0.031 ± 0.003 and 0.06 ± 0.01 M^{-1} s^{-1}, respectively in DMSO solution (*24*).

Formal reduction potentials for both hemin and CoTCP anchored to TiO_2 surfaces that had been pretreated with aqueous solutions of known pH were also measured spectroelectrochemically in CH_3CN electrolytes (Figure 3-5). Plots of the $M^{III/II}$ potential versus pH used for surface pretreatment show a significant shift in formal potentials. The hemin $Fe^{III/II}$ potential varied linearly from pH 1-14 with a slope of 40 mV per pH unit. In the case of CoTCP, the $M^{III/II}$ reduction potential varied between pH 4-9 with an average slope of 66 mV per pH unit and was pH independent at higher and lower proton concentrations.

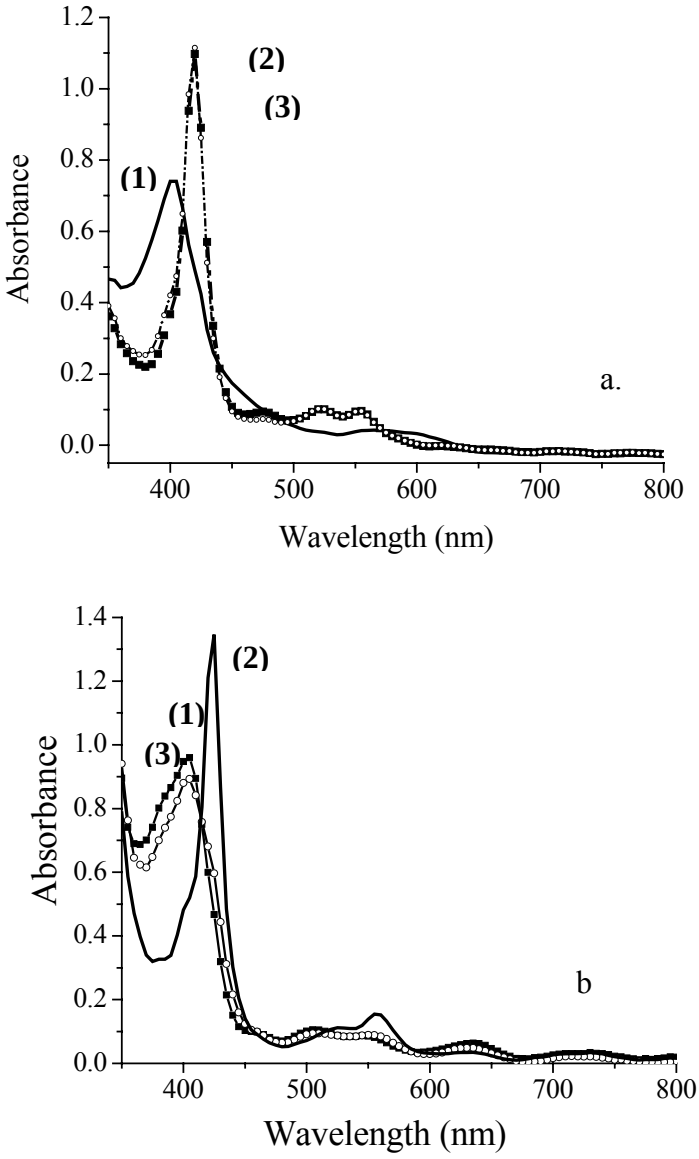

Figure 3-4. (a) The UV-visible absorbance spectra of (1) — hemin (2) –■– heme, and (3) –o – the spectra recorded 2days after the addition of $CHCl_3$ in DMSO electrolyte. (b) The UV-visible absorbance spectra of (1) –■– hemin/TiO_2, (2) — heme/TiO_2, and (3) – o – the spectra obserbed in 30min after the addition of $CHCl_3$ in DMSO electrolyte.

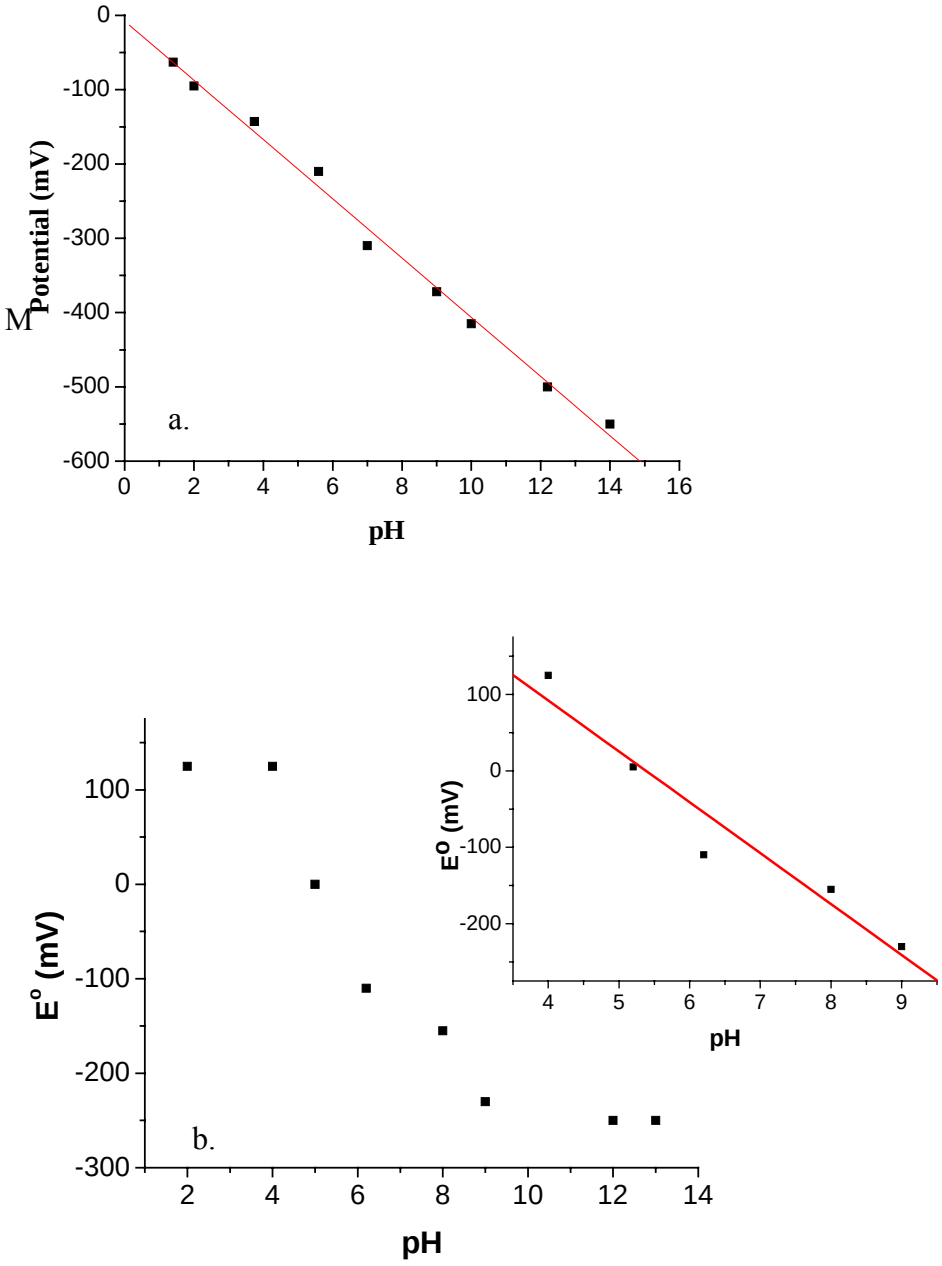

Figure 3-5. Formal $Fe^{III/II}$ reduction potential (E°) vs Ag/AgCl of (a) hemin/TiO_2 in a 50:50 CH_3CN/DMSO electrolyte as a function of the pH surface pretreatment of TiO_2. The best-fit line has a slope of 40 mV per pH unit. (b) CoTCP/TiO_2 in a CH_3CN electrolyte as a function of the pH surface pretreatment of the TiO_2. The inset shows a linear fit to the data from pH 4 to 9 with a slope of 66 mV per pH unit.

Measuring accurate hemin reduction potentials in aqueous solution was not feasible due to significant broadening of the absorption bands and poor solubility. However, it was possible for CoTCP. Typical spectroelectrochemical data for CoTCP/TiO_2 in aqueous electrolyte are shown in Figure 3-6. An increase in solution pH resulted in more negative formal potentials throughout the range of pH 1-10. The linear correlation was observed with an average slope of 52 mV ± 4 per pH unit (inset Figure 3-6). The $Co^{III/II}$TCP formal potentials with no TiO_2 present were also measured by spectroelectrochemistry at pH 6 and 9 and -583 and - 682 mV, respectively.

The heme/TiO_2 reactivity with CCl_4 was quantified at pH 4 and 8. Band gap illumination ($\lambda < 390$ nm) of hemin/TiO_2 in the presence of acetate was found to reduce the metal center to yield heme/TiO_2 at both pH values. The dark addition of CCl_4 was found to generate the initial hemin/TiO_2 absorption spectrum. The kinetics was first-order as shown in Figure 3-7. The observed rate constants, k_{obs}, were $3.9 \pm 0.7 \times 10^{-4}$ and $2.0 \pm 0.1 \times 10^{-3}$ s^{-1} at pH 4 and 8, respectively. The rate constants for heme loss and hemin formation were within the same experimental error.

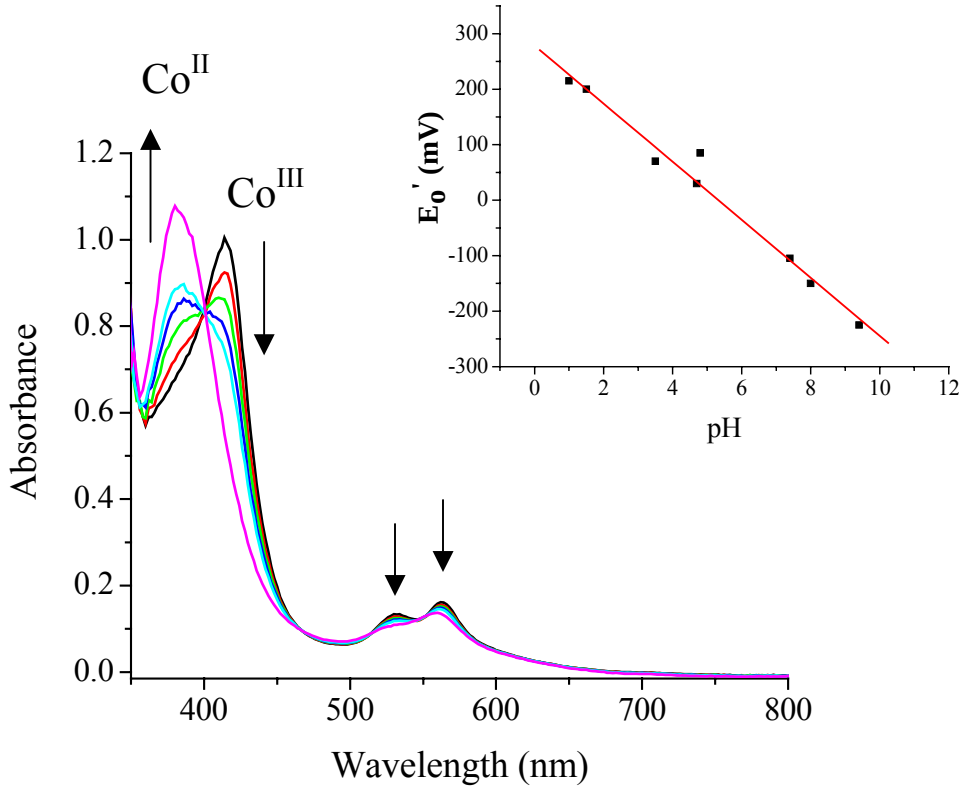

Figure 3-6. Representative spectroelectrochemical data of CoTCP/TiO_2 in pH 8 aqueous electrolyte as a function of applied potential (V_{appl} = -50, -100, -150, -200, and -270 mV). The inset shows formal potentials of CoTCP/TiO_2 in aqueous solution as a function of pH. The best-fit line has a slope of 52 mV per pH unit.

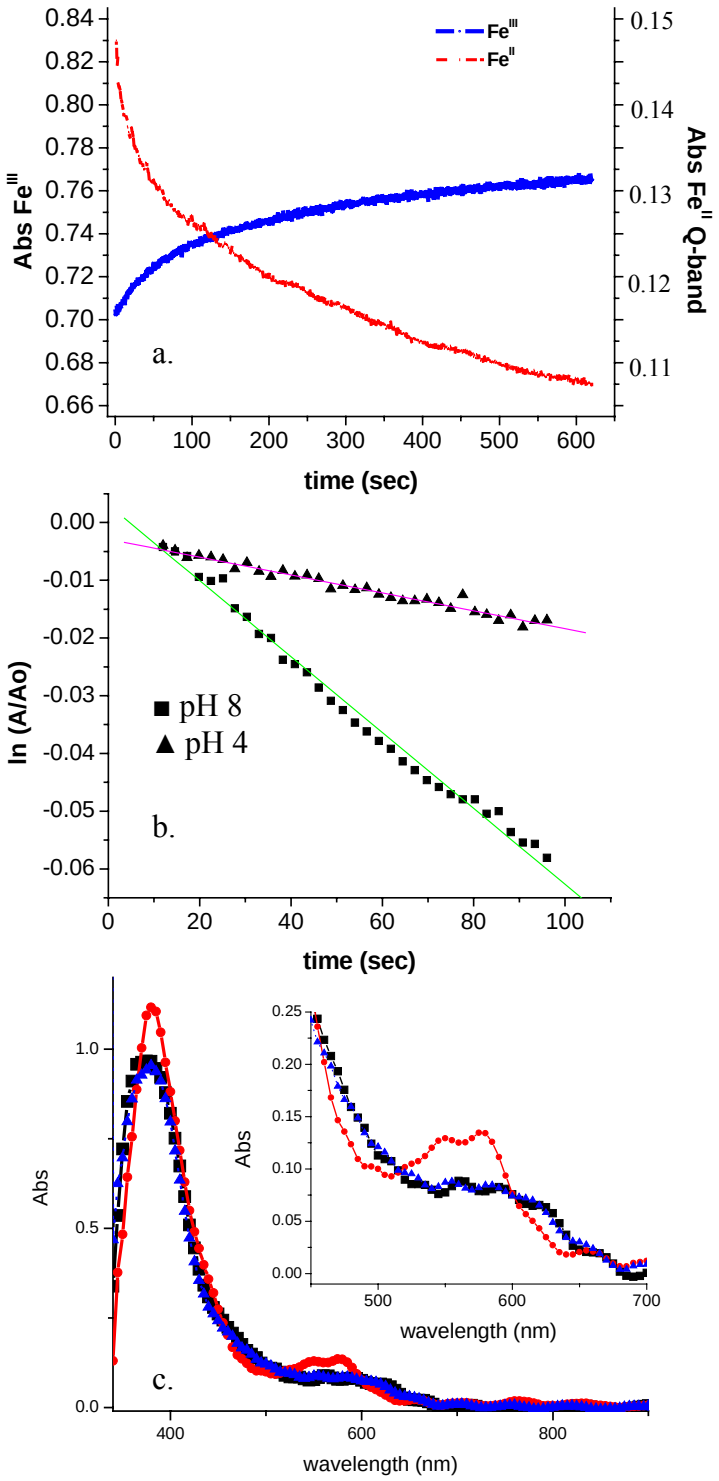

Figure 3-7. Reaction of heme/TiO_2 with 0.2 mM CCl_4 in aqueous solutions at pH 4 and 8. Panel a shows the absorption changes after the addition of CCl_4 at 575 nm (Fe^{II} Q-band) and at 360 nm (Fe^{III} Soret band) in pH 4. Panel b shows first-order kinetic analysis of data in panel a and corresponding data (not shown) at pH 8. Panel c shows the UV-vis spectra of (i) -■- hemin/TiO_2, (ii) -·- heme/TiO_2, and (iii) -△- the final product after the reaction of heme/TiO_2 with CCl_4 in pH 8 aqueous solution. The inset shows an expanded scale in the Q-band region.

3.4 Discussion

High surface area nanocrystalline (anatase) TiO_2 films were utilized as supports for hemin and CoTCP catalysts. These same TiO_2 films have been used extensively for solar cell applications and the high surface coverages (~10^{-8} mol/cm^2), and large adduct formation constants (K ~10^5 M^{-1}) measured here were consistent with that literature(*39, 40*). There exist several potential advantages of these mesoporous films over the colloidal suspensions previously used for environmental studies (*17-20*). The most obvious is that the films can be introduced and removed from a wide variety of environments including ground and ocean water. They do not suffer from aggregation or salting out common in colloidal suspensions. In addition, the mesoporous structure allows facile diffusion of RX or other pollutants to catalytic sites in the film. Most significant for this study is that the catalysts can electronically communicate with the outside world for environmental photocatalysis and electrocatalysis applica tions.

We find that the reactivity of heme and Co^{II}TCP with CCl_4 and $CHCl_3$ is greatly enhanced when they are immobilized on the surface of TiO_2. Such synergy between molecular and heterogeneous catalysts has previously been observed; however, the origins remain speculative (*24, 38*). The electrochemical, spectroscopic, and organohalide reactivity studies described herein have identified some of the factors that underlie this synergy. A significant shift in the formal reduction potential of the catalysts was observed upon surface binding, such that the catalysts bound to TiO_2 were always stronger reductants than the catalysts in fluid solution. This fortuitous change in potentials

underlies, at least in part, the enhanced organohalide reactivity on the TiO_2 surface. Next, we discuss the origins of this effect and of relevant literature data.

The mechanism by which the semiconductor bound catalysts can be reversibly oxidized and reduced is not obvious and deserves some discussion (*41*). The metal-based reduc tion potentials of these catalysts reside energetically within the forbidden energy gap of TiO_2 (Figure 3-8). Therefore, without band gap illumination, it is not possible for TiO_2 to directly reduce or oxidize these catalysts. We note that with a more negative applied bias, or band gap illumination, it is possible to mediate the reduction with TiO_2 conduction band electrons (*24*). More generally, the dark redox chemistry is initiated with catalysts bound to the tin oxide substrate and extends to the TiO_2 catalysts by intermolecular electron hopping. Complete oxidation of all the catalysts thus requires that there are no electronically isolated regions of the film and that a pathway for hopping to each catalyst is present. Bonhote and co-workers have indeed shown that a percola tion threshold exists for oxidation of amines anchored to nanocrystalline TiO_2 thin films (*42*). In the present work, saturation surface coverages led to absorbances >2 in the Soret region (400-430 nm) due to the high extinction coefficients of porphyrins (Table 3-1). Therefore, spectroelectrochemical measurements were performed at about 1/3 the maximum surface coverage. This coverage was either above the percolation threshold or catalysts had sufficient translational mobility to undergo lateral intermolecular electron transfer.

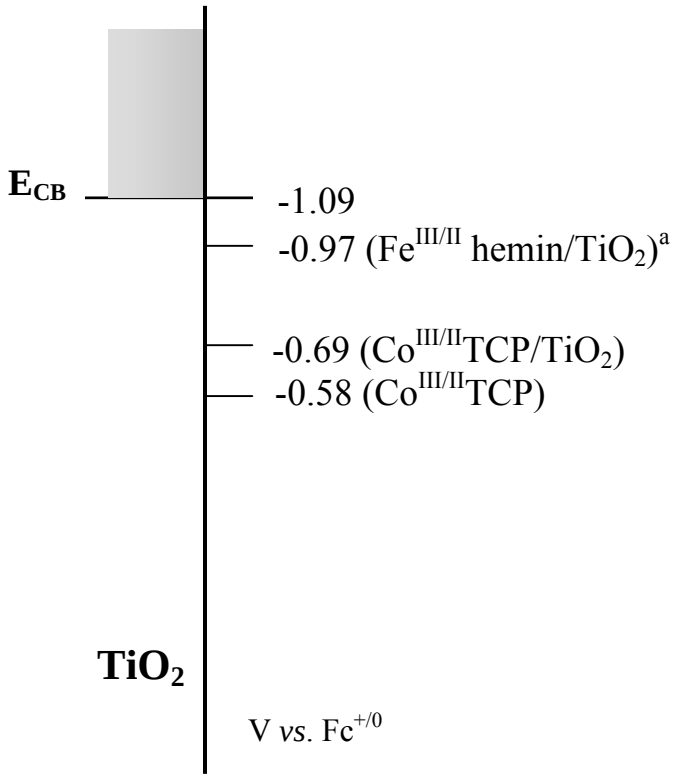

Figure 3-8. Interfacial energetics at catalyst/TiO_2 interfaces at pH = 6. The conduction band edge position was taken from refs *23* and *51*. The CoTCP data were measured herein. [a]Hemin/TiO_2 could not be measured in water, so the potential difference between $Co^{III/II}$ and $Fe^{III/II}$ in DMSO was assumed to be the same in water. While data are shown for pH = 6, the conduction band edge and the $M^{III/II}$ potentials show nearly Nernstian pH dependences, so the relative energetics are approximately correct at any pH.

The results of the spectroelectrochemical measurements show that surface binding has a profound affect on the formal potentials and RX reactivity of the catalysts (Table 3-1). The formal potentials measured in nonaqueous solution were dependent on the concentration of protons at the TiO_2 surface. The surface bound catalysts displayed nearly Nernstian shifts in the formal reduction potentials with pH. In aqueous solution, both environmental pH and interaction with the metal oxide surface contributed to the formal potential shifts of the transition metals catalysts. For example, at pH 6, the $Co^{III/II}$ formal potential shifted about 100 mV upon surface binding.

The near Nernstian shift with pH in aqueous solution has previously been observed for hemes and related macrocyles and is consistent with a proton coupled electron-transfer mechanism (*43-46*). Reduction of M^{III}-OH produces M^{II}-H_2O; hence, one electron and one proton are transferred. Rusling and co-workers, for example, have reported a similar pH dependence of the $Fe^{III/II}$ potentials of hemoglobin and myoglobin modified electrodes (*43, 45*). The reduced form of hemin and CoTCP and related compounds is known to react with a wide variety of organohalides (*8, 10, 20, 32, 33, 47-53*). Here, we have shown a clear correlation between the $M^{III/II}$ potential and the reaction rate constants.

The shifts in formal potential with surface binding are more difficult to explain. In nonaqueous solution, the results reported herein clearly show that they originate at least in part from the interfacial proton concentration. This observation is important as TiO_2 is known to be hydroscopic, and the exact processing conditions can lead to different surface potentials and hence reactivity. In addition, Zaban and co-workers

have shown that molecular dyes with pH independent formal reduction potentials become pH dependent when attached to TiO_2 (*54, 55*). The mechanism for this behavior is not fully understood but is thought to result from the influence of the electrostatic field caused by the adsorp tion of H^+ and OH^- ions on the semiconductor surface. This equilibrium also drives the well-known 59 mV/pH shifts of the conduction and valence band edge potentials. These same workers have shown that the distance between the dye and the semiconductor surface influenced the magnitude of the effect (*26*). Dyes within the Helmholtz layer showed a Nernstian shift, while those more distant showed a <59 mV/pH unit change (*55*). These observations could also explain why hemin/TiO_2 shows a weaker pH dependence than does CoTCP/TiO_2, as the former is separated from the surface by a flexible ethylene spacer.

3.5 Conclusions

We have shown that binding molecular catalysts to TiO_2 surfaces enhances their reactivity toward organohalide pollutants as compared with fluid solution. The increase in reactivity can be attributed to a negative shift in $M^{III/II}$ reduction potential (toward the vacuum level) upon surface binding. Interfacial as well as solution pH were shown to influence the thermodynamics and kinetics of RX reactivity. The results can be rationally understood on the basis of proton coupled electron transfer and the well-known Bronsted acid-base equilibrium of metal oxide surfaces. The ability to tune the reactivity of surface bound molecular catalysts by pH has profound impacts toward their reactivity with various RX pollutants.

3.6 References

1. McGuire, M. M.; Carlson, D. L.; Vikesland, P. J.; Kohn, T.; Grenier, A. C.; Langley, L. A.; Roberts, A. L.; Fairbrother, D. H. Applications of surface analysis in the environmental sciences: dehalogenation of chlorocarbons with zerovalent iron and iron-contain ing mineral surfaces. *Anal. Chim. Acta* **2003**, *496*, 301-313.

2. Satapanajaru, T.; Shea, P. J.; Comfort, S. D. Green rust and iron oxide formation influences metolachlor dechlorination during zerovalent iron treatment. *Environ. Sci. Technol.* **2003**, *37*, 5219-5227.

3. Fernandez-Sanchez, J. M.; Sawvel, E. J.; Alvarez, P. J. J. Effect of Fe^{O} quantity on the efficiency of integrated microbial-Fe^{O} treatment processes. *Chemosphere* **2004**, *54*, 823-829.

4. Burris, D. R.; Delcomyn, C. A.; Smith, M. H.; Roberts, L. A. Reductive dechlorination of tetrachloroethylene and trichloroethylene catalyzed by vitamin B-12 in homogeneous and heterogeneous systems. *Environ. Sci. Technol.* **1996**, *30*, 3047-3052

5. Lesage, S.; Brown, S.; Millar, K. A different mechanism for the reductive dechlorination of chlorinated ethenes: Kinetic and spectroscopic evidence. *Environ. Sci. Technol.* **1998**, *32*, 2264-2272.

6. Assaf-Anid, N.; Hayes, K. F.; Vogel, T. M. Reductive dechlorination of carbon tetrachloride by cobalamin (II) in the presence of dithiothreitol-Mechanistic study, effect of redox potential, and pH. *Environ. Sci. Technol.* **1994**, *28*, 246-252.

7. Nonnenberg, C.; van der Donk, W. A.; Zipse, H. Reductive dechlorination of trichloroethylene: A computational study. *J. Phys. Chem. A* **2002**, *106*, 8708-8715.

8. Gantzer, C. J.; Wackett, L. P. Reductive dechlorination catalyzed by bacterial transition-metal coenzymes. *Environ. Sci. Technol.* **1991**, *25*, 715-722.

9. Rich, A. E.; DeGreeff, A. D.; McNeill, K. Synthesis of (chlorovinyl) cobaloxime complexes, model complexes of proposed intermediates in the B-12-catalyzed dehalogenation of chlorinated ethylenes. *Chem. Commun.* **2002**, 234-235.

10. Chiu, P. C.; Reinhard, M. Metallocoenzyme-mediated reductive transformation of carbon tetrachloride in titanium(III) citrate aqueous solution. *Environ. Sci. Technol.* **1995**, *29*, 595-603.

11. Glod, G.; Angst, W.; Holliger, C.; Schwarzenbach, R. P. Corrinoid-mediated reduction of tetrachloroethene, trichloroethene, and trichlorofluoroethene in homogeneous aqueous solution: Reaction kinetics and reaction mechanisms. *Environ. Sci. Technol*. **1997**, *31*, 253-260.

12. Glod, G.; Brodmann, U.; Angst, W.; Holliger, C.; Schwarzenbach, R. P. Cobalamin-mediated reduction of *cis*- and *trans*-dichloroethene, 1,1-dichloroethene, and vinyl chloride in homogeneous aqueous solution: Reaction kinetics and mechanistic considerations. *Environ. Sci. Technol*. **1997**, *31*, 3154-3160.

13. Perlinger, J. A.; Buschmann, J.; Angst, W.; Schwarzenbach, R. P. Iron porphyrin and mercaptojuglone mediated reduction of polyhalogenated methanes and ethanes in homogeneous aqueous solution. *Environ. Sci. Technol*. **1998**, *32*, 2431-2437

14. Kadish, K. M.; Lin, X. Q.; Han, B. C. Chloride-binding reactions and electrochemistry of (TPP)Co^{II} and (TPP)Co^{III}Cl in dichloromethane. *Inorg. Chem*. **1987**, *26*, 4161-4167.

15. Doro, I.; Baram, D.; Berkowitz, B. Use of nanosized catalysts for transformation of chloro-organic pollutants. *Environ. Sci. Technol* **2005**, *39*, 1283-1290.

16. Ukrainczyk, L.; Chibwe, M.; Pinnavaia, T. J.; Boyd, S. A. Reductive dechlorination of carbon tetrachloride in water catalyzed by mineral-supported biomimetic cobalt macrocycles. *Environ. Sci. Technol.* **1995**, *29*, 439-445.

17. Hong, A. P.; Bahnemann, D. W.; Hoffmann, M. R. Cobalt(II) tetrasulfophthalocyanine on titanium dioxide-A new efficient electron relay for the photocatalytic formation and depletion of hydrogen peroxide in aqueous suspensions. *J. Phys. Chem*. **1987**, *91*, 2109-2117.

18. Hong, A. P.; Bahnemann, D. W.; Hoffmann, M. R. Cobalt(II) tetrasulfophthalocyanin on titanium dioxide. 2. Kinetics and mechanisms of the photocatalytic oxidation of aqueous sulfur dioxide. *J. Phys. Chem*. **1987**, *91*, 6245-6251.

19. Maldotti, A.; Molinari, A.; Amadelli, R. Photocatalysis with organized systems for the oxofunctionalization of hydrocarbons by O_2. *Chem. Rev*. **2002**, *102*, 3811-3836.

20. Kuhler, R. J.; Santo, G. A.; Caudill, T. R.; Betterton, E. A.; Arnold, R. G. Photoreductive dehalogenation of bromoform with titanium dioxide cobalt macrocycle hydrid catalysts. *Environ. Sci. Technol*. **1993**, *27*, 2104-2111.

21. Orth, W. S.; Gillham, R. W. Dechlorination of trichloroethene in aqueous solution using Fe^0. *Environ. Sci. Technol*. **1996**, *30*, 66-71.

22. Nzengung, V. A.; Castillo, R. M.; Cates, W. P.; Mills, G. L. Abiotic transformation of perchloroethylene in homogeneous dithionite solution and in suspensions of dithionite-treated clay minerals. *Environ. Sci. Technol.* **2001**, *35*, 2244-2251.

23. Kriegman-King, M. R.; Reinhard, M. Transformation of carbon tetrachloride in the presence of sulfide, biotite, and vermiculite. *Environ. Sci. Technol.* **1992**, *26*, 2198-2206.

24. Obare, S. O.; Ito, T.; Balfour, M. H.; Meyer, G. J. Ferrous hemin oxidation by organic halides at nanocrystalline TiO_2 interfaces. *Nano Lett.* **2003**, *3*, 1151-1153.

25. Nozik, A. J. Photoelectrochemistry: Applications to Solar Energy Conversion. *Annu. Rev. Phys. Chem.* **1978**, *29*, 189-222.

26. Gerischer, H. Neglected problems in the pH dependence of the flatband potential of semiconductors covered with oxide layers. *Electrochim. Acta* **1989**, *34*, 1005-1009.

27. Heimer, T. A.; D'Arcangelis, S. T.; Farzad, F.; Stipkala, J. M.; Meyer, G. J. An acetylacetonate-based semiconductor-sensitizer linkage. *Inorg. Chem.* **1996**, *35*, 5319-5324.

28. Bard, A. J.; Faulkner, L. R. *Electrochemical Methods Fundamentals and Applications*; John Wiley and Sons: New York, 2001.

29. Cao, F.; Oskam, G.; Searson, P. C.; Stipkala, J. M.; Heimer, T. A.; Farzad, F.; Meyer, G. J. Electrical and optical properties of porous nanocrystalline TiO_2 films. *J. Phys. Chem.* **1995**, *99*, 11974-11980.

30. Tieman, R. S.; Coury, L. A., Jr.; Kirchhoff, J. R.; Heineman, W. R. The electrochemistry of hemin in dimethyl sulfoxide. *J. Electroanal. Chem.* **1990**, *281*, 133-145.

31. Whitten, D. G.; Baker, E. W.; Corwin, A. H. Spectral studies of the d^6 metalloporphyrins. Ligand and solvent field effects on ferrous and cobaltic mesoporphyrin IX. *J. Org. Chem.* **1963**, *28*, 2363-2368.

32. Wade, R. S.; Castro, C. E. Oxidation of iron(II) porphyrins by alkyl halides. *J. Am. Chem. Soc.* **1973**, *95*, 226-230.

33. Larson, R. A.; Cervini-Silva, J. Dechlorination of substituted trichlorometanes by an iron(II) porphyrin. *Environ. Toxicol. Chem.* **2000**, *19*, 543-548.

34. Magdesieva, T. V.; Ivanov, P. S.; Kravchuk, D. N.; Butin, K. P. Electrochemical arylation of N-containing chelate and mactocyclic complexes of transition metals with the aid of diphenyliodonium salts. *Russ. J. Electrochem.* **2003**, *39*, 1245-1252.

35. Bettelheim, A.; White, B. A.; Raybuck, S. A. Murray, R. W. Electrochemical polymerization of amino-, pyrrole-, and hydroxy-substituted tetrapheylporphyrins. *Inorg. Chem.* **1987**, *26*, 1009-1017.

36. Lin, X. Q.; Boisselier-Cocolios, B.; Kadish, K. M. Electrochemistry, spectroelectrochemistry, and ligand addition reactions of an easily reducible cobalt porphyrin. Reaction of ((tetracyanotetraphenylporphinato) cobalt(II)($(CN)_4TPP)Co^{II}$) in pyridine and in pyridine/methylene chloride mixtures. *Inorg. Chem.* **1986**, *25*, 3242-3248.

37. *Merck Index*, Merck and CO., Inc.: Whitehouse Station, NJ, 1968; p 520.

38. Ozer, R. R.; Ferry, J. L. Photocatalytic oxidation of aqueous 1,2-dichlorobenzene by polyoxometalates supported on the NaY zeolite. *J. Phys. Chem. B* **2002**, *106*, 4336-4342.

39. O'Regan, B.; Gratzel, M. A low-cost, high-efficiency solar cell based on dye-sensitized colloidal TiO_2 films. *Nature* **1991**, *353*, 737-740.

40. Qu, P.; Meyer, G. J. Dye sensitization of electrodes. In *Electron Transfer in Chemistry*; Balzani, V., Ed.; John Wiley and Sons: New York 2001; Ch. 2, Part 2, Vol. IV, pp 355-411.

41. Argazzi, R.; Bignozzi, C. A.; Heimer, T. A.; Castellano, F. N.; Meyer, G. J. Enhanced spectral sensitivity from ruthenium(II) polypyridyl based photovoltaic devices. *Inorg. Chem.* **1994**, *33*, 5741-5749.

42. Bonhote, P.; Gogniat, E.; Tingry, S.; Barbe, C.; Vlachopoulos, N.; Lenzmann, F.; Comte, P.; Gratzel, M. Efficient lateral electron transport inside a monolayer of aromatic amines anchored on nanocrystalline metal oxide films. *J. Phys. Chem. B* **1998**, *102*, 1498-1507.

43. Nassar, A.-E. F.; Zhang, Z.; Hu, N.; Rusling, J. F.; Kumosinski, T. F. Proton-coupled electron transfer from electrodes to myoglobin in ordered biomembrane-like films. *J. Phys. Chem. B* **1997**, *101*, 2224-2231.

44. Blair, D. F.; Ellis, W. R., Jr.; Wang, H.; Gray, H. B.; Chan, S. I. Spectroelectrochemical study of cytochrome *c* oxidase: pH and temperature dependences of the cytochrome potentials. *J. Biol. Chem.* **1986**, *261*, 11524-11537.

45. Chen, X.; Hu, N.; Zeng, Y.; Rusling, J. F.; Yang, J. Ordered electrochemically active films of hemoglobin, didodecyldimethylammonium ions, and clay. *Langmuir* **1999**, *15*, 7022-7030.

46. Marques, H. M. Cyclic voltammetry of imidazolemicroperoxidase-8: Modeling the control of the redox potential of the cytochromes. *Inorg. Chem.* **1990**, *29*, 1597-1599.

47. Brault, D. Model studies in cytochrome P-450-mediated toxicity of halogenated compounds: Radical processes involving iron porphyrins. *Environ. Health Perspect.* **1985**, *64*, 53-60.

48. Castro, C. E.; Wade, R. S.; Belser, N. O. Biodehalogenation: Reactions of cytochrome P-450 with polyhalomethanes. *Biochemistry* **1985**, *24*, 204-210.

49. Brault, D.; Neta, P. Reactions of iron(III) porphyrins with peroxyl radicals derived from halothane and halomethanes *J. Phys. Chem.* **1984**, *88*, 2857-2862.

50. Nassar, A. F.; Bobbitt, J. M.; Stuart, J. D.; Rusling, J. F. Catalytic reduction of organohalide pollutants by myoglobin in a biomembrane-like surfactant film. *J. Am. Chem. Soc.* **1995**, *117*, 10986-10993.

51. Dobson, D. J.; Saini, S. Porphyrin-modified electrodes as biomimetic sensors for the determination of organohalide pollutants in aqueous samples. *Anal. Chem.* **1997**, *69*, 3532-3538.

52. Zheng, G.; Stradiotto, M.; Li, Lijuan. An electrochemical and spectroelectrochemical (IR) investigation of the reduction of RCo(II)TPP (R) = benzyl or butyl; TPP = tetraphenylporphyrin: mechanistic implications in the CoTPP catalyzed electrocarboxylation of alkyl halides. *J. Electroanal. Chem.* **1998**, *453*, 79-88.

53. Alonso, F.; Beletskaya, I. P.; Yus, M. Metal-mediated reductive hydrodehalogenation of organic halides. *Chem. Rev.* **2002**, *102*, 4009-4091.

54. Zaban, A.; Ferrere, S.; Sprague, J.; Gregg, B. A. pH-Dependent redox potential induced in a sensitizing dye by adsorption onto TiO_2. *J. Phys. Chem. B* **1997**, *101*, 55-57.

55. Zaban, A.; Ferrere, S.; Gregg, B. A. Relative energetics at the semiconductor/sensitizing dye/electrolyte interface. *J. Phys. Chem. B* **1998**, *102*, 452-460.

56. Fitzmaurice, D. Using spectroscopy to probe the band energetics of transparent nanocrystalline semiconductor films. *Solar Energy Mater. Solar Cells* **1994**, *32*, 289-305.

Chapter 4: Multi-Electron Transfer from Heme-Functionalized Nanocrystalline TiO_2 to Organohalide Pollutants

4.1 Introduction

A significant challenge in the photochemical sciences is to identify assemblies that can store and transfer multiple electrons to a substrate when illuminated with light. Multi-electron transfer (MET) processes avoid high-energy free radical intermediates and can yield desired reaction products under mild conditions. The synthesis of chromophoric molecular compounds capable of MET is challenging, although some notable breakthroughs have recently been realized.[1-3] Nanomaterials, on the other hand, that can harvest solar energy and store multiple electrons are easily synthesized but often lack the selectivity of molecular catalysts.[4,5]

In this Chapter, we describe a new and broadly applicable approach for photodriven molecular MET catalysis. Hemin (iron protoporphyrin IX) has been anchored to ~15 nm TiO_2 nanocrystallites (anatase) in ~8 μm thick mesoporous thin films. Band gap excitation of these materials in methanol or aqueous (pH 4 or 8) solutions leads to the reduction of hemin to heme ($Fe^{III} \rightarrow Fe^{II}$) and the production of $TiO_2(e^-)$, heme/$TiO_2(e^-)$. Well-defined molecular catalysts (hemes) anchored to mesoporous nanocrystalline (anatase TiO_2) thin films were found to trap, store, and transfer multiple electrons to organohalide pollutants. The mechanisms and second-

order rate constants for the reduction of bromobenzene, chlorobenzene, dichlorobenzene, and trichloroethylene were quantified. The evidence of MET processes were supported with the reaction of heme/$TiO_2(e^-)$ with 6-bromo-1-hexene as a radical clock.

4.2 Experimental section

Materials

Aryl halides (bromobenzene, clorobenzene, and dichlorobenzene, and trichloroethylene) were used as received. Titanium(IV) isopropoxide was obtained from Aldrich Chemical Co. Iron(III) protoporphyrin IX chloride (hemin) was obtained from Fluka. All solvents were of HPLC grade and were obtained from Fisher Scientific. Deionized water was used for the measurements in aquesou soulutions.

Nanocrystalline TiO_2 thin films and functionarization of heme catalysts

Mesoporous nanocrystalline TiO_2 films were prepared by the hydrolysis of Ti(*i*-OPr)$_4$ by a sol-gel method previously described in the literature.[7] Anatase TiO_2 nanoparticles prepared in this manner were ~15 nm in diameter, and the film thickness was ~10 μm. Hemin was attached to nanocrystalline TiO_2 films from micromolar DMSO solutions at room temperature.

Photoreduction from hemin/TiO_2 to heme/$TiO_2(e^-)$

TiO_2 films or hemin (protoporphyrin IX chloride)-functionalized TiO_2 films were immersed in solutions of neat methanol or, in some cases, aqueous solutions of 6.7×10^{-4} M acetic acid (pH = 4) or 0.1 M sodium citrate (pH = 8) and were purged for > 30 min with N_2. Band gap excitation resulted in the reduction of hemin to heme, and continued photolysis led to the appearance of the well-known absorption of TiO_2 electrons, $TiO_2(e^-)$, that absorb light throughout the visible and into the infrared region, Figure 4-1.[8]

Kinetic Analysis of Organohalide Reactivity

A Varian Cary 50 UV-visible spectrophotometer was used to acquire time-resolved spectra for the reaction of $TiO_2(e^-)$ and/or heme/$TiO_2(e^-)$ with aryl halides and trichloroethylene. An aliquot of N_2 saturated RX in MeOH or H_2O was added to $TiO_2(e^-)$ or heme/$TiO_2(e^-)$ thin film immersed in MeOH or an aqueous solution. The disappearance of heme (Fe^{II}) Soret absorbance at 420 nm and $TiO_2(e^-)$ absorption at 800 nm, and the appearance of hemin (Fe^{III}) Soret band at 400 nm were analyzed with a first-order kinetic model where pseudo-first-order kinetic rate constants, $k_{obs,}$ were obtained.

Gas chromatography mass spectrometry

The products formed by photocatalysis in THF were analyzed by a Shimadzu GC17A/QP5050A GC/MS (Shimadzu Columbia, MD). The GC17A is equipped with a

low polarity (5% phenyl-, 95% methyl-siloxane) capillary J & W DB5-MS column (30 m length, 0.25 mm ID, 0.25 μm film thickness). The products formed in THF solution was transfer to a 2 mL GC/MS vial. The reaction mixture was injected into the autosampler of the GC/MS. The injector temperature was 220 °C and the transfer interface was at 280 °C. The split ratio was 10 and the H_2 gas column flow rate was kept at 1.0 mL/min. An EI quadrupole based mass spectrometer served as the detector with a scan range of 40-900 amu and an ionizing electron energy of 70 eV.

4.3. Results

The catalysts were photoreduced from Fe^{III}/TiO_2 (or TiO_2) to $Fe^{II}/TiO_2(e^-)$ (or $TiO_2(e^-)$) by band gap illumination in N_2 saturated MeOH or aqueous (pH 4 or 8) solution. Valence band holes are known to irreversibly oxidize methanol (or carboxylates) that allows the concentration of $TiO_2(e^-)$ to build up under steady-state photolysis.[5,9] Under the experimental conditions investigated, we estimate that each TiO_2 nanoparticle contains on average ~50 hemes and 600 $TiO_2(e^-)$.[8] Concentrations of $TiO_2(e^-)$ could be controlled by photolysis time, and the heme surface coverage could be independently tuned through equilibrium binding.[10]

The photogenerated hemes and $TiO_2(e^-)$ were stable under anaerobic conditions for several days. Organohalide (RX) pollutants, trichloroethylene (TCE), 1,2-dichlorobenzene, 1-bromobenzene, and 1-chlorobenzene, introduced to the external

solutions were found to initiate redox reactivity. The experiments were performed in the dark to preclude secondary photolytic reactions. Figure 4-1 shows the changes in absorbance with time after 1,2-dichlorobenzene (4-1a) and trichloroethylene (4-1b) were added to the external solvent. The spectral changes observed were qualitatively similar for all the organohalides investigated. The concentration of $TiO_2(e^-)$ decreased rapidly to less than 10% of the initial value, after which time the heme was oxidized to hemin (inset Figure 4-1). The first-order rate constants for the appearance of oxidized heme (hemin) and the loss of heme were, within experimental error, the same. At long reaction times, the initial hemin/TiO_2 absorption spectrum was observed, consistent with quantitative reactivity based on heme.

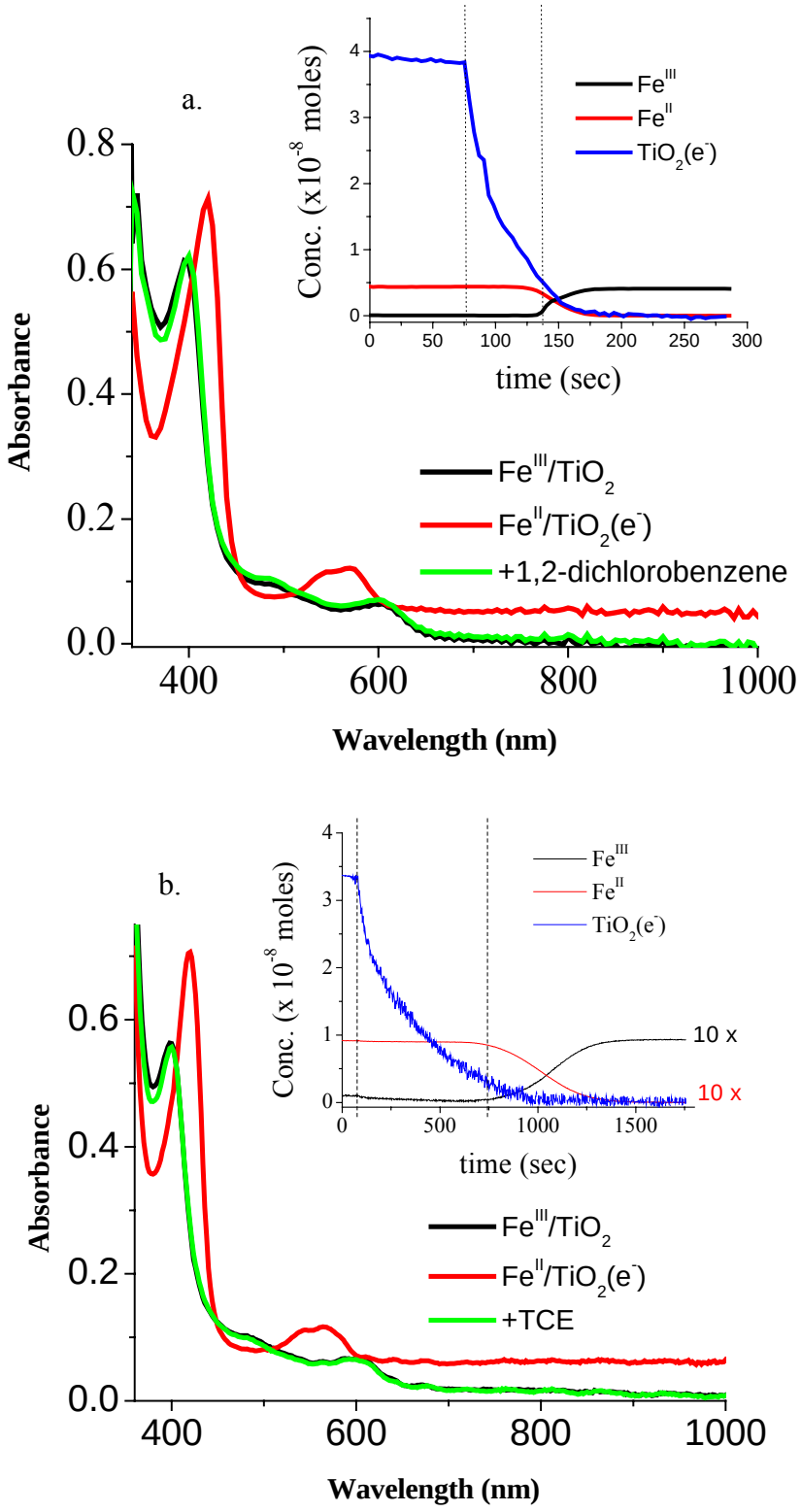

Figure 4-1. UV-visible absorbance spectra of hemin/TiO_2 (—), after photolysis: heme/$TiO_2(e^-)$ (—), and after addition of (a)1,2-dichlorobenzene and (b) trichloroethylene to yield hemin/TiO_2 (—). The inset shows time-resolved concentration changes upon addition of RX. The first vertical line indicates the time of RX injection (75 s), and the second line corresponds to the time when >90% of the $TiO_2(e^-)$ was consumed and heme oxidation begins.

Comparative studies with titanium dioxide electrons in the absence of heme and heme alone were investigated. Heme is a naturally occurring porphyrin that is known to reduce a variety of alkyl halides[11] but was unreactive toward TCE or the arylhalides in methanol. The $TiO_2(e^-)$s showed measurable reactivity with the arylhalides but none with TCE.

Figure 4-2 shows that the concentration of $TiO_2(e^-)$ decreased to near zero within 20 s upon addition of 1,2'-dichlorobenzene when heme was anchored to the semiconductor surface. In contrast, under the same conditions, the $TiO_2(e^-)$ decreased by only about half after 30 min in the absence of heme. Both reactions were found to be first-order in aryl halide. In general, the second-order rate constants for aryl halide reduction by $TiO_2(e^-)$ was 80-150 times larger in the presence of heme (Table 4-1). Neither $TiO_2(e^-)$ nor heme alone showed measurable reactivity with TCE after 3 days in both MeOH (Table 4-1) and pH 8 aqueous solution (Figure 4-3). However, the reaction proceeded rapidly for heme/$TiO_2(e^-)$ in methanol (Table 4-1), and at pH 8 (Figure 4-3), $k = 0.22 \pm 0.02\ M^{-1}s^{-1}$.

Table 4-1. Rate constants for Organohalid Reduction by $TiO_2(e^-)$ and heme/$TiO_2(e^-)$ in Methanol.

	$TiO_2(e^-)$	Heme/$TiO_2(e^-)$
Organohalide	k ($M^{-1}s^{-1}$)	k ($M^{-1}s^{-1}$)
Bromobenzene	0.430 ± 0.040	36.47 ± 1.10
Chlorobenzene	0.050 ± 0.006	3.780 ± 0.13
Dichlorobenzene	0.070 ± 0.002	10.42 ± 0.27
Trichloroethylene	No Rxn.	0.760 ± 0.03

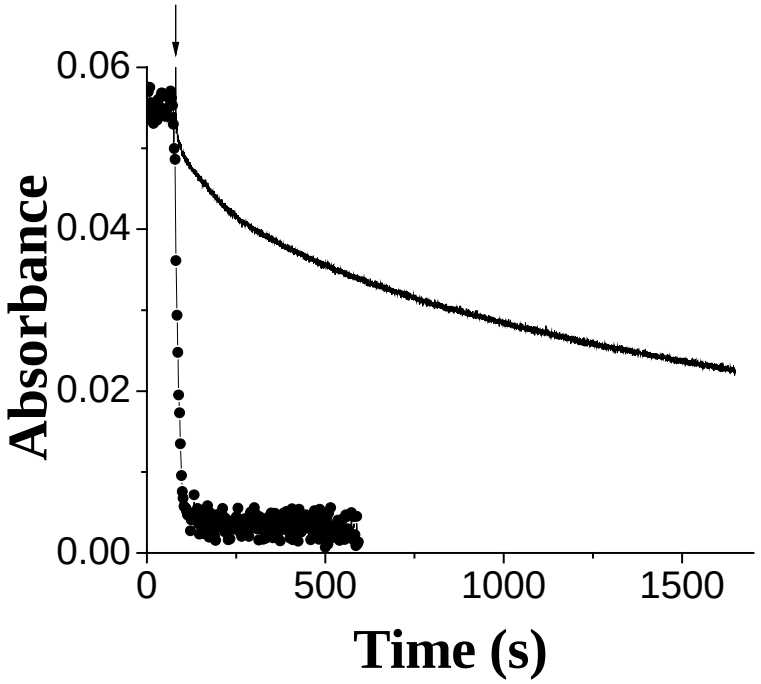

Figure 4-2 Absorbance at 1000 nm of heme/$TiO_2(e^-)$ (· · ·) and $TiO_2(e^-)$ (-) as a function of time. The arrow indicates the point at which 1,2-dichlorobenzene was added to the external methanol solution.

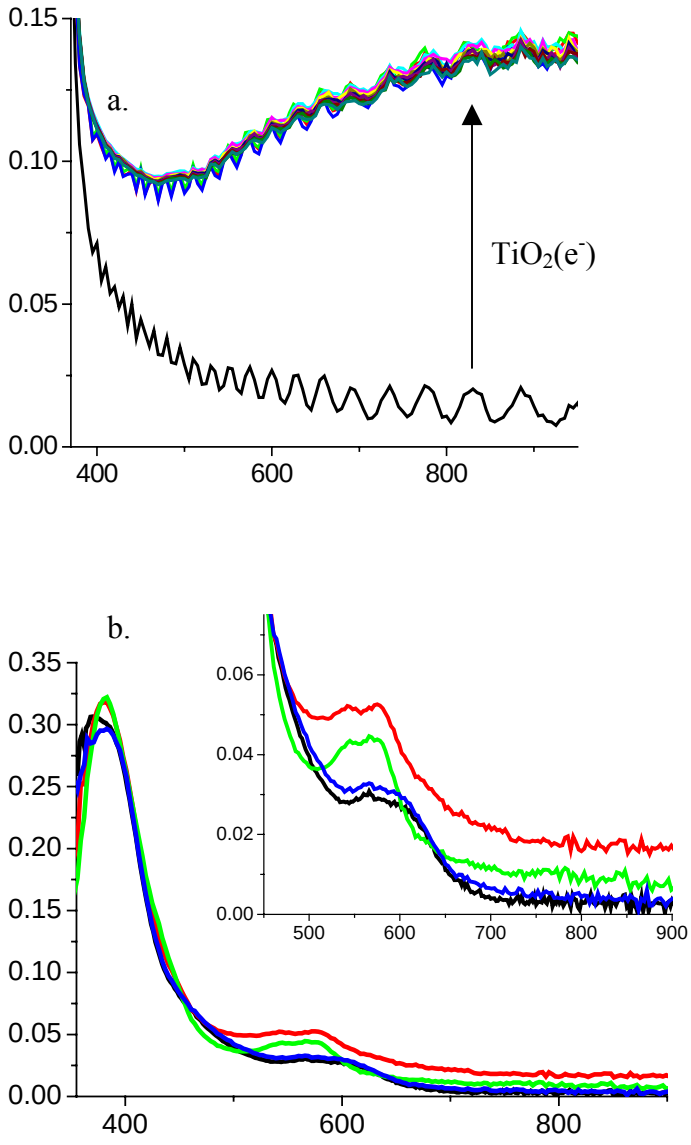

Figure 4-3. UV-vis absorption spectra of TCE reaction with a) $TiO_2(e^-)$ that shows no reactivity for 3 hours after addition of TCE and b) heme/$TiO_2(e^-)$ that shows the competion of the reaction in 1 hour after the addition of TCE. UV-visible absorbance spectra of hemin/TiO_2 (—), after photolysis, heme/$TiO_2(e^-)$ (—), after addition of TCE to yield heme/TiO_2 (—), and the completion of the reaction to yield hemin/TiO_2 (—).

The cooperative reactivity was further investigated with radical clocks that yield characteristic products from one- and two- electron transfer reactions.[13] As shown in Scheme 4-1, 6-bromo-1-hexene yields 1-methylcyclopentane through two single-electron transfer reactions, while a rapid two-electron transfer produces 1-hexene. Reactions of 6-bromo-1-hexene with $TiO_2(e^-)$ and heme/$TiO_2(e^-)$ in THF were analyzed by GC-MS. 1-Methylcyclopentane was the sole product observed for $TiO_2(e^-)$. For reactions of 6-bromo-1-hexene with heme/$TiO_2(e^-)$, both 1-hexene and 1-methylcyclopentane were formed in relative yields of 69 ± 5 and 31 ± 5%, respectively.

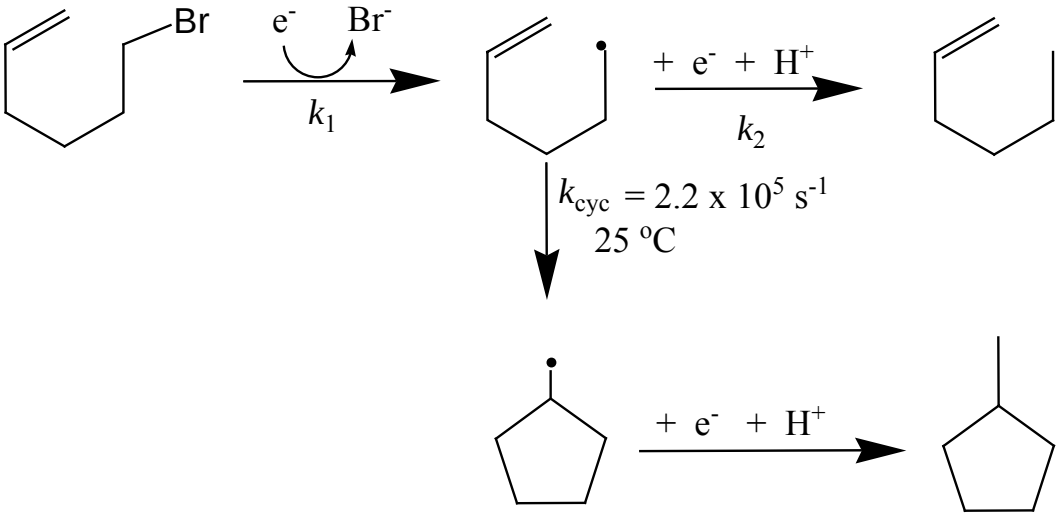

Scheme 4-1. The electron transfer pathways of the radical clock, 6-bromo-1-hexene that yields a) 1-hexene as a product of two-electron transfer process and b) 1-methylcyclopentane as a product of two single electron transfer processes.

4.4 Discusstion

Each heme functionalized TiO_2 nanoparticle was found to store >500 reducing equivalents upon illumination. A synergy effect between the molecular catalysts and the semiconductor was observed. We have quantified the kinetics for TCE and aryl halide reduction by hemes anchored to $TiO_2(e^-)$, Table 4-1. It is noteworthy that these same reactions are not observed for hemes in fluid solution and do not occur, or are much slower, for $TiO_2(e^-)$s alone under otherwise similar conditions.

Similar spectroscopic changes were observed when all the organohalides were reacted with the heme/ $TiO_2(e^-)$. In all cases, the concentration of $TiO_2(e^-)$ was found to decrease to near zero before the hemes were oxidized to hemin, Figure 4-1. The spectral changes are consistent with at least two mechanistic pathways: (1) a heme-mediated reduction; or (2) reduction first by $TiO_2(e^-)$ and then by heme/TiO_2. The first pathway requires that the $TiO_2(e^-) \rightarrow$Fe(III) charge transfer be faster than Fe(II) $\rightarrow$ RX. The latter pathway requires rapid reduction of RX by the $TiO_2(e^-)$.

(1) Mediated Mechanism:

$Heme/TiO_2(ne^-) + RX \rightarrow Hemin/TiO_2(ne^-) + RX^{\bullet-}$ Slow (4-a)

$Hemin/TiO_2(ne^-) \rightarrow Heme/TiO_2((n-1)e^-)$ Fast (4-b)

$Heme/TiO_2 + RX \rightarrow Hemin/TiO_2 + RX^{\bullet-}$ (4-c)

(2) Stepwise Mechanism:

$Heme/TiO_2(ne^-) + RX \rightarrow Heme/TiO_2((n-1)e^-) + RX^{\bullet-}$ (4-d)

$Heme/TiO_2(e^-) + RX \rightarrow Heme/TiO_2 + RX^{\bullet-}$ (4-e)

$Heme/TiO_2 + RX \rightarrow Hemin/TiO_2 + RX^{\bullet-}$ (4-f)

Comparative studies with $TiO_2(e^-)$ that were not functionalized with hemes were very slow or, in the case of TCE, did not react at all. The second-order rate constants by heme/$TiO_2(e^-)$ were 80-150 times larger than $TiO_2(e^-)$ in the absence of heme. Such data are most consistent with heme-mediated RX reduction and suggest cooperativity between hemes and the semiconductor conduction band electrons (Figure 4-4). We note that there was no spectroscopic evidence for RX adsorption to TiO_2 or to hemin-functionalized TiO_2 in the dark.

In the case of the reaction with TCE, $TiO_2(e^-)$ or heme alone did not show measurable reactivity for 3 days. However, heme/$TiO_2(e^-)$ in methanol and aqueous solution (pH 4 and 8) reacted rapidly with TCE. A possible explanation for this is that the first reduction potential of TCE is too negative, $E^\circ = -0.69 \pm 0.01$ V, and the reduction occurs by the more thermodynamically favorable two-electron pathway, $E^\circ = +0.52 \pm 0.01$ V vs NHE.[12]

Radical clock studies clearly demonstrate that rapid microsecond multi-electron transfer reduction occurs at the heme/TiO_2 interface. Reactions of 6-bromo-1-hexene with heme/$TiO_2(e^-)$ that produced 69% 1-hexene demonstrate multi-electron transfer. The formation of 1-hexene indicates that the second electron was transferred to RX at a rate faster than that of the free-radical cyclization reaction. In other words, the heme/$TiO_2(e^-)$ nanocrystallites delivered two electrons to RX within 4.5 μs. On the other hand, the only product of the reactions with $TiO_2(e^-)$ was 1-Methylcyclopentane. This indicates that the second electron was transferred slower, > 4.5 μs, in the absence of heme. The radical clock studies support the evidence of two-electron reduction pathway for heme/$TiO_2(e^-)$ with RX.

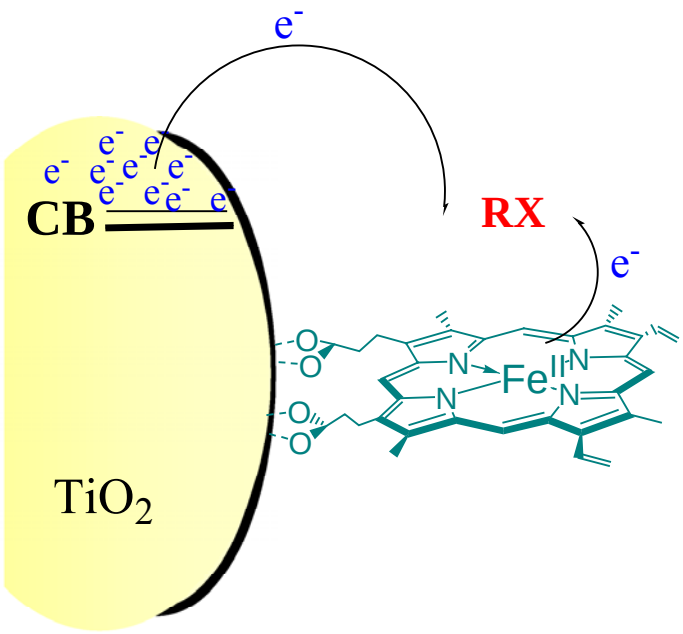

Figure 4-4. The possible multi-electron transfer processes of heme/$TiO_2(e^-)$ reaction with organohalide pollutants.

4.5 Conclusions

We have quantified the kinetics for aryl halide and TCE reduction by heme anchored to TiO_2 particles. The reactions with heme/$TiO_2(e^-)$ were much faster than $TiO_2(e^-)$ or heme alone. The evidence for a multi-electron transfer process was supported by radical clock studies. The semiconducting nature of the mesoporous TiO_2 thin films allows the reactive states to be controlled with light and/or applied potential,[10,14] behavior that is difficult, if not impossible, to achieve with colloidal solutions.[15] In principle, the relative concentrations of conduction band electrons and hemes can be systematically tuned to yield desired reaction products. We emphasize also that the approach here is not limited to naturally occurring heme catalysts or to TiO_2 and can be extended to a wide variety of naturally occurring or synthetic catalysts and nanomaterials for other environmental or catalytic applications. Future studies of heme/$TiO_2(e^-)$ will focus on the mechanistic details for multi-electron transfer as well as identification of the RX reduction products.

4.6 References

1. Heyduk, A. F.; Nocera, D. G. Hydrogen produced from hydrohalic acid solutions by a two-electron mixed-valence photocatalyst. *Science* **2001**, *293*, 1639.

2. Konduri, R.; de Tacconi, T. R.; Rajeshwar, K.; MacDonnell, F. M. Multielectron Photoreduction of a Bridged Ruthenium Dimer, $[(phen)_2Ru(tatpp)Ru(phen)_2][PF_6]_4$: Aqueous Reactivity and Chemical and Spectroelectrochemical Identification of the Photoproducts *J. Am. Chem. Soc*. **2004**, *126*, 11621.

3. Fukuzumi, S.; Okamoto, K.; Tokuda, Y.; Gros, C. P.; Guilard, R. Dehydrogenation versus Oxygenation in Two-Electron and Four-Electron Reduction of Dioxygen by 9-

Alkyl-10-methyl-9,10-dihydroacridines Catalyzed by Monomeric Cobalt Porphyrins and Cofacial Dicobalt Porphyrins in the Presence of Perchloric Acid. *J. Am. Chem. Soc*. **2004**, *126*, 17059.

4. Hirakawa, T.; Kamat, P. V. Charge separation and catalytic activity of Ag@TiO_2 core-shell composite clusters under UV-irradiation. *J. Am. Chem. Soc*. **2005**, *127*, 3928.

5. Hoffmann, M. R.; Martin, S. T.; Choi, W.; Bahnemann, D. W**.** Environmental Applications of Semiconductor Photocatalysis. *Chem. Rev*. **1995**, *95*, 69.

6. Rothenberger, G.; Moser, J.; Gratzel, M.; Serpone, N.; Sharma, D. K**.** Charge carrier trapping and recombination dynamics in small semiconductor particles. *J. Am. Chem. Soc.* **1985**, *107*, 8054.

7. Heimer, T. A.; D'Arcangelis, S. T.; Farzad, F.; Stipkala, J. M.; Meyer, G. J. An acetylacetonate-based semiconductor-sensitizer linkage. *Inorg. Chem*. **1996**, *35*, 5319.

8. Rothenberger, G.; Fitzmaurice, D.; Gratzel, M**.** Spectroscopy of conduction band electrons in transparent metal oxide semiconductor films: optical determination of the flatband potential of colloidal titanium dioxide films. *J. Phys. Chem.* **1992**, *96*, 5983.

9. Linsebigler, A. L.; Lu, G. Q.; Yates, J. T. Photocatalysis on TiO_2 surfaces: principles, mechanisms, and selected results. *Chem. Rev*. **1995**, *95*, 735.

10. Obare, S. O.; Ito, T.; Balfour, M. H.; Meyer, G. J. Ferrous hemin oxidation by organic halides at nanocrystalline TiO_2 interfaces. *Nano Lett*. **2003**, *3*, 1151.

11. (a) Wade, R. S.; Castro, C. E. Oixidation of heme proteins by alkyl halides *J. Am. Chem. Soc*. **1973**, *95*, 226. (b) Brault, D. Model studies in cytochrome P-450-mediated toxicity of halogenated compounds: radical processes involving iron porphyrins. *Environ. Health Perspect.* **1985**, *64*, 53.

12. Totten, L.; Roberts, A. L. Calculated one- and two-electron reduction potentials and related molecular descriptors for reduction of alkyl and vinyl halides in water *Crit. Rev. Environ. Sci. Technol.* **2001**, *31*, 175.

13. Chatgilialoglu, C.; Ingold, K. U.; Scaiano, J. C. Rate constants and Arrhenius parameters for the reactions of primary, secondary, and tertiary alkyl radicals with tri-n-butyltin hydride. *J. Am. Chem. Soc*. **1981**, *103*, 7739.

14. Obare, S. O.; Ito, T.; Meyer, G. J. Controlling reduction potentials of semiconductor-supported molecular catalysts for environmental remediation of organohalide pollutants. *Environ. Sci. Technol.* **2005**, *39*, 6266

15. (a) Hong, A. P.; Bahnemann, D. W.; Hoffmann, M. R. Cobalt(II) tetrasulfophthalocyanine on titanium dioxide-A new efficient electron relay for the

photocatalytic formation and depletion of hydrogen peroxide in aqueous suspensions *J. Phys. Chem*. **1987**, *91*, 6245. (b) Ukrainczyk, L.; Chibwe, M.; Pinnavaia, T. J.; Boyd, S. A. Reductive dechlorination of carbon tetrachloride in water catalyzed by mineral-supported biomimetic cobalt macrocycles. *Environ. Sci. Technol.* **1995**, *29*, 439. (c) Maldotti, A.; Molinari, A.; Amadelli, R. Photocatalysis with organized systems for the oxofunctionalization of hydrocarbons by O_2 *Chem. Rev*. **2002**, *102*, 3811.

Chapter 5: Heme Mediated Reduction of Organohalide Pollutants at Nanocrystalline TiO_2 Thin Film Interfaces

5.1 Introduction

Organohalide pollutants are commonly found in groundwater and have been linked to Serious health problems (Tesfamichael and Kaluarachchi 2004; Simmons *et al.,* 2002; Duran and Esposite 2000; U.S.EPA 2000a). In fact, seventeen of the fifty pollutants most commonly found in urban area groundwater are organohalides. About 44% of pollutants on the EPA's contaminants candidate list are organohalides (U.S.EPA 1998b). Thus organohalide removal, or degradation to benign products, represents a major environmental challenge (U.S.EPA 2000c).

A common approach for organohalide remediation has been to use electron transfer reactions from semiconductors, metals, or transition metal compounds (Obare and Meyer 2004; McGuire *et al.,* 2003; Lee and Batchelor 2003; Burris *et al.,* 1996). Indeed both the oxidation and reduction of organohalide pollutants have been well documented in laboratory experiments. Reductive dechlorination with "zero valent" iron has been employed in the US and Canada for some time (Fernandez-Sanchez *et al.,* 2004; Satapanajaru *et al.,* 2003; Eykholt and Davenport 1998). A significant challenge for reductive dehalogenation with molecular catalysts is maintaining the active redox state of the catalyst in the environment. This is a particularly problematic in aerobic and acidic

environments where proton and dioxygen reduction is generally more facile than is the reduction of organohalide poisons such as trichloroethylene.

Recently we initiated experiments with molecular catalysts bound to semiconductor nanocrystallites dispersed in mesoporous thin films (Obare *et al.,* 2003; Obare *et al.,* 2005). The semiconducting nanoparticles allowed the active state of the catalysts to be maintained with light and/or an applied potential for applications in environmental photocatalysis and electrocatalysis. In addition, the enormous surface area of the thin films afforded high concentrations of catalysts (approaching one molar within the film) while still at monolayer or lower surface coverage. Furthermore, by interconnecting the nanoparticles in a mesoporous thin film, the common difficulty of colloidal precipitation or 'salting out' in high ionic strength environmental fluids was eliminated. The mesopores within the thin films (Barbe *et. al.,* 1997) extend to the substrate and allow pollutants to freely diffuse to the surface bound catalysts.

In the course of this work an unexpected synergy between the catalysts and the semiconductor nanoparticles was discovered (Obare *et al.,* 2003). Organohalide reactivity was greater for catalyst/semiconductor materials than for the sum of the semiconductor and the catalyst alone. This behavior was explained, at least in part, by more favorable energetics for organohalide reduction at the semiconductor-catalyst interface (Obare *et al.,* 2005). In addition, evidence for multi-electron transfer (MET) reactivity at the molecular-semiconductor interface was found (Obare *et al.,* 2006). MET processes avoid high-energy free radical intermediates and can yield desired reaction products under environmentally significant conditions. A long term goal of this research is to utilize MET processes with molecular catalysts and semiconductor materials that are

highly turned to selectively react with specific pollutants to yield desired reaction products.

Herein, we describe our most recent studies of environmental redox catalysis at semiconductor-catalyst interfaces. Well-defined molecular catalysts (hemes) anchored to mesoporous nanocrystalline (anatase) TiO_2 thin films were reacted with organohalide pollutants (CCl_4, $CHCl_3$, propachlor, and trichloroethylene) in both water and methanol. Insights into the dechlorination reaction mechanisms were gained from electrochemical, spectroscopic, and mass spectroscopy studies. The reactions were found to be enhanced significantly when excess electrons were present in the TiO_2 nanoparticles.

5.2 Experimental Section

Materials

Dimethyl sulfoxide (DMSO), acetic acid, potassium nitrate, and nitric acid were obtained from Fisher Scientific. Sodium acetate was obtained from J.T. Baker. Titanium (IV) isopropoxide (Aldrich), methanol (Fisher), tetrabutylammonium hexafluorophosphate (TBAH) (Fluka), sodium hydroxide (Aldrich), iron(III) *meso*-tetraphenyl porphyrin chloride (Frontier Scientific), and iron(III) protoporphyrin chloride (Fluka), were used as received. Deionized water was used in aqueous measurements and reactions.

Nanocrystalline TiO_2 thin film preparation

Transparent TiO_2 films consisting of ~ 15 nm diameter anatase particles were prepared by the hydrolysis of $Ti(iOPr)_4$ using a sol-gel technique previously described in the literature (Heimer *et al*., 1996). The TiO_2 particles were cast as mesoporous thin (~10μm) films onto transparent fluorine-doped tin oxide (FTO) or microscope glass slides and heated at 420 °C for 30 min. Freshly prepared TiO_2 films were soaked in 2-8 μM hemin/DMSO solutions overnight at room temperature. Hemin/TiO_2 films were rinsed with MeOH, pH 4 (6.7×10^{-4} M acetic acid), or pH 8 (0.6 M sodium acetate) priories to the reaction. The pH values were measured using an Orion Model 420A pH meter.

The photoreduction from Fe^{III} to Fe^{II} was performed in N_2-saturated solutions with bandgap ($h\nu > 3.2$ eV) excitation of TiO_2. Bandgap excitation generates electron-hole pairs in the TiO_2 nanocrystallites. The conduction band electrons can reduce Fe^{III} to Fe^{II} and the valence-band hole can oxidize solvent or ions. If photolysis is continued after all the hemes are reduced, electrons in TiO_2 are generated, $TiO_2(e^-)$. The RX pollutants were introduced in the dark after photoreduction.

Electrochemistry/electrocatalysis

Hemin/TiO_2 thin films deposited on transparent FTO electrodes were placed in $NaOH/H_2O$ (pH 8) or acetic acid/H_2O (pH 4) electrolyte in a glass container. The ionic strength was increased to 1.0 M with KCl. The electrolyte was purged with N_2 gas for at least 30 min before the measurements. Cyclic voltammetry was used to measure formal potentials of the molecular catalysts. A BAS model CV-50 W potentiostat was used in a

standard three-electrode arrangement with a Pt gauze counter electrode, a Ag/AgCl reference electrode, and the TiO_2 thin film as the working electrode.

Hemin/TiO_2 thin films deposited onto FTO electrodes were placed in a standard quartz cuvette for the determination of electrocatalysis products. The cuvette was sealed with a rubber septum and then purged with N_2 gas for at least 30 min before applying a potential. A BAS model CV-50 W potentiostat was also used to apply –1.0 V potentials for 4 hours. A N_2 atmosphere was kept throughout the measurements.

Kinetic analysis of organohalide reactivity

A Varian Cary 50 UV-visible spectrophotometer was used to acquire time-resolved spectra for the reaction of heme/TiO_2, heme/$TiO_2(e^-)$, and $TiO_2(e^-)$ with RX. An aliquot of N_2 saturated RX in H_2O was added to heme/TiO_2 thin film immersed in MeOH or an aqueous solution (pH 4 or 8). The disappearance of heme Q-band absorbance at 575 nm and the appearance of hemin Q-band area at 500 nm were analyzed with a first-order kinetic model. Pseudo-first-order kinetic rate constants, $k_{obs,}$ were obtained by fitting to Equation (5a).

$$\ln (\Delta A/A_0) = -k_{obs}\, t \qquad (5a)$$

where ΔA = initial absorption – absorption at time equal to t, and A_0 is the initial absorption.

Gas chromatography mass spectrometry

The products formed by electrocatalysis and photocatalysis at pH 8 aqueous solutions were analyzed by a Shimadzu GC17A/QP5050A GC/MS (Shimadzu Columbia, MD). The GC17A is equipped with a low polarity (5% phenyl-, 95% methyl-siloxane) capillary J & W DB5-MS column (30 m length, 0.25 mm ID, 0.25 μm film thickness). The products were extracted from the aqueous solution with pentane. Typically a ~2 mL aliquot of pentane was added to ~ 10 mL of RX reaction mixture. The solutions were mixed manually and allowed to separate. A syringe was used to extract the upper pentane layer and transfer it to a 2 mL GC/MS vial. The reaction mixture was injected into the autosampler of the GC/MS. The injector temperature was 220 °C and the transfer interface was at 280 °C. The split ratio was 10 and the H_2 gas column flow rate was kept at 1.0 mL/min. An EI quadrupole based mass spectrometer served as the detector with a scan range of 40-900 amu and an ionizing electron energy of 70 eV. For CCl_4, the oven temperature was ramped from 40 °C, held for 10 min, to 80 °C at a rate of 7.2 °C/min. The pressure program was 1.0 kPa, ramp 2.7 kPa/min to 16 kPa, and held for 5 min. For propachlor, the oven temperature was ramped from 40 °C, held for 2 min, to 170 °C at a rate of 7.3 °C/min. The pressure program was 48.9 kPa, ramp 3 kPa/min to 99 kPa, and held for 5 min.

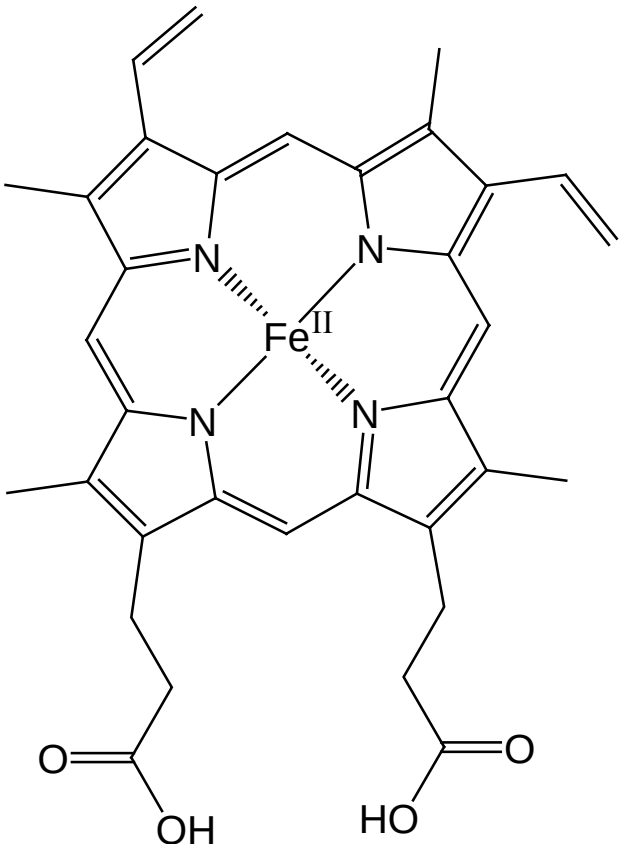

Figure 5-1. Iron (II) protoporphyrin IX (heme)

5.3 Results

Hemin/TiO_2 adsorption isotherms

Mesoporous nanocrystalline TiO_2 thin films were prepared by a sol-gel technique that has been previously described (Heimer *et al*., 1996). The films were comprised at anatase nanocrystallites (~ 15 nm diameter) interconnected in a mesoporous film approximately ~10 μm thick. The BET surface area was 120 ± 10 m^2/g and the pore volume was 0.5 ± 0.1 cc/g for similarly prepared TiO_2 (Barbe *et. al.*, 1997). Hemin (iron(III) protoporphyrin IX chloride) dissolved in DMSO was found to bind to the TiO_2 surface. Adsorption isotherms were constructed at 25 °C (Fig. 5-2). The concentration of hemin anchored to TiO_2 was determined spectroscopically with Beer's Law. UV-visible absorption spectra of the hemin/TiO_2 and hemin in DMSO were within experimental error the same. Hemes (Fe^{II}) have an intense Soret band ~400 nm and lower energy Q-bands between 450 – 650 nm, Fig. 5-3 (Tieman *et al.,*1990; Larson and Cervini-Silva 2000).

The equilibrium binding was found to follow the Langmuir adsorption isotherm model, Equation 5b.

$$\theta = K[A] / (1 + K[A]) \qquad (5b)$$

where θ is the fractional surface coverage, [A] is the hemin concentration, and K is the equilibrium constant. At hemin concentrations over ~15 μM, the surface coverage was found to saturate, θ = 1. For a 1 cm^2 geometric area, this corresponded to a surface

coverage of ~ 10^{-8} moles, and approximately 500 hemes per particle. Double reciprocal plots, Equation 5c, allowed the equilibrium binding constants to be determined, K = 1 x 10^5 M^{-1} (Fig. 5-2 inset).

$$1/\theta = 1 + 1/K[A] \qquad (5c)$$

Hemin/TiO_2 thin films were stable with no desorption for periods of days in MeOH or pH 4 and 8 aqueous solutions. Iron(III) *meso*-tetraphenyl porphyrin chloride, which lacks the carboxylic acid functional groups, did not bind to TiO_2 surfaces under the same conditions.

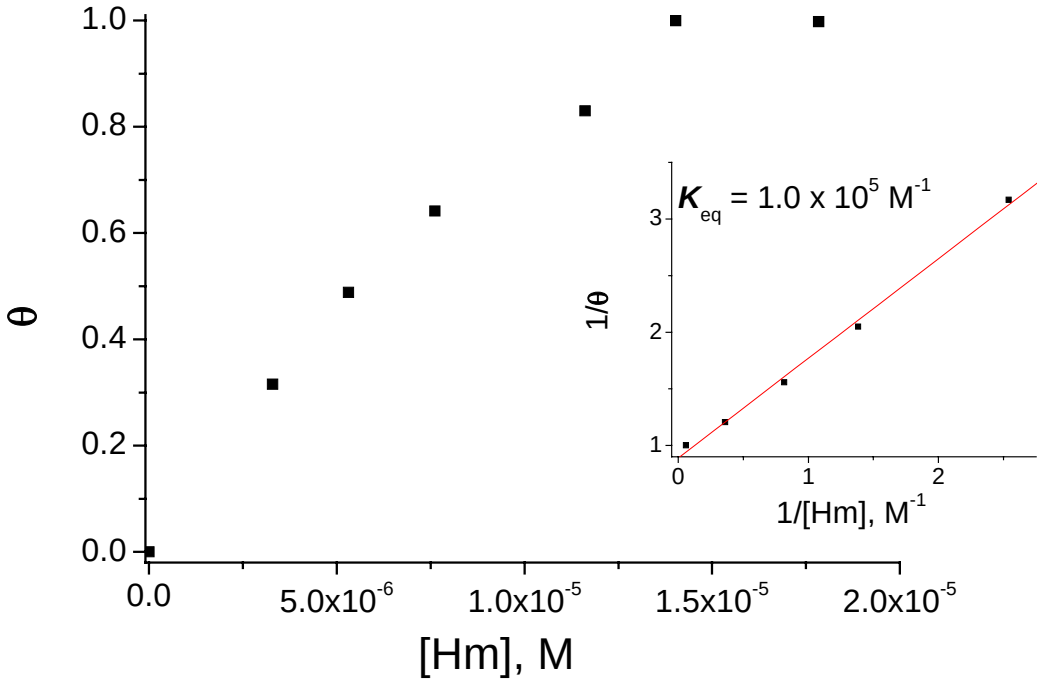

Figure 5-2. Equilibrium binding of hemin to nanocrystalline TiO_2 thin films in DMSO at room temperature, where θ in the fractional surface coverage. The inset shows a double-reciprocal plot of the data from which an equilibrium constant was abstracted, K = 1 x 10^5 M^{-1}.

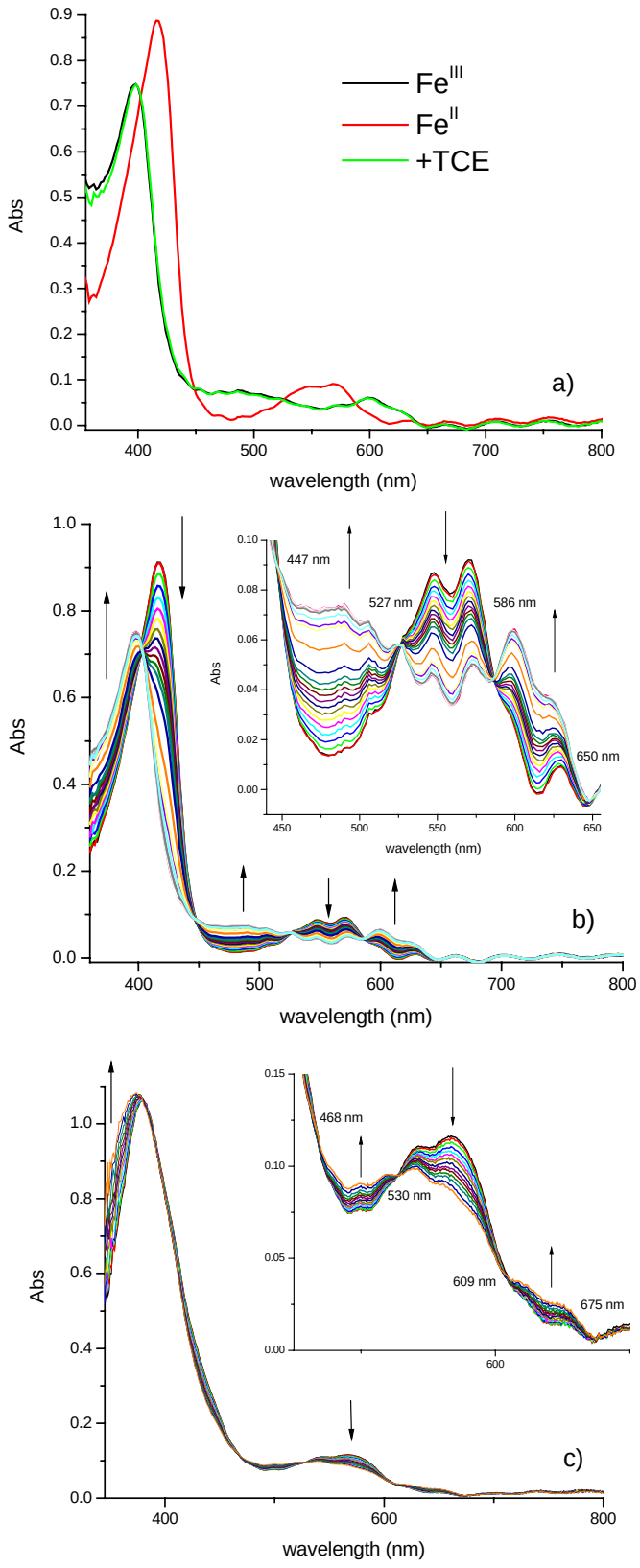

Figure 5-3. a) UV-visible absorbance spectrum of hemin/TiO_2 (—), heme/TiO_2 (—), and the final product after addition of TCE (—) in MeOH. b) The spectral changes observed after addition of 1.6 x 10^{-4} M TCE to heme/TiO_2 in MeOH and c) pH 4 aqueous solution. The arrows show the direction of absorption change after TCE addition.

Electrochemical measurements of hemin/TiO_2 in aqueous solutions

Formal $Fe^{III/II}$ reduction potentials (E°) of hemin/TiO_2 was estimated in $NaOH/H_2O$ (pH 8) and KNO_3/H_2O (pH 4) electrolyte by cyclic voltammetry. As the applied potential was ramped from 0.0 V to –1.2 V *vs.* Ag/AgCl at scan rates of 1-20 mV/s, two waves were observed, the first was assigned to $Fe^{III} \rightarrow Fe^{II}$ reduction and the second was due to TiO_2 reduction. Upon reversing the potential scan, the oxidation of TiO_2 and of Fe^{II} was observed. The $Fe^{III/II}$ redox chemistry is termed quasi-reversible as the peak-to-peak separation was > 60 mV and the peak oxidation current was typically less than the reduction (Bard and Faulkner 2001). The half-wave potentials were taken as the formal reduction potential, $E°(Fe^{III/II})$, and were -340 mV and –600 mV *vs.* Ag/AgCl in pH 4 and 8, respectively. Cyclic voltammetry measurements were also made in 0.1 M TBAH/MeOH electrolyte. However, the TiO_2 and $Fe^{III} \rightarrow Fe^{II}$ reductions were badly overlapped at all scan rates. From this data, we concluded that the $E°(Fe^{III/II})$ was more negative in methanol than in water.

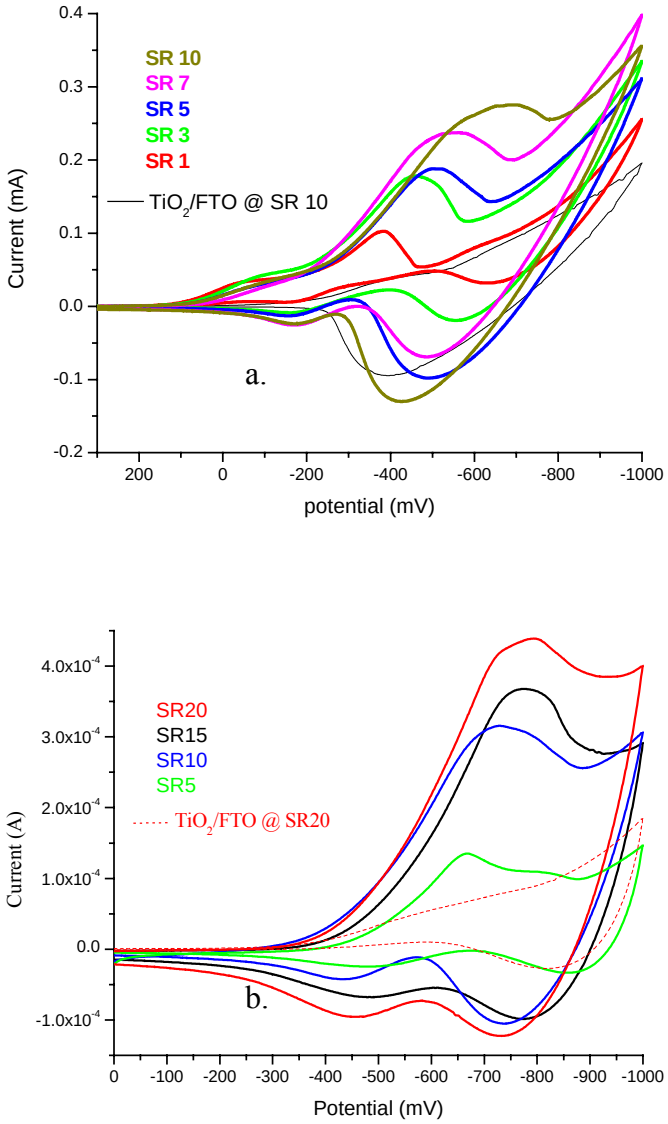

Figure 5-4. Cyclic voltammetry of hemin/TiO_2 in aqueous solution in a) pH 4 KNO_3/H_2O and b) pH 8 $NaOH/H_2O$ electrolytes. The half-wave potentials were taken as the formal reduction potentials, and were estimated to be –340 mV and –600 mV vs. Ag/AgCl in pH 4 and 8, respectively.

Reaction of heme/TiO_2 with organohalides

Hemin (Fe^{III}) was photoreduced to heme (Fe^{II}) with bandgap illumination ($\lambda <$ 370 nm) in N_2 saturated methanol or in pH 4 or 8 acetate aqueous solution (Linsebigler *et al.*,1995; Hoffman *et al.*,1995). Valence band holes are known to react with MeOH (Kawai and Sakata 1980; Tamaki *et al.*, 2006) or carboxylate (Hoffman *et al.*, 1994) that serve as sacrificial donors. The heme and hemin Soret and lower energy absorption bands were well separated in MeOH (Fig. 5-3a and b). However, broadened and overlapped absorption bands were observed in aqueous solutions (Fig. 5-3c). When hemin (Fe^{III}) was reduced to heme (Fe^{II}) a red shift of the Soret band and an absorption increase ~ 570 nm were observed in both MeOH and aqueous solutions. The anaerobic dark addition of N_2 saturated RX/MeOH (or RX/H_2O) stock solutions resulted in oxidation of heme/TiO_2 to that of hemin/TiO_2 (Fig. 5-3a). The heme/TiO_2 to hemin/TiO_2 conversion shows isosbestic points at λ_{iso} = 408, 447, 527, 586, and 650 nm in MeOH (Fig. 5-3b) and λ_{iso} = 468, 530, 609, and 675 nm in aqueous solutions (Fig. 5-3c).

The loss of heme/TiO_2 and the concurrent formation of hemin/TiO_2 were found to be exponential (Fig. 5-5a). The surface concentrations were calculated spectroscopically by standard addition of the heme/TiO_2 and hemin/TiO_2 absorbance spectra at each observation time. Observed rate constants (k_{obs}) were abstracted from the absorption changes for the disappearance of heme/TiO_2 and the appearance of hemin/TiO_2. Figure 5-6 shows a plot of k_{obs} *vs.* [heme] for the reaction of $[CCl_4] = 4.5 \times 10^{-4}$ M at pH 8 acetate solution. The reactions were found to be first-order in heme at low surface coverages ($< 4 \times 10^{-9}$ mole/cm^2). Similar results were observed with 1×10^{-2} M $CHCl_3$ and 1.7×10^{-4} M TCE.

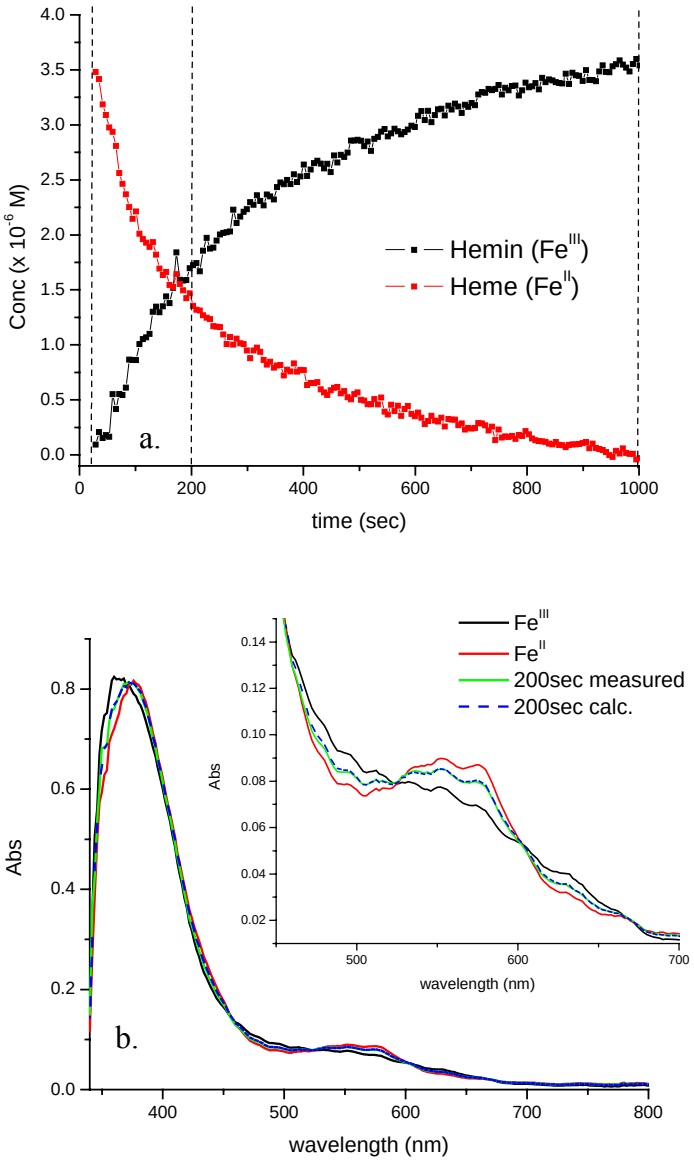

Figure 5-5. a) Plots of heme/TiO_2 (-●-) and hemin/ TiO_2 (—) surface concentrations after the addition of 2.9 x 10^{-4} M CCl_4 in pH 8 aqueous solution. The surface concentrations were determined by standard addition of the observed spectra for 350 – 800 nm. b) Experimental and calculated data are shown before the addition of CCl_4 (Fe^{II}), 200 sec after the addition of CCl_4, and after the reaction was complete (Fe^{III}). The times these spectra were recorded are indicated with arrows in a). The Q-band region is expanded in the inset of b).

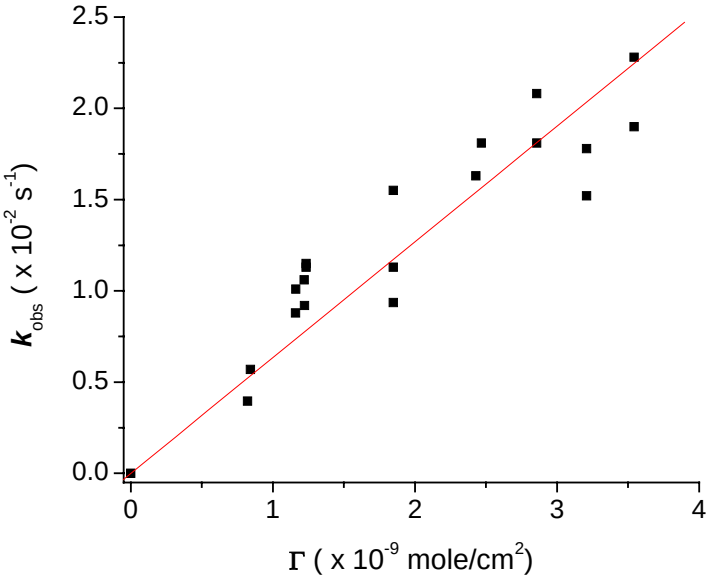

Figure 5-6. The observed rate constant for reduction of 4.5 x10^{-4} M CCl_4 in pH 8 aqueous solution as a function of the heme surface coverage.

Second-order rate constants were determined from plots of k_{obs} vs. [RX] for each organohalide at the same heme surface coverage, 4 x 10^{-9} mole/cm^2 (Fig. 5-7). Propachlor and TCE concentrations were low in aqueous solutions due to their limited solubility (Fig. 5-7b). Second-order rate constants increased in order of CCl_4 ≥ propachlor > $CHCl_3$ > TCE in MeOH, and CCl_4 > propachlor > TCE > $CHCl_3$ in both pH 4 and 8 (Table 5-1). The reactions were faster in MeOH compared to aqueous solutions with the exception of CCl_4 that had similar rate constants in both media.

The durability of heme/TiO_2 thin films was tested by repeatedly using the same film in the reaction with 2.9 x 10^{-4} M CCl_4 at pH 8. After each RX reaction, the hemin/TiO_2 film was washed with H_2O and then pH 8 acetate solution before the anaerobic photo-reduction back to heme/TiO_2 and addition of CCl_4. After the first cycle, the k_{obs} decreased by ~1/3 but remained the same within an experimental error for the next 27 cycles. The k_{obs} values slowly decreased between the 28th and 30th cycles. After 31 cycles of washing, photo-reduction, and CCl_4 reactions, the material was no longer redox active.

Table 5-1. Second-order rate constants for reduction of organohalides reactions by heme/TiO_2 at room temperature [a].

RX	$\boldsymbol{k}$ ($M^{-1}s^{-1}$) MeOH	$\boldsymbol{k}$ ($M^{-1}s^{-1}$) pH 4	$\boldsymbol{k}$ ($M^{-1}s^{-1}$) pH 8
CCl_4	64 ± 2	14.1 ± 0.7	69 ± 3
$CHCl_3$	18.7 ± 0.5	0.63 ± 0.03	1.33 ± 0.07
Propachlor	61 ± 3	9.8 ± 0.5	9.9 ± 0.6
TCE	9.8 ± 0.6	8.3 ± 0.6	3.8 ± 0.2

[a] All experiments were performed with a heme surface coverage of 4 x 10^{-9} mole/cm^2.

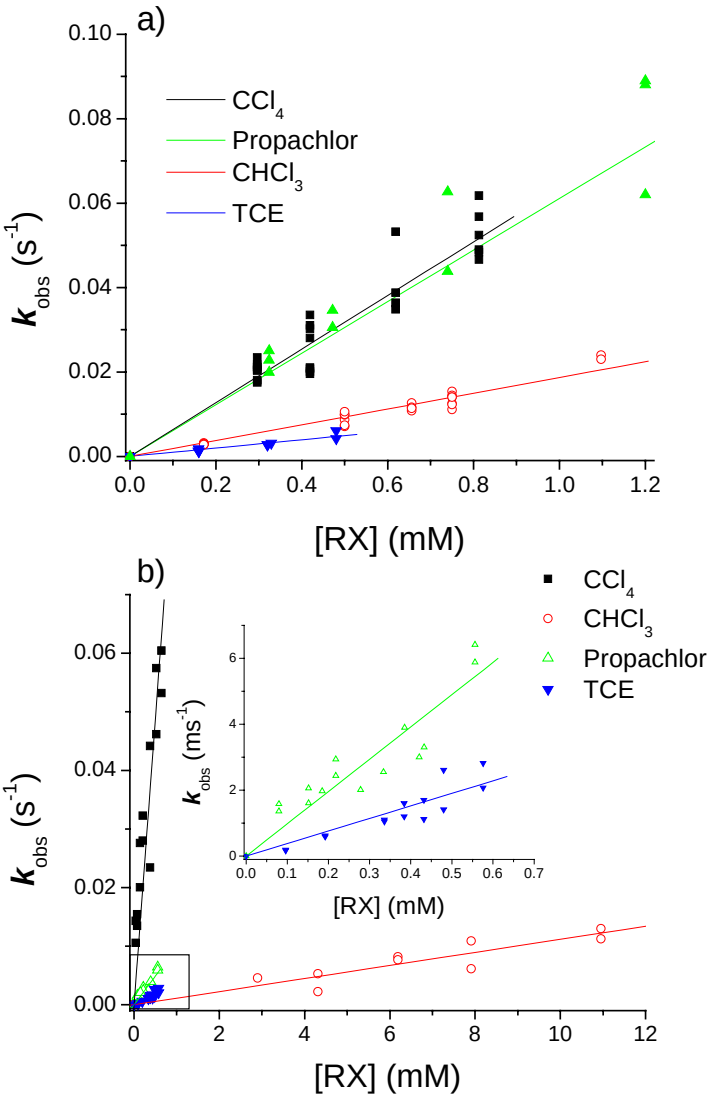

Figure 5-7. Plots of the observed rate constants vs the indicated RX concentration in a) MeOH and b) in pH 8 acetate aqueous solution. The inset of b) shows and expanded plot for propachlor and TCE.

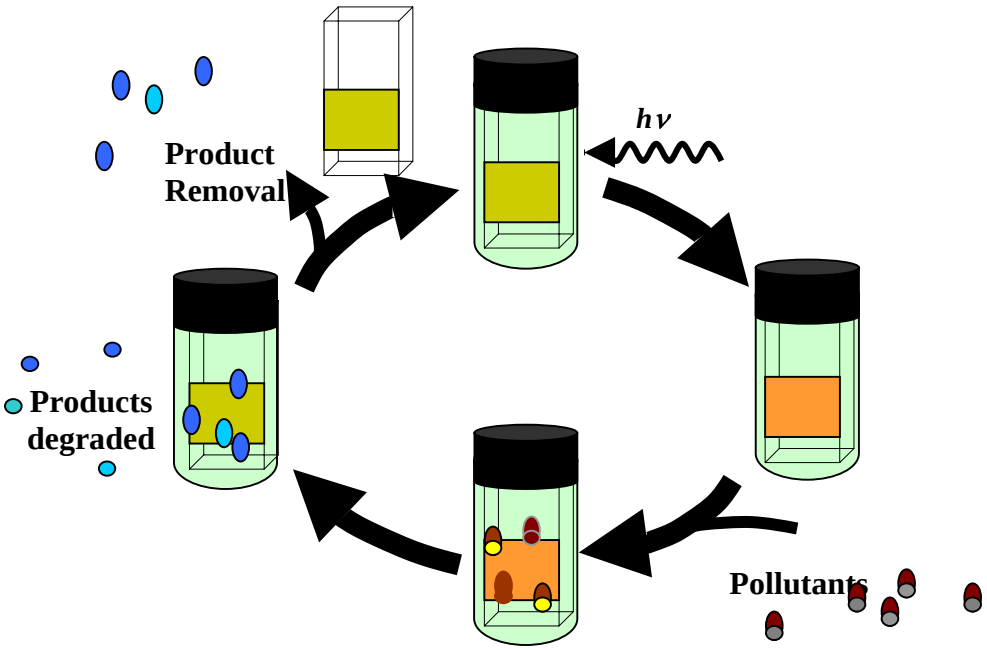

Figure 5-8. The durability of heme/TiO_2 thin films was determined with 2.9 x 10^{-4} M CCl_4 at pH 8. After 31 cycles of washing, photoreduction, and CCl_4 reactions, the material was no longer redox active.

Organohalide reaction with heme/$TiO_2(e^-)$ and with $TiO_2(e^-)$ alone

Bandgap irradiation of TiO_2 thin films in MeOH or acetate aqueous solution resulted in the appearance of the well-known UV-visible absorption spectrum of TiO_2 electrons, $TiO_2(e^-)$, Fig. 5-9a (Fitzmaurice 1994; Rothenberger *et al.*,1992; Hirakawa and Kamat 2005). Similarly, bandgap irradiation of hemin/TiO_2 yielded first the spectrum of heme/TiO_2 and with continued photolysis, the absorption of $TiO_2(e^-)$ throughout the visible and into the infrared region (Fig. 5-9b). Heme/$TiO_2(e^-)$ thin films were stable for at least 3 days. No photodegradation or desorption of heme was observed for 1 hr of photolysis.

The visible absorption spectra of $TiO_2(e^-)$, Fe^{II}, and Fe^{III} allowed their concentrations to be quantified spectroscopically after the addition of RX. Experiments were performed for CCl_4, propachlor, and TCE in pH = 4 and 8 aqueous solutions. Typical data is shown in Fig. 5-9b inset for heme/$TiO_2(e^-)$ reduction of 1.4×10^{-4} M CCl_4. In all cases, it was found that the $TiO_2(e^-)$ concentration decreased to near zero in the presence of heme, followed by the oxidation of Fe^{II} to Fe^{III}.

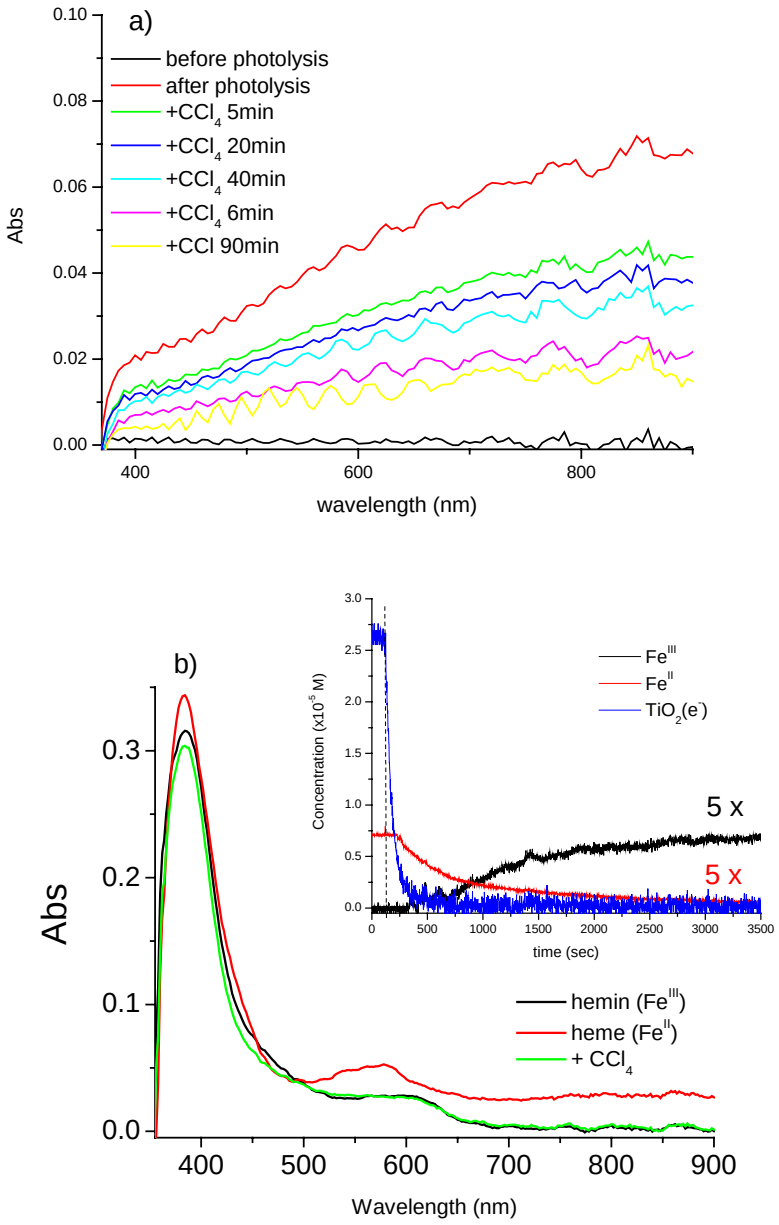

Figure 5-9. a) The UV-visible absorption spectra observed after bandgap excitation of a TiO_2 thin film immersed in pH 4 H_2O. b) UV-visible absorption spectrum of (—) hemin/TiO_2, the spectrum after ultra band gap illumination assigned to (—) heme/$TiO_2(e^-)$, and the final spectrum (—) after addition of CCl_4 into the external pH 4 solution. The final CCl_4 concentration was 1.4 x 10^{-4} M. The inset shows time-resolved concentration observed after the addition of CCl_4. The arrow indicates the time of CCl_4 injection (120 s).

Exposure of $TiO_2(e^-)$ without heme to CCl_4, $CHCl_3$, and propachlor resulted in the slow and incomplete loss of $TiO_2(e^-)$. The observed rate constants for CCl_4 in pH 8 aqueous solution increased linearly with the $TiO_2(e^-)$ concentration (Fig. 5-10c). The reaction was first-order in $TiO_2(e^-)$. On the other hand, the presence of heme on the surface had a profound effect on the reactivity. Heme/$TiO_2(e^-)$ reacted 20 times faster with CCl_4 (Fig. 5-10a and b) and 10 times faster with propachlor than did $TiO_2(e^-)$ under the same conditions. The concentration of $TiO_2(e^-)$ was controlled with irradiation time and calculated by the extinction coefficient, $\varepsilon_{TiO2(e-)}$ at 800 nm = 1,300 $M^{-1}cm^{-1}$ (Kay *et al*., 1994).

Addition of TCE into the pH 8 external solution of $TiO_2(e^-)$ showed no evidence for TCE reduction as the $TiO_2(e^-)$ absorbance remained unchanged. However, a rapid decrease in the concentration of TiO_2 electrons (k_{obs} = 1.0 x 10^{-3} s^{-1}) was observed with heme/$TiO_2(e^-)$ after TCE addition under the same conditions (Fig. 5-11b). Once most of TiO_2 electrons were consumed, heme/TiO_2 was oxidized to hemin/TiO_2, with an observed rate constant of k_{obs} = 1.1 x 10^{-3} s^{-1}. If one assumes that all the redox reactivity of TCE was heme mediated, a turnover for heme can be calculated by Equation (5d).

$$N = [\text{ heme} + TiO_2(e^-)] / \text{heme} \qquad (5d)$$

The highest turnover number measured was 82 with 2.36 x 10^{-7} moles heme and 1.92 x 10^{-5} moles $TiO_2(e^-)$ at pH 8. The assumption that heme mediates TCE reduction was based on the observation that $TiO_2(e^-)$ do not react with TCE under these same conditions.

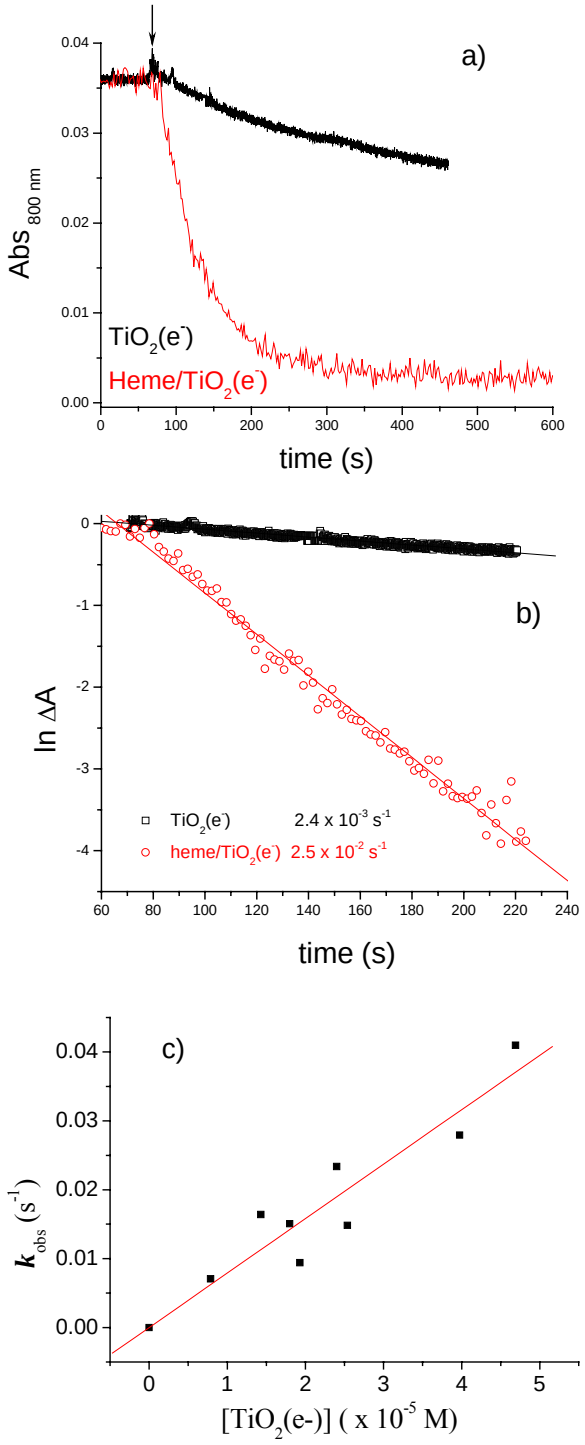

Figure 5-10. a) The absorption at 800 nm of a $TiO_2(e^-)$ and a heme/$TiO_2(e^-)$ thin film recorded as a function of time. The arrow indicates the time at which CCl_4 was injected (60 s) into the external pH 8 aqueous solution. The CCl_4 concentration was 4.5 x10^{-4} M. b) Natural log plots of the data in a) from which observed rate constants were abstracted, k_{obs} = 2.4 x 10^{-3} s^{-1} for $TiO_2(e^-)$ and k_{obs} = 2.5 x 10^{-2} s^{-1} for heme/$TiO_2(e^-)$. c) Plot of the observed rate constants for CCl_4 reduction as a function of $TiO_2(e^-)$.

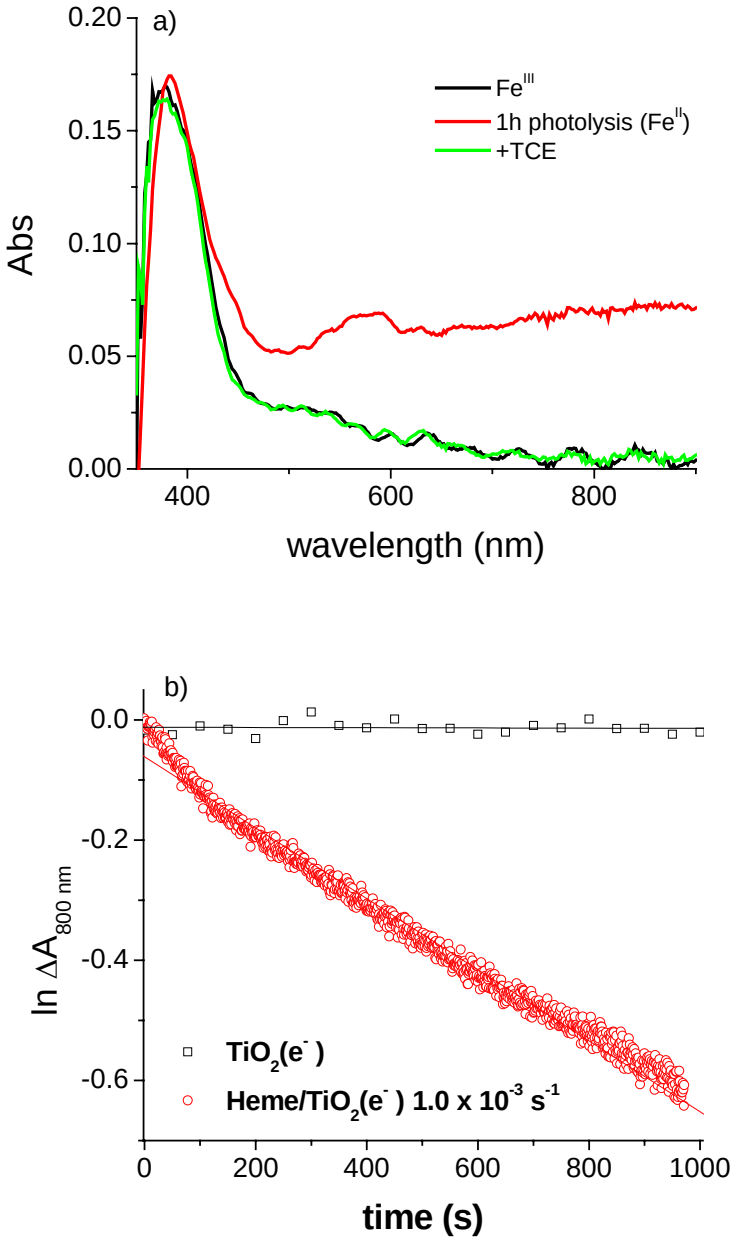

Figure 5-11. a) The UV-vis absorption spectrum of hemin/TiO_2 (—), the spectrum after ultra band gap illumination assigned to heme/$TiO_2(e^-)$ (—), and the final spectrum (—) after addition of TCE into the external pH 8 aqueous solution. The final TCE concentration was 2.5 x 10^{-4} M. b) Natural log plots of data from reactions of $TiO_2(e^-)$ (□) and heme/$TiO_2(e^-)$ (o). $TiO_2(e^-)$ shows no reactivity with TCE. The reaction of heme/$TiO_2(e^-)$ with TCE from which an observed rate constant was abstracted, k_{obs} = 1.0 x 10^{-3} s^{-1}.

Products analysis by GC/MS

The products of CCl_4 and propachlor reduction by heme/$TiO_2(e^-)$ in aqueous pH 8 solution were analyzed by GC/MS. Electrocatalysis was initially performed at an applied potential of -1.0 V (*vs*. Ag/AgCl). This potential reduced all hemin to heme and established a $TiO_2(e^-)$ concentration of 1.9×10^{-5} M. The RX of interest was then added to the external electrolyte and the potential was applied for 4 hours. The products from dark reactions of photochemically generated heme/$TiO_2(e^-)$ with RX, like those described for Fig. 5-9 and Fig. 5-10, were also analyzed. Control experiments performed with FTO electrodes without heme or TiO_2 showed no dechlorinated products. In all cases, the aqueous solutions were extracted with pentane as described in the experimental section.

Propachlor (m/z 211; Retention time 20.5 min): The major product of electrocatalysis was deschloropropachor that appeared at a retention time (RT) of 17 min. The formation of this product as a function of electrocatalysis time was determined by analyzing an aliquot of the reaction mixture every 20 min. Deschloropropachlor (*m/z* 177) was the only product observed in the first 200 min. This product was also found in heme/$TiO_2(e^-)$ reactions prepared by bandgap excitation.

CCl_4 (m/z-Cl 117; Retention time 4.1 min): The major product of electrocatalysis was $CHCl_3$ (*m/z* 118) at RT = 3.5 min. Identification was confirmed by independent analysis of $CHCl_3$/pentane. $CHCl_3$ was also the main product from heme/$TiO_2(e^-)$ reactions prepared by bandgap excitation.

5.4 Discussion

Heme catalysts were found to bind to anatase TiO_2 nanocrystallites interconnected in mesoporous thin films. Adsorption isotherms were well described by the Langmuir model from which equilibrium constants of $K = 10^5\ M^{-1}$ and saturation surface coverages of $\Gamma_{max} = 1.0 \times 10^{-8}$ mol/cm^2 were abstracted. Although the error is somewhat large, we estimate that about 500-1000 hemes are anchored to each 15 nm anatase nanoparticle (Hoertz *et al.,* 2002) at saturation surface coverages. The data reported herein was performed at about 1/5 saturation surface coverage or 150 hemes per particle. Although the nature of the hemin and heme binding to TiO_2 remain unknown, it almost certainly involves the carboxylic acid groups, Figure 1-1. In this regard we found no evidence for surface binding with an iron porphyrin that did not contain carboxylic acid functional groups, iron(III) *meso*-tetraphenyl porphyrin chloride.

Hemes were chosen as catalysts as they are known to react with a wide variety of organohalides in natural and synthetic systems. Indeed, reductive dehalogenation with heme porphyrins have been studied in a considerable detail (Brault 1985; Chiu and Reinhard 1995; Gantzer and Wackett 1991; Larson and Cervini-Silva 2000). The ability of many micro-organisms to dehalogenate pollutants is often linked to heme biochemistry in cytochrome P450 or in other heme containing proteins (Castro *et al.,*1985; Dawson and Sono 1987; Guengerich and Macdonald 1984). Heme modified electrodes have also been characterized for environmental remediation (Nassar *et al.,*1995).

Titanium dioxide (TiO_2) has also received much attention for the treatment of organohalide pollutants in water (Karches *et al.,* 2002; Mora-Sero *et al.,* 2005; Choi and

Hoffmann 1995). The anatase form of TiO_2 has a bandgap of 3.2 eV and is perhaps the most well studied semiconductor photocatalyst for environmental remediation (Pozzo *et al.,* 2002; Hoffmann *et al.,*1995). Ultraviolet excitation of TiO_2 can initiate both reductive and oxidiative dehalogenation reactions. A broad distribution of reaction products with little selectivity are often observed, even under tightly controlled laboratory conditions (Alonso *et al.,* 2002; Adewuyi 2005). It was therefore anticipated that functionalizing the TiO_2 surface with hemes would improve the selectivity and reactivity of the semiconductor material.

The formal $Fe^{III/II}$ reduction potential for the hemes anchored to TiO_2 were measured by cyclic voltammetry in aqueous electrolyte. A quasi-reversible wave was observed prior to TiO_2 reduction that was reasonably assigned to $Fe^{III/II}$ redox chemistry. The half-wave potential measured was taken as an estimation of the formal $Fe^{III/II}$ reduction potentials that shifted -260 mV from pH 4 to 8. Similar shifts with pH have been reported at hemoglobin modified electrodes (Chen *et al.*, 1999), functionalized TiO_2 (Zaban *et al.,*1997) and cytochrome oxidase (Blair *et al.,*1986). The observed behavior reported here is consistent with proton coupled electron transfer, Equation 5e, where P is the porphyrin ring.

$$PFe^{III}\text{-}OH + e^- + H^+ \rightarrow PFe^{II}\text{-}OH_2 \qquad (5e)$$

In methanol electrolytes we found that the direct reduction and re-oxidation of TiO_2 obscured this molecular redox process. The negative and gradual onset of the TiO_2

reduction in methanol electrolyte suggests that heme/TiO_2 is a stronger reductant in methanol than in water at the pH values investigated.

The dark addition of organohalides pollutants after the photoreduction of hemin/TiO_2 to heme/TiO_2 was performed to prevent secondary photochemical reactions that could have complicated analysis. The TiO_2 thin films are transparent in the visible and near infra-red regions which allow the $Fe^{III/II}$ and $TiO_2(e^-)$ redox chemistry to be characterized spectroscopically in a transmission mode with excellent signal-to-noise ratios. Below we present the results of mechanistic studies beginning first with heme/TiO_2 and concluding with materials where additional TiO_2 electrons were introduced with light or applied potentials.

Heme/TiO_2 and RX Reactions.

A rate law for the reactions was determined by independently varying the organohalide concentrations and the heme surface coverage and measuring the observed rates, Equation 5f.

$$r = k\,[RX]^1\,[heme]^1 \qquad (5f)$$

The reactions were first-order in heme and in organohalide concentration. The same rate law was previously determined for related hemes and organohalides in homogeneous solution (Wade and Castro 1973). The second-order rate constants for heme/TiO_2 with CCl_4 and $CHCl_3$ increased in the order of MeOH ≥ pH 8 > pH 4, when the heme surface coverage was 4×10^{-9} mole/cm^2. This trend follows the expected shift in the heme $Fe^{III/II}$

formal reduction potential and is consistent with faster reactions at larger driving forces (Obare *et al.,* 2005). In addition, consistent with one electron reduction potentials, $E^o(CCl_4^{0/-})$ = +85 mV and $E^o(CHCl_3^{0/-})$ = –145 mV *vs*. NHE (Totten and Roberts 2001), the reactions with CCl_4 were consistently faster than those with $CHCl_3$.

In the case of propachlor reduction, the rate constants were within an experimental error the same at both pH 4 and 8, 9.8 ± 0.5 $M^{-1}s^{-1}$ and 9.9 ± 0.6 $M^{-1}s^{-1}$. Similar pH independent results have been previously reported for the hydrolysis of chloroacetamide herbicides in water (Liu *et al.*, 2001). For example, the alachlor hydrolysis rate constants were 3.6 x 10^{-2} and 3.2 x 10^{-2} d^{-1} at pH 5 and 8 respectively (Sharma 2002). The redox mechanism from heme/TiO_2 to propachlor are not fully understood but the lack of a pH dependence, where one would be anticipated, suggest a composite mechanism where electron transfer is not rate limiting.

The second-order rate constant for heme/TiO_2 with TCE *decreased* from 8.3 ± 0.6 $M^{-1}s^{-1}$ at pH 4 to 3.8 ± 0.2 $M^{-1}s^{-1}$ at pH 8. Similar pH dependence was previously reported for the reaction of TCE with Fe supported in slag (Kang *et al.,* 2006). In the reaction of TCE with super-reduced corrinoids, the reaction products were also pH dependent (Glod *et al.,*1997). Acetylene was favored at higher pH and dichloroethylene at lower pH. Such competing reaction pathways in homogenous solution may also exist at TiO_2 interfaces and further studies with identification of the reaction products will be made in future research.

Heme/$TiO_2(e^-)$ and RX Reactions.

The electrochemical, photochemical, or chemical reduction of TiO_2 is known to generate reducing equivalents in the solid (Hoffmann *et al.*,1995; Linsebigler *et al.*,1995; Fitzmaurice 1994). A blue-black color appears with characteristic spectroscopic properties that is quite stable under anaerobic conditions. A molecular description of these states is lacking and remains somewhat contentious. Literature references that describe this coloration as due to localized Ti(III) states or to free conduction band electrons can be found (Hoffmann *et al.*,1995; Linsebigler *et al.*,1995; Fitzmaurice 1994). Here we refer to them simply as $TiO_2(e^-)$ or if heme is present on the surface, heme/$TiO_2(e^-)$. In methanol we estimate that about 600 electrons can be stored in an individual TiO_2 nanoparticle while in water the value is about a factor of 3 less.

Our initial motivation for studying organohalide reactions with heme/$TiO_2(e^-)$ was that the $TiO_2(e^-)$ would regenerate the Fe(II) state after RX reactions and allow larger concentrations of reaction products to be isolated. Similar approaches have been used in the past wherein excess reductants were added to catalyst/RX solutions to regenerate the catalysts after reactions with RX (Chiu and Reinhard 1995; Larsen and Cervini-Silva 2000; Glod *et al.*, 1997). We find however, that the presence of $TiO_2(e^-)$ does far more than simply regenerate the Fe(II) state of the heme. In fact, it appears that the materials are capable of multi-electron transfer reaction mechanisms not available to the hemes (Obare e*t al*., 2006).

For example, the observed rate constant for CCl_4 reduction was about 20 times faster for heme/$TiO_2(e^-)$ than it was for $TiO_2(e^-)$, $k_{obs} = 5.0 \times 10^{-2}$ s^{-1} and $k_{obs} = 2.4 \times 10^{-3}$ s^{-1}. Furthermore, at this CCl_4 concentration the observed rate for heme/TiO_2 in the

absence of excess electrons was k_{obs} = 3.2 x 10^{-2} s^{-1}. For aqueous reactions with TCE, no reactivity was observed over several hours with $TiO_2(e^-)$ but the reactions with heme/$TiO_2(e^-)$ were quite rapid, k_{obs}= 1.0 x 10^{-3} s^{-1}. This is somewhat surprising from a thermodynamic point of view as it is clear that the $TiO_2(e^-)$ are more potent reductants than are hemes under all conditions examined.

An advantage of the heme/$TiO_2(e^-)$ and RX reactions is that the concentrations of heme, hemin, and $TiO_2(e^-)$ can be quantified spectroscopically. This provides some insights into the mechanism for RX dechlorination. In all cases, the same general behavior was observed: the concentration of $TiO_2(e^-)$ decreased until near zero at which time the oxidation of heme to hemin was observed. The rate constants for the disappearance of heme and the formation of hemin were within experimental error the same. This behavior is consistent with at least two separate mechanisms. One we call the "stepwise mechanism" in which the $TiO_2(e^-)$ reacted first followed by the hemes. The second is termed the "mediated mechanism" wherein all the reactivity occurred through the hemes.

Stepwise Mechanism:

i) $\text{Heme/TiO}_2(ne^-) + RX \rightarrow \text{Heme/TiO}_2((n-1)e^-) + RX^{\bullet-}$

ii) $\text{Heme/TiO}_2(ne^-) + RX \rightarrow \text{Heme/TiO}_2 + RX^{\bullet-}$

iii) $\text{Heme/TiO}_2 + RX \rightarrow \text{Hemin/TiO}_2 + RX^{\bullet-}$

Mediated Mechanism:

i) $\text{Heme/TiO}_2(ne^-) + RX \rightarrow \text{Hemin/TiO}_2(ne^-) + RX^{\bullet-}$
Slow

ii) $Hemin/TiO_2(ne^-) \rightarrow Heme/TiO_2((n-1)e^-)$
Fast

iii) $Heme/TiO_2 + RX \rightarrow Hemin/TiO_2 + RX^{\bullet -}$

The mediated mechanism requires that regeneration of heme be rapid relative to RX reduction such that hemin is not observed until all the $TiO_2(e^-)$ have reacted. The stepwise mechanism requires that the $TiO_2(e^-)$ rapidly react with RX. We tend to disfavor this latter mechanism in all cases as RX reactions with $TiO_2(e^-)$ were always sluggish and incomplete or, in the case of TCE, did not occur at all. However, the situation may be more complicated as the presence of hemes on the semiconductor surfaces may alter the reaction rate constants for $TiO_2(e^-)$ even when $Fe^{III/II}$ redox chemistry is not directly involved.

A case where the mediated mechanism appeared to be present was identified in these studies, the reaction of heme/$TiO_2(e^-)$ with TCE at pH 8. No reaction was observed after the addition of TCE to $TiO_2(e^-)$ in the absence of heme under these conditions. Furthermore, the observed rate constant for the loss of the TiO_2 electrons was within experimental error the same as the rate constant for oxidation of heme to hemin, k_{obs}= 1.1 x 10^{-3} s^{-1}. This data is fully consistent with the mediated mechanism described above wherein heme reduction of TCE is the rate determining step. It is noteworthy that electron transfer from $TiO_2(e^-)$ to hemin never became rate limiting as has been previously suggested for outer-sphere mediators (Larsen and Cervini-Silva 2000; Glod e*t al*., 1997). Therefore, binding catalysts to the electron source (i.e. $TiO_2(e^-)$) provided more favorable electron transfer kinetics. Further studies are required to unambiguously identify the mechanisms for chloroform, propachlor and carbon tetrachloride reduction.

A product was identified after aqueous propachlor and CCl_4 reduction by both electrocatalysis and photocatalysis. Propachlor reduction yielded deschloropropachlor, Reaction 5g.

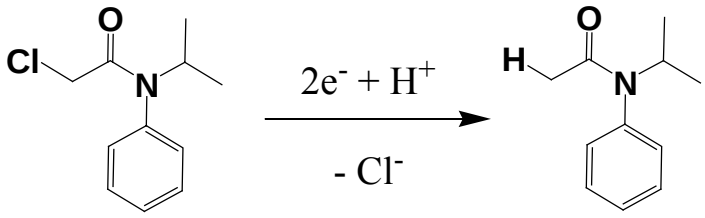

(5g)

The reduction of CCl_4 yielded $CHCl_3$, Reaction 4h. A dissociative electron transfer pathway for the aerobic reduction of CCl_4 has previously been established (Pause *et al.*, 2000; Chiu and Reinhard 1995; Kriegman-King and Reinhard 1992).

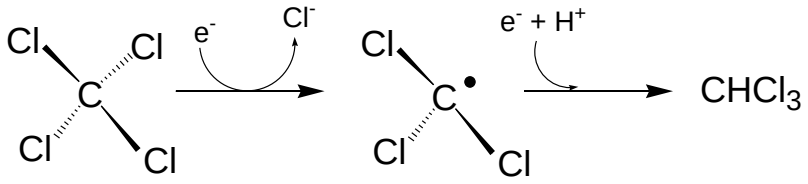

(5h)

Both reactions pathways 5g and 5h require reduction by two electrons or dissociative electron transfer followed by protonation. The two electron transfer reduction potentials of CCl_4 and TCE are favored by 500 mV over the one electron reduction (Totten and Roberts 2001). Further studies are underway to identify these mechanistic steps and include them in more detailed modeling of this interesting interfacial reactivity.

5.5 Conclusions

Heme (iron(II) protoporphyrin IX) bound to mesoporous nanocrystalline (anatase) TiO_2 thin films, heme/TiO_2, showed enhanced reactivity with CCl_4, $CHCl_3$, propachlor, and trichloroethylene in MeOH, and pH 4 and 8 aqueous solution. The reactions were found to be first-order in heme/TiO_2 and in organohalide. The heme $Fe^{III/II}$ reduction potential became more negative with increasing pH, behavior attributed to proton coupled electron transfer. The rate constants for reduction of CCl_4 and $CHCl_3$ increased with pH while propachlor and trichloroethylene did not. Reactions of organohalides with excess electrons trapped in TiO_2, $TiO_2(e^-)$, and heme/$TiO_2(e^-)$ were also quantified. Rate constants for the reactions of heme/$TiO_2(e^-)$ with CCl_4, propachlor, and TCE were much larger than those without a surface bound heme catalyst. Rapid and efficient electron transfer from $TiO_2(e^-)$ to hemin was observed under all conditions. Therefore, the strategy of utilizing light and/or applied potential to maintain the active redox state of catalysts anchored to semiconductor surfaces was successful. The synergetic enhancement of the organohalide reactivity was an additional benefit that may be exploited for practical environmental applications.

5.6 Acknowledgments

This work was supported by the National Science Foundation and Collaborative Research Activities for Environmental Molecular Science (CRAEMS) Program. We thank Dr. Phil Mortimer for discussions of the GC-MS product analysis.

5.7 References

ADEWUYI, Y. G. (2005) Sonochemistry in environmental remediation. 2. Heterogeneous sonophotocatalytic oxidation processes for the treatment of pollutants in water. *Environ. Sci. Technol.* **39**, 8557.

ALONSO, F., BELETSKAYA, I. P., and YUS. M. (2002) Metal-mediated reductive hydrodehalogenation of organic halides. *Chem. Rev*. **102**, 4009.

BARBE, C. J., ARENDSE, F., COMTE, P., JIROUSEK, M., LENZMANN, F., SHKLOVER, V., AND GRATZEL, M. (1997) Nanocrystalline titanium oxide electrodes for photovoltaic applications. *J. Am. Ceram. Soc*. **80**, 3157.

BARD, A. J. and FAULKNER, L. R. (2001) *Electrochemical Methods Fundamentals and Applications*. New York: John Wiley & Sons.

BLAIR, D. F., ELLIS, JR. W. R., WANG, H., GRAY, H. B., and CHAN, S. I. (1986) Spectroelectrochemical study of cytochrome *c* oxidase: pH and temperature dependences of the cytochrome potentials. *J. Biol. Chem.* **261**, 11524.

BRAULT, D. (1985) Model studies in cytochrome P-450-mediated toxicity of halogenated compounds: radical processes involving iron porphyrins. *Environ. Health Perspectives* **64,** 53.

BURRIS, D. R., DELCOMYN, C. A., SMITH, M. H., and ROBERTS, L. A. (1996) Reductive dechlorination of tetrachloroethylene and trichloroethylene catalyzed by vitamin B-12 in homogeneous and heterogeneous systems. *Environ. Sci. Technol.* **30**, 3047.

CASTRO., C. E., WADE, R. S., and BELSER, N. O. (1985) Biodehalogenation: reactions of Cytochrome P-450 with polyhalomethanes. *Biochemistry* **24**, 204.

CHEN, X., HU, N., ZENG, Y., RUSLING J. F., and YANG, J. (1999) Ordered electrochemically active films of hemoglobin, didodecyldimethylammonium ions, and clay. *Langmuir* **15**, 7022.

CHIU, P. C. and REINHARD, M. (1995) Metallocoenzyme-mediated reductive transformation of carbon tetrachloride in titanium (III) citrate aqueous solution. *Environ. Sci. Technol*. **29**, 595.

CHOI, W. and HOFFMANN, M. R. (1995) Photoreductive mechanism of CCl_4 degradation on TiO_2 particles and effects of electron donors. *Environ. Sci. Technol*. **29**, 1646.

DAWSON, J. H. and SONO, M. (1987) Cytochrom P-450 and chloroperoxidase: Thlolate-ligated heme enzymes. Spectroscopic determination of their active site structures and mechanistic implications of thlolate ligation. *Chem. Rev*. **87**, 1255.

DURAN, N. and ESPOSITE, E. (2000) Potential applications of oxidative enzymes and phenoloxidase-like compounds in wastewater and soil treatment: a review. *Appl. Catal. B: Environ.* **28**, 83.

EYKHOLT, G. R. and DAVENPORT, D. T. (1998) Dechlorination of the chloroacetanilede herbicides alachlor and metolachlor by iron metal. *Environ. Sci. Technol.* **32**, 1482.

FERNANDEZ-SANCHEZ, J. M., SAWVEL, E. J., and ALVAREZ, P. J. J. (2004) Effect of Fe-0 quantity on the efficiency of integrated microbial-Fe-0 treatment processes. *Chemosphere* **54**, 823.

FITZMAURICE, D. (1994) Using spectroscopy to probe the band energetics of transparent nanocrystalline semiconductor films. *Solar Energy Materials and Solar Cells* **32**, 289.

GANTZER, C. J. and WACKETT, L. P. (1991) Reductive dechlorination catalyzed by bacterial transition-metal coenzymes. *Environ. Sci. Technol.* **25**, 715.

GLOD, G., ANGST, W., HOLLIGER, C., and SCHWARZENBACH, R. P. (1997) Corrinoid-mediated reduction of tetrachloroethene, trichloroethene, and trichlorofluoroethene in homogeneous aqueous solution: reaction kinetics and reaction mechanisms. *Environ. Sci. Technol.* **31**, 253.

GUENGERICH. F. P. and MACDONALD T. L. (1984) Chemical mechanisms of catalysis by cytochromes P-450: A unified view. *Acc. Chem. Res*. **17**, 9.

HEIMER, T.A., D' ARCANGELIS, S. T., FARZAD, F., STIPKALA, J. M., and MEYER, G. J. (1996) An acetylacetonate-based semiconductor-sensitizer linkage. *Inorg. Chem*. **35**, 5319.

HIRAKAWA, T. and KAMAT, P. V. (2005) Charge separation and catalytic activity of $\underline{Ag@TiO_2}$ core-shell composite clusters under UV-irradiation. *J. Am. Chem. Soc*. **127**, 3928.

HOERTZ, P. G., THOMPSON, D. W., FRIEDMAN, L. A., and MEYER, G. J. (2002) Ligand-Localized electron trapping at sensitized semiconductor interfaces. *J. Am. Chem. Soc*. **124**, 9690.

HOFFMAN, A. J., CARRAWAY, E. R., and HOFFMANN, M. R. (1994) Photocatalytic production of H_2O_2 and organic peroxides on quantum-sized semiconductor colloids. *Environ. Sci. Technol*. **28**, 776.

HOFFMAN, M. R., MARTIN, S. T., CHOI, W., and BAHNEMANN, D. W. (1995) Environmental applications of semiconductor photocatalysis. *Chem. Rev*. **95**, 69.

KANG, W., HWANG, I., and PARK, J. (2006) Dechlorination of trichloroethylene by a steel converter slag amended with Fe(II). *Chemosphere* **62**, 285.

KARCHES. M., MORSTEIN, M., ROHR, P. R., POSSO, R. L., GIOMBI, J. L., and BALTANAS, M. A. (2002) Plasma-CVD-coated glass beads as photocatalyst for water contamination. *Catal. Today* **72**, 267.

KAWAI, T. and SAKATA, T. (1980) Photocatalytic hydrogen production from liquid methanol and water. *J. Chem. Soc. Chem. Comm*. 15, 694.

KAY, A., HUMPHRY-BAKER, R., and GRATZEL, M. (1994) Artificial photosynthesis. 2. Investigations on the mechanism of photosensitization of nanocrystalline TiO_2 solar cells by chlorophyll derivatives. *J. Phys. Chem*. **98**, 952.

KRIEGMAN-KING, M. R. and REINHARD, M. (1992) Transformatin of carbon tetrachloride in the presence of sulfide, biotite, and vermicullte. *Environ. Sci. Technol*. **26**, 2198.

LARSON, R. A. and CERVINI-SILVA, J. (2000) Dechlorination of substituted trichloromethanes by an iron(II) porphyrin. *Environ. Toxicol. Chem*. **19**, 543.

LEE, W. and BATCHELOR, B. (2003) Reductive capacity of natural reductants. *Environ. Toxicol. Chem*. **37**, 535.

LINSEBIGLER, A. L., LU, G., and YATE, J. T. (1995) Photocatalysis on TiO_2 surfaces: principles, mechanisms, and selected results. *Chem. Rev*. **95**, 735.

LIU, B., MCCONNELL, L. L., and TORRENTS, A. (2001) Hydrolysis of chlorpyrifos in natural waters of the Chesapeake bay. *Chemosphere*, **44**, 1315.

McGUIRE, M. M., CARLSON, D. L., VIKESLAND, P. J., KOHN, T., GRENIER, A. C., LANGLEY, L. A., ROBERTS, A. L., and FAIRBROTHER, D. H. (2003) Applications of surface analysis in the environmental sciences: dehalogenation of chlorocarbons with zero-valent iron and iron-containing mineral surfaces. *Anal. Chim. Acta*. **496**, 301.

MORA-SERO, I., VILLARREAL, T. L., BISQUERT, J., PITARCH, A., GOMEZ, R., and SALVADOR, P. (2005) Photoelectrochemical behavior of nanostructured TiO_2 thin-

film electrodes in contact with aqueous electrolytes containing dissolved pollutants: a model for distinguishing between direct and indirect interfacial hole transfer from photocurrent measurements. *J. Phys. Chem. B* **109**, 3371.

NASSAR, A. F., BOBBITT, J. M., STUART, J. D., and RUSLING, J. F. (1995) Catalytic reduction of organohalides pollutants by Myoglobin in a biomembrane-like surfactant film. *J. Am. Chem. Soc.* **117**, 10986.

OBARE, S. O., ITO, T., and MEYER, G. J. (2006) Multi-electron transfer from heme-functionalized nanocrystalline TiO_2 to organohalide pollutants. *J. Am. Chem. Soc*. **128**, 712.

OBARE, S. O., ITO, T., and MEYER, G. J. (2005) Controlling reduction potentials of semiconductor-supported molecular catalysts for environmental remediation of organohalide pollutants. *Environ. Sci. Technol*. **39**, 6266.

OBARE, S. O. and MEYER, G. J. (2004) Nanostructured materials for environmental remediation of organic contaminants in water. *J. Environ. Sci. Health A* **39,** 2549.

OBARE, S. O., ITO, T., BALFOUR, M. H., and MEYER, G. J. (2003) Ferrous hemin oxidation by organic halides at nanocrystalline TiO_2 interfaces. *Nano Lett*. **3**, 1151.

PAUSE, L., ROBERT, M., and SAVEANT, J. M. (2000) Reductive cleavage of carbon tetrachloride in a polar solvent. An example of a dissociative electron transfer with significant attractive interaction between the caged product fragments. *J. Am. Chem. Soc.* **122**, 9829.

POZZO, R. L., GIOMBI, J. L., BALTANAS, M. A., and CASSANO, A. E. (2002) Radiation extinction of slurried TiO_2 as a function of mechanical action and ionic composition of the suspending media: a key factor in the photocatalytic efficiency. *Appl. Catal. B. Envion*. **38**, 61.

ROTHENBERGER, G., FITZMAURICE, D., and GRATZEL, M. (1992) Spectroscopy of conduction band electrons in transparent metal oxide semiconductor films: optical determination of the flatband potential of colloidal titanium dioxide films. *J. Phys. Chem*. **96**, 5983.

SATAPANAJARU, T., SHEA, P. J., and COMFORT, S. D. (2003) Green rust and iron oxide formation influences metolachlor dechlorination during zerovalent iron treatment. *Environ. Sci. Technol.* **37**, 5219.

SHARMA, K., K. (2002) Degradation of alachlor in water and tropical soils of India. *Bull. Environ. Contam. Toxicol.* **68**, 394.

SIMMONS, J. E., RICHARDSON, S. D., SPETH, T. F., MILTNER, R. J., RICE, G., SCHENCK, K. M., HUNTER, E. S., and TEUSCHLER, L. K. (2002) Development of a

research strategy for integrated technology-based toxicological and chemical evaluation of complex mixtures of drinking water disinfection by products. *Environ. Health. Perspectives* **110**, 1013.

TAMAKI, Y., FURUBE, A., MURAI, M., HARA, K., KATOH, R., and TACHIYA, M. (2006) Direct observation of reactive trapped holes in TiO_2 undergoing photocatalytic oxidation of adsorbed alcohols: evaluation of the reaction rates and yields. *J. Am. Chem. Soc.* **128**, 416.

TESFAMICHAEL, A. A. and KALUARACHCHI, J. J. (2004) Uncertainty analysis of pesticide residues in drinking water risk assessment. *Human Ecological Risk Assessment* **10**, 1129.

TIEMAN, R. S., COURY JR, L. A., KIRCHHOFF, J. R., and HEINEMAN, W. R. (1990) The electrochemistry of hemin dimethylsulfoxide. *J. Electroanal. Che*m. **281**, 133.

TOTTEN, L. A. and ROBERTS, A. L. (2001) Calculated one- and two-electron reduction potentials and related molecular descriptors for reduction of alkyl and vinyl halides in water. *Crit. Rev. Environ. Sci. Technol*. **31**, 175.

U.S. EPA (2000) a) Federal Register, www.epa.gov/safewater/gwr/gwrprop.pdf. b) Drinking water contaminant candidate list. c) Conducting a risk assessment of mixtures of disinfections byproduct of chemical mixtures. Washington, DC. U. S. Environmental Protection Agency.

WADE, R. S. and CASTRO, C. E. (1973) Oxidation of Iron (II) porphyrins by alkyl halides. *J. Am. Chem. Soc*. **95**, 226.

ZABAN, A., FERRERE, S., SPRAGUE, J., and GREGG, B. A. (1997) pH-Dependent redox potential induced in a sensitizing dye by adsorption onto TiO_2. *J. Phys. Chem. B.* **101**, 55.

Chapter 6: Effects of Axial Ligands on Heme/TiO_2 Reactivity: One- and Multi-Electron Reduction of Organohalide Pollutants

6.1 Introduction

Remediation of organohalides (RX) in wastewater and groundwater is an important goal (1). Due to the prevalent of organohalides in the pharmaceutical and chemical industries, they will continue to be introduced into a wide range of environments. The removal of organohalides contaminants either *in situ* or above ground treatment is the active research area, and many remediation processes have been proposed over the years (1-3).

Reductive dehalogenation has been extensively studied (4-17) and their degradation products have been isolated (9-12). A common material for reductive dehalogenation studies is zero-valent iron (4, 9-12, 14). Highly reduced molecular compounds, for example, Co^{I} porphyrins (18, 19), are also reactive toward organohalides pollutants. Semiconductors (e.g., TiO_2, ZnO, and Fe_2O_3) illuminated with light have also been shown to reductivelydehalogenate organohalides, such as poly-halogenated biphonyls (PCBs), halogenated alkanes, and pesticides (8, 15-17). However, these materials often generate a distribution of products and sometimes produce secondary pollutants that can be more toxic than the original organohalides compounds. Therefore, maintaining the reduced state of the catalysts and controlling the RX reactions to produce desired products are a vital challenge in the environment.

Iron porphyrins, such as heme, are one of naturally occurring and play important roles in biological systems. They are known to be redox catalysts (4, 13, 20-21). The studies of living organisms in both biotic and abiotic condition for reductive bioremediation of organohalides have shown that the halogenated compounds can undergo biotransformations (11, 13, 22-28). The mechanism of how electrons are transferred from electron donors (heme catalysts) to electron acceptors (organohalides pollutants) is a great interest. For example, carbene complexes of P-450 hemes (23) have been reported that were suggestive of an inner-sphere electron transfer mechanism (29, 30). Investigating reductive dehalogenation by heme porphyrins may help determine the nature of complex microbial pathways.

In Chapter 2, we reported the enhanced reactivity of heme catalysts anchlored to nanocrystalline mesoporous TiO_2 thin films relative to fluid solution (31). This synergistic effect was due, in part, to the shifts in $Fe^{III/II}$ formal reduction potentials upon surface binding (32). The reactive state of heme could be maintained with light or an applied potential. Furthermore, as described in Chapter 4, we recently found evidence of multi-electron transfer (MET) reactivity with these materials (33). The MET process is an efficient method for the degradation of pollutants that can be fine tuned with regard to selectivity and reactivity with specific organic compounds (33, 34).

In this Chapter, we investigated the effect of axial ligands on heme-modified semiconductor reactivity ($Fe^{II}P/TiO_2$ and bis(pyr)$Fe^{II}P/TiO_2$) with halomethanes in pH 4 aqueous solutions. Axial ligation to iron is one of the critical variables in heme catalysis. Pyridines are often used (35-38) because of the sharp characteristic α and β

bands obtained by obsorption spectroscopy. Pyridine ligation to iron porphyrin is also known to autoreduce the ferric state to the ferrous state (39-46). Although explanations for autoreduction by pyridine are still lacking, we also found that hemin (Fe^{III}) autoreduced on the surface of TiO_2 in the presence of pyridine. The results reported herein describe the equilibrium constant of pyridine binding to heme catalysts on TiO_2 ($Fe^{II}P/TiO_2$), the reactivity of the catalysts at nanocrystalline TiO_2 interfaces, the electron transfer mechanism of bis(pyr)$Fe^{II}P/TiO_2$ reactions, as well as the thermodynamic correlation between formal $Fe^{III/II}$ reduction potentials of catalysts (FeP/TiO_2 and bis(pyr)FeP/TiO_2) and the second-order rate constants for the reduction of halomethanes.

6.2 Experimental Section

Materials. Dimethyl sulfoxide (DMSO), pyridine, acetic acid, potassium nitrate, and nitric acid were obtained from Fisher Scientific. Sodium acetate was obtained from J.T. Baker. Titanium (IV) isopropoxide (Aldrich), methanol (Fisher), sodium hydroxide (Aldrich), iron(III) *meso*-tetraphenyl porphyrin chloride (Frontier Scientific), tetrabutylammonium hexafluorophosphate (TBAH) (Fluka), and iron(III) protoporphyrin chloride (Fluka), were used as received. Deionized water was used in aqueous measurements and reactions.

Preparation of FeP/TiO_2 and $(pyr)FeP/TiO_2$ nanocrystalline thin films. Transparent TiO_2 films consisting of ~ 10 nm diameter anatase particles were prepared by the hydrolysis of $Ti(iOPr)_4$ using a sol-gel technique previously described in the literature

(47). The TiO_2 particles were cast as mesoporous thin (~10μm) films onto transparent fluorine-doped tin oxide (FTO) or microscope glass slides and heated at 420 °C for 30min.

Freshly prepared TiO_2 films were soaked in 2-8 μM hemin/DMSO solutions overnight at room temperature. Once iron porphyrins were anchored, they remained strongly bound to the surface in aqueous solutions. For the preparation of FeP/TiO_2, hemin/TiO_2 films were rinsed with pH 4 aqueous solution (6.7 x 10^{-4} M acetic acid) priories to the reaction. The pH values were measured using an Orion Model 420A pH meter. For the preparation of (pyr)FeP/TiO_2, hemin/TiO_2 films were placed diagonally in a standard quartz cuvette containing pyridine solution. The cuvette was sealed with a rubber septum and then purged with N_2 gas for at least 30 min. The photoreduction from Fe^{III} to Fe^{II} was performed with band gap ($h\nu$ > 3.2 eV) excitation of TiO_2 to produce bis(pyr)Fe^{II}P/TiO_2. Band gap excitation generates electron-hole pairs in the TiO_2 nanocrystallites. The conduction band electrons can reduce Fe^{III} to Fe^{II} and the valence-band hole can oxidize solvent or ions. In pyridine solution, Fe^{II} porphyrins were known to have two pyridine axial ligands (48). The bis(pyr)FeP/TiO_2 films were then rinsed with pH 4 acetic acid solution to wash the excess pyridine priories to the reaction. When bis(pyr)Fe^{II}P/TiO_2 films were exposed to air, the iron complexes were oxidized to ferric forms, (pyr)Fe^{III}P/TiO_2.

Binding constants of pyridine to Fe^{II}P/TiO_2 in pH 4 aqueous solution. Binding constants were typically measured from the absorbances of 4 x 10^{-9} mole/cm^2 surface coverage of FeP/TiO_2. A slide coated with Fe^{III}P/TiO_2 was placed in a quartz cuvette.

The photoreduction of $Fe^{III}P/TiO_2$ was performed in N_2-saturated pH 4 acetic acid aqueous solution by band gap excitation of TiO_2 ($\lambda < 370$ nm). After a few minutes of the illumination, $Fe^{III}P/TiO_2$ was reduced to $Fe^{II}P/TiO_2$. Various concentrations of deoxygenated pyridine/pH 4 solutions were added to $Fe^{II}P/TiO_2$ into the external pH 4 aqueous solution. Spectroscopic measurements were made on a Varian Cary 50 UV-visible spectrophotometer. A N_2 atmosphere was kept throughout the measurements.

Spectroelectrochemistry. A (pyr)FeP/TiO_2 functionalized FTO electrode was placed in a standard quartz cuvette. As electrolytes, acetic acid/KNO_3 (0.1M) was used in aqueous solution and tetrabutylammonium hexafluorophosphate (TBAH) was used in methanol. The cuvette was sealed with a rubber septum and then purged with N_2 gas for at least 30 min before applying a potential. A PAR™ Model 173 Potentiostat was used to apply the desired potentials in a standard three-electrode arrangement with a Pt gauze counter electrode and a Ag/AgCl reference electrode. A N_2 atmosphere was kept throughout the measurements. A Cary 50 spectrometer was used to measure absorbance spectral changes. Each potential was held until the UV-vis spectrum became time-independent at which the equilibrium was assumed.

Kinetic analysis of heme complexes reactivity with organohalides. A Varian Cary 50 UV-visible spectrophotometer was used to acquire time-resolved spectra for the reactions of $Fe^{II}P/TiO_2$ and bis(pyr)$Fe^{II}P$ /TiO_2 with halogenated methanes. The $Fe^{III}P/TiO_2$ or (pyr)$Fe^{III}P$ /TiO_2 thin film immersed in pH 4 aqueous solution was purged with N_2. Band gap excitation resulted in the reduction of ferric iron to ferrous

iron. The photogenerated $Fe^{II}P/TiO_2$ and bis(pyr)$Fe^{II}P$ /TiO_2 complexes were stable at least for 3 days under anaerobic conditions. An aliquot of N_2 saturated RX in H_2O was added to $Fe^{II}P/TiO_2$ or bis(pyr)$Fe^{II}P$ /TiO_2 thin film immersed in pH 4 aqueous solution. The experiments were performed in the dark to preclude secondary photocatalytic reactions. The disappearance of Fe^{II} and the appearance of Fe^{III} Soret absorbance were analyzed with a first-order kinetic model. Pseudo-first-order kinetic rate constants, $k_{obs,}$ were obtained by fitting to Equation (6a).

$$\ln (\Delta A/A_0) = -k_{obs}\, t \qquad (6a)$$

where ΔA = initial absorption – absorption at time equal to t, and A_0 is the initial absorption.

Multi-electron transfer (MET) of bis(pyr)$Fe^{II}P/TiO_2(e^-)$ with CCl_4 in MeOH. The films of bis(pyr)$Fe^{II}P/TiO_2$ was prepared as described above. If photolysis is continued after all the catalysts are reduced, electrons in TiO_2, $TiO_2(e^-)$, are generated to form bis(pyr)$Fe^{II}P/TiO_2(e^-)$. An aliquot of CCl_4/MeOH solution was added to the external solution of MeOH under N_2 atmosphere.

Gas chromatography mass spectrometry. The products formed by electrocatalysis and photocatalysis at pH 8 aqueous solutions were analyzed by a Shimadzu GC17A/QP5050A GC/MS (Shimadzu Columbia, MD). The GC17A is equipped with a low polarity (5% phenyl-, 95% methyl-siloxane) capillary J & W DB5-MS column (30

m length, 0.25 mm ID, 0.25 μm film thickness). The products were extracted from the aqueous solution with pentane. Typically a ~2 mL aliquot of pentane was added to ~ 10 mL of RX reaction mixture. The solutions were mixed manually and allowed to separate. A syringe was used to extract the upper pentane layer and transfer it to a 2 mL GC/MS vial. The reaction mixture was injected into the autosampler of the GC/MS. The injector temperature was 220 °C and the transfer interface was at 280 °C. The split ratio was 10 and the H_2 gas column flow rate was kept at 1.0 mL/min. An EI quadrupole based mass spectrometer served as the detector with a scan range of 40-900 amu and an ionizing electron energy of 70 eV. The oven temperature was ramped from 40 °C, held for 10 min, to 80 °C at a rate of 7.2 °C/min. The pressure program was 1.0 kPa, ramp 2.7 kPa/min to 16 kPa, and held for 5 min.

6.3 Results

UV-vis spectra of heme complexes. The UV-vis absorption spectra of FeP in aqueous solution (20, 49) and bis(pyr)FeP in benzene (48, 50) and aqueous solution (51) were previously reported and aided our analysis. The UV-vis absorption spectra of bis(pyr)Fe^{II}P in pyridine solution (data not shown) and bis(pyr)Fe^{II}P on nanocrystalline TiO_2 surface, bis(pyr)Fe^{II}P/TiO_2 in pyridine (Figure 6-1a), were the same within the experimental error (Soret = 416nm, Q_α = 526 nm, Q_β = 556nm). Similarly, the UV-vis absorption spectra of bis(pyr)Fe^{II}P/TiO_2 in pyridine and pH 4 acetic acid aqueous solution were, within the experimental error, the same (Figure 6-1a). Soret region of bis(pyr)Fe^{II}P/TiO_2 in pH 4 broadened compared to in pyridine solution but the Q-band

region stayed the same in both solvents. In MeOH solution, λ_{max} of bis(pyr)$Fe^{II}P/TiO_2$ were similar to pH 4 solution, however, extinction coefficient became larger (table 6-1).

Figure 6-1a and b show the normalized absorption spectra of ferric and ferrous forms of FeP/TiO_2 and (pyr)FeP/TiO_2 in pH 4. The two axial pyridine ligands shifted the Soret band toward the red (lower energy) for both ferric and ferrous forms. A similar result has been shown previously with heme proteins where red shifts of spectral absorption changes were observed when pyridine was added (51, 52). For heme complexes on nanocrystalline anatase TiO_2 surface in pH 4, $\Delta\lambda_{max}$ for ferric and ferrous forms between FeP/TiO_2 and (pyr)FeP/TiO_2 were 30 nm and 32 nm, respectively (Figure 6-1b and c). Table 6-1 is the summary of absorption spectra for ferric and ferrous forms of FeP/TiO_2 and (pyr)FeP/TiO_2. There was no clear Q-band absorption of ferric forms for both FeP/TiO_2 and (pyr)FeP/TiO_2, and therefore, the λ_{max} of Soret bands were used to determine whether complexes had the pyridine axial ligands (Figure 6-1b). Ferrous forms of heme complexes have unique and distinct absorption spectra (Figure 6-1c). Both Soret bands and the Q-band region were well separated and easily detected when pyridine ligands were bound to heme. $Fe^{II}P/TiO_2$ has a broad Q-band at λ_{max} = 575 nm, and bis(pyr)$Fe^{II}P/TiO_2$ has two sharp Q-bands at Q_α = 556 nm and Q_β = 526 nm.

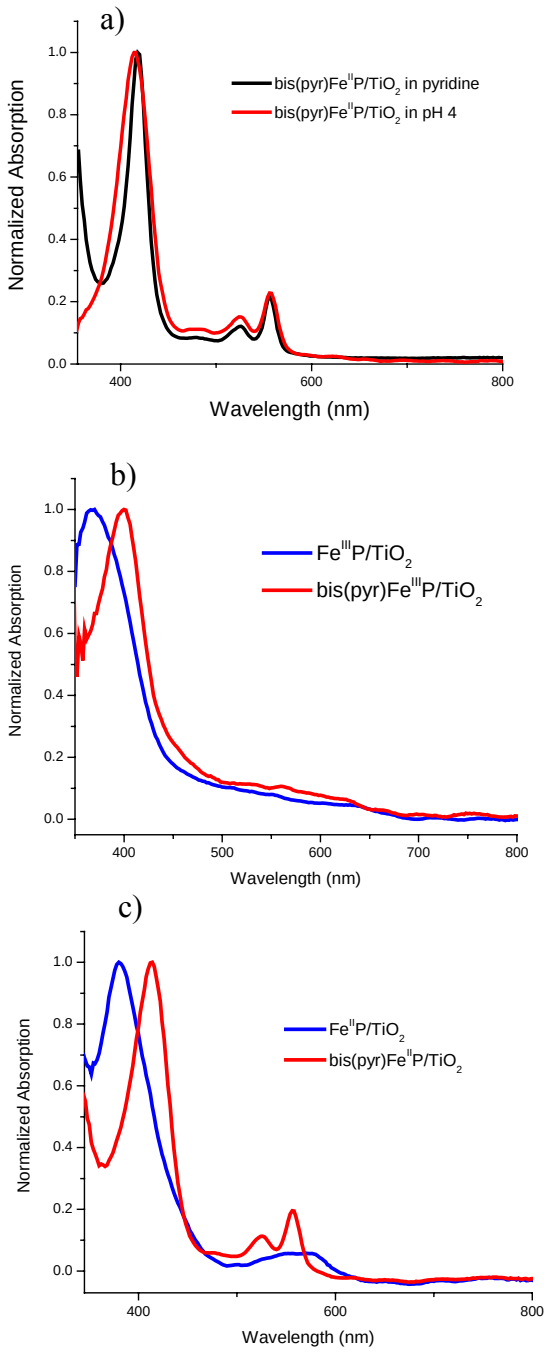

Figure 6-1. a) UV-visible absorbance spectrum of bis(pyr)Fe^{II}P/TiO$_2$ in pyridine (—) and pH 4 acetic acid aqueous solution(—). b) UV-visible absorbance spectrum of ferric forms of heme complexes, Fe^{III}P/TiO$_2$ (—) and (pyr)Fe^{III}P/TiO$_2$ (—) in pH 4 acetic acid aqueous solution. c) UV-visible absorbance spectrum of ferrous forms of heme complexes, Fe^{II}P/TiO$_2$ (—) and bis(pyr)Fe^{II}P/TiO$_2$ (—) in pH 4 acetic acid aqueous solution.

Table 6-1. Spectroscopic and redox properties of heme complexes in pH 4 and MeOH at room temperature.

		Soret (nm)	ε (cm^{-1} M^{-1})	Q (nm)	ε (cm^{-1} M^{-1})	*E° (mV)
$Fe^{III}P/TiO_2$	pH 4	368	105,000			
$Fe^{II}P/TiO_2$	pH 4	382	105,000	575	10,000	-900
$(pyr)Fe^{III}P/TiO_2$	pH 4	398	105,000			
	MeOH	398	142,000			
$bis(pyr)Fe^{II}P/TiO_2$	pH 4	414	145,000	556; 526	30,000; 20,000	-160
	MeOH	414	230,000	554, 522	50,000; 30,000	-140

* Formal reduction potential was measured vs. $Fc^{+/0}$.

Autoreduction of hemin/TiO_2 (Fe^{III}) to (pyr)$Fe^{II}P/TiO_2$. Autoreduction of $Fe^{III}P$ to $Fe^{II}P$ by pyridine has been reported previously (39-46). In this study, we placed the films of hemin/TiO_2 (Fe^{III}) in a standard quartz cuvette containing pyridine solution. The absorption at 418 nm, 526 nm, and 558 nm for bis(pyr)$Fe^{II}P/TiO_2$ (Data not shown) increased slowly as the absorption of hemin/TiO_2 decreased. Isosbestic points were observed at 409, 442, 508, 568, and 560 nm.

Addition of pyridine to $Fe^{II}P/TiO_2$ in pH 4. Binding constants of pyridine to $Fe^{II}P/TiO_2$ was determined in N_2 saturated pH 4 acetic acid solution. After reducing $Fe^{III}P/TiO_2$ by bandgap illumination of TiO_2 to form $Fe^{II}P/TiO_2$, various concentrations of pyridine/pH 4 solution was added. Figure 6-2a. shows the typical spectroscopic changes after the addition of excess pyridine/pH 4 solution to the external aqueous solution. Isosbestic points were observed at λ_{iso} = 392, 456, and 570 nm. The addition of > 1.0 x 10^{-2} M pyridine resulted in over 90 % conversion from $Fe^{II}P/TiO_2$ to bis(pyr)$Fe^{II}P/TiO_2$. The final spectrum after the addition of pyridine to $Fe^{II}P/TiO_2$ was overlapped with an absorption spectrum of bis(pyr)$Fe^{II}P/TiO_2$ prepared for RX reactions (Fig 6-2a. inset). The λ_{max} of the spectra were within the experimental error the same (λ_{max} = 414 nm, 526 nm, and 556 nm).

The axial ligation reactions of iron porphyrins have been reported previously with pyridine (40, 41, 52) and imidazole molecules (35, 53). Two steps of axial ligand addition to iron porphyrins have been suggested (40, 41). The first step is the intermediate formation of the mono pyridine complexes ((pyr)$Fe^{II}P/TiO_2$).

$$Fe^{II}P/TiO_2 + pyr \overset{K_1}{\rightleftharpoons} (pyr)Fe^{II}P/TiO_2 \qquad (6b)$$

The product of the first step is not usually detectable since the equilibrium constant of the second step, K_2, is in general larger than K_1. The second step of axial ligand addition can be written as:

$$(pyr)Fe^{II}P/TiO_2 + pyr \overset{K_2}{\rightleftharpoons} bis(pyr)Fe^{II}P/TiO_2 \qquad (6c)$$

Since $K_2 >> K_1$, the equilibrium constant of two pyridine ligation to $Fe^{II}P/TiO_2$ is the sum of equations (6b) and (6c), and can be expressed as a single step:

$$Fe^{II}P/TiO_2 + 2\ pyr \overset{\beta_2}{\rightleftharpoons} bis(pyr)Fe^{II}P/TiO_2 \qquad (6d)$$

Where β_2 is the sum of two stepwise constants, $K_1 * K_2$. Therefore, equilibrium constant of two axial ligation for the formation of $bis(pyr)Fe^{II}P/TiO_2$ (β_2) can be determined by following Equations:

$$\beta_2 = [\ bis(pyr)Fe^{II}P/TiO_2\ ] / [\ Fe^{II}P/TiO_2\ ]\ [pyr]^2 \qquad (6e)$$

$$[\ bis(pyr)Fe^{II}P/TiO_2\ ]/[\ Fe^{II}P/TiO_2\ ] = \beta_2 * [pyr]^2 \qquad (6f)$$

$$\log [\ bis(pyr)Fe^{II}P/TiO_2\ ]/[\ Fe^{II}P/TiO_2\ ] = \log \beta_2 + 2 * \log [pyr] \qquad (6g)$$

The ratio between the products, $bis(pyr)Fe^{II}P/TiO_2$, and the precursor heme, $Fe^{II}P/TiO_2$, can be given by the spectral changes upon addition of pyridine at wavelengths of interest. The calculations were typically done by the Equations (6h). (40, 41, 52)

$$[\text{bis(pyr)}Fe^{II}P/TiO_2] / [Fe^{II}P/TiO_2] = (A - A_0) / (A_\infty - A) \qquad (6h)$$

where A is the absorbance of interest, A_0 is the absorbance of $Fe^{II}P/TiO_2$, and A_∞ is the absorbance in the large excess of pyridine to form > 95 % bis(pyr)$Fe^{II}P/TiO_2$ (Fig 6-2). Then the equation (6g) can be written in the form of Equation (6i).

$$\log (A - A_0) / (A_\infty - A) = \log \beta_2 + 2 * \log [\text{pyr}] \qquad (6i)$$

The total pyridine concentration is experimentally known. The plots of log ($A-A_0$ / A_∞-A) vs. log [pyr] were constructed. The equilibrium constant, β_2, was estimated from the intercept of the graph which yields a slope of 2. Figure 6-2b. shows the experimental points fitted by a straight line that gave a slope of 2.0± 0.1. The intercept of the graph in Figure 6-2b was 4.97 that yielded the binding constant of $9.3 \pm 0.4 \times 10^4$ M^{-2}.

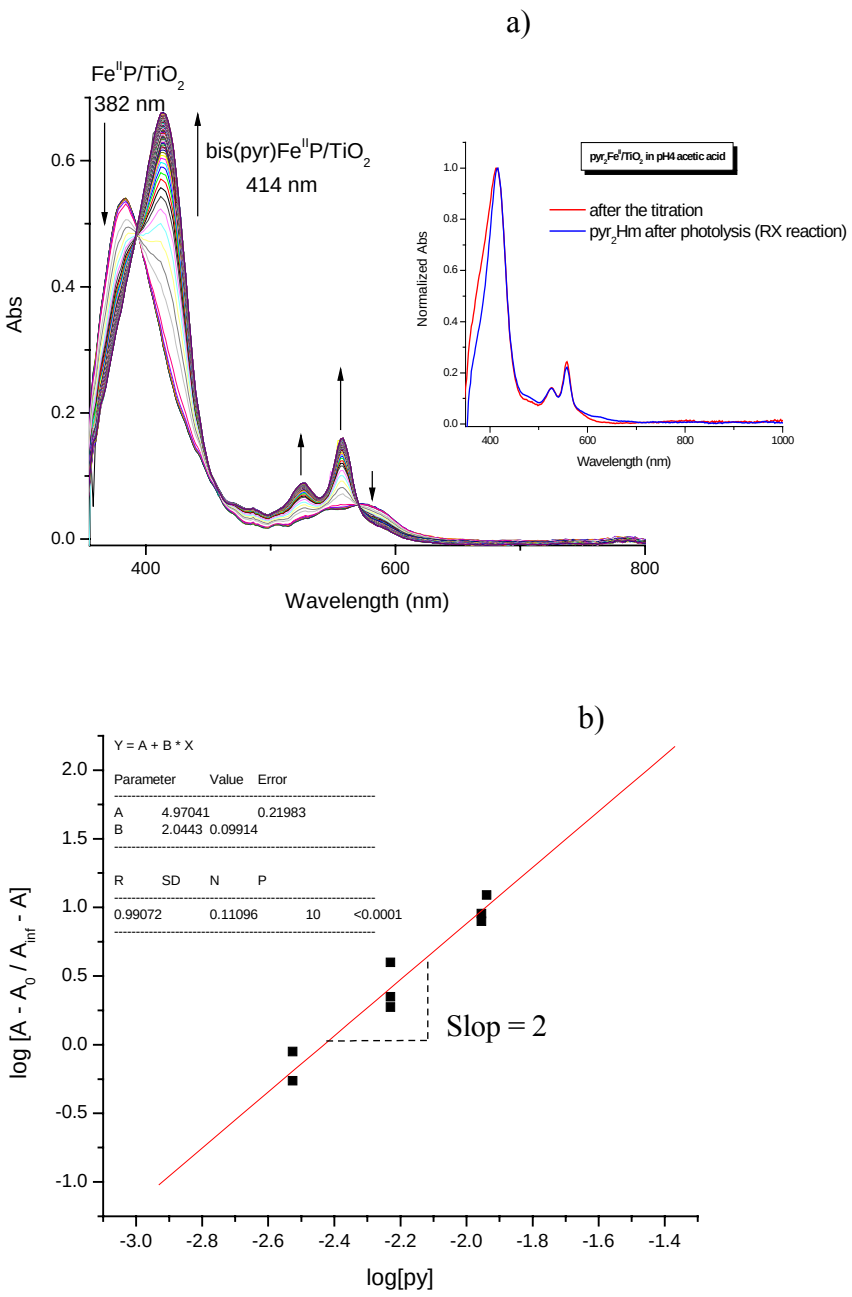

Fig 6-2. a) The spectral changes observed after addition of 1.1 x 10^{-2} M pyridine to $Fe^{II}P/TiO_2$ in pH 4 aqueous solution. The arrows show the direction of absorption change after the addition. The inset shows the UV-visible absorbance spectrum of the final bis(pyr)$Fe^{II}P/TiO_2$ spectrum from a. (—) and bis(pyr)$Fe^{II}P/TiO_2$ prepared for RX reactions (—). b) The plot of log $(A-A_0)/(A_\infty-A)$ vs. log [pyr]. The binding constant of pyridine to $Fe^{II}P/TiO_2$ estimated from the intercept of the fitted line was $\beta_2 = 9.3 \pm 0.4 \times 10^4$ M^{-2}.

Formal reduction potential of (pyr)$Fe^{III/II}P/TiO_2$ in pH4 and MeOH. Formal $Fe^{III/II}$ reduction potential (E°) of hemin anchored to nanocrystalline anatase TiO_2 surface, $Fe^{III/II}P/TiO_2$, in pH 4 aqueous solution was estimated in our previous study (34). Spectroelectrochemistry measurements were used to estimate the formal reduction potential (E°) of (pyr)$Fe^{III/II}P/TiO_2$ in pH 4 acetic acid/KNO_3 and MeOH/TBAH electrolytes. Upon stepping the applied potential to a new value, the absorption spectra were taken every 3-5 min until the steady-state concentration did not change as a function of time. The absorption spectra of the catalysts, (pyr)$Fe^{III/II}P/TiO_2$, showed isosbestic points as they were reduced or oxidized (Figure 6-3). Isosbestic points were observed at λ_{iso} = 398, 452, 474, 576, and 654 nm in pH 4 and λ_{iso} = 406, 447, 511, and 579 nm in MeOH. The formal reduction potential of the catalysts corresponded to the equilibrium potential where the concentrations of ferric and ferrous forms were equal (Figure 6-3 inset). The reduction potential of (pyr)$Fe^{III/II}P/TiO_2$ in pH 4 and MeOH electrolytes were -160 mV and -140 mV vs. $Fc^{+/0}$, respectively (Table 6-1).

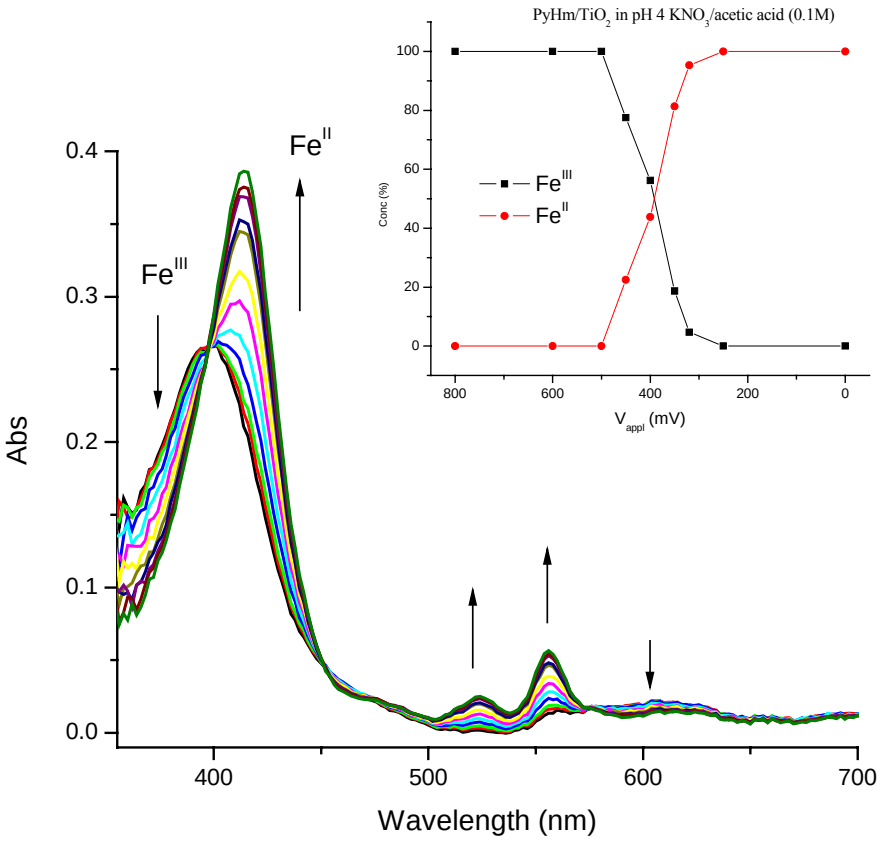

Figure 6-3. The spectroelectrochemical data of (pyr)FeP/TiO_2 in pH 4 acetic acid/KNO_3 electrolyte. The Soret band shifts from 398 nm (Fe^{III}) to 414 nm (Fe^{II}) with negative applied potential. The arrow shows the direction of absorption change upon applying negative potential. Isosbestic points were observed at λ_{iso} = 398, 452, 474, 576, and 654 nm. The inset shows the plot of % concentration of Fe^{III} and Fe^{II} vs. applied potential. The formal reduction potential of (pyr)FeP/TiO_2 in pH 4 was -160 mV vs. $Fc^{+/0}$.

Reaction of $Fe^{II}P/TiO_2$ and bis(pyr)$Fe^{II}P/TiO_2$ toward organohalide pollutants. The reactivity of $Fe^{II}P/TiO_2$ and bis(pyr)$Fe^{II}P/TiO_2$ with halogenated methanes were quantified in pH 4 acetic acid aqueous solution. The catalysts were photoreduced to ferrous forms with bandgap illumination ($\lambda > 370$ nm) in N_2 saturated pH 4 aqueous solution. The anaerobic dark addition of RX/H_2O stock solutions resulted in oxidation of $Fe^{II}P/TiO_2$ to $Fe^{III}P/TiO_2$ (or bis(pyr)$Fe^{II}P/TiO_2$ to (pyr)$Fe^{III}P/TiO_2$). The typical data is shown in Figure 6-4. The final spectra after the addition of RX was found to generate the initial ferric absorption spectra (Figure 6-4a). The disappearance of reduced forms and the appearance of oxidized forms of heme complexes were monitored to measure k_{obs} rate constants. The observed rate constants for the loss of ferrous forms and the formation of ferric forms were the same within the experimental error. The bis(pyr)$Fe^{II}P/TiO_2$ to (pyr)$Fe^{III}P/TiO_2$ conversion showed isosbestic points at λ_{iso} = 396, 454, 472, and 577 nm (Figure 6-4b) that were similar to spectroelectrochemistry measurements (Figure 6-3). For the conversion of $Fe^{II}P/TiO_2$ to $Fe^{III}P/TiO_2$ after addition of RX/H_2O, isosbestic points were observed at λ_{iso} = 468, 530, 609, and 675 nm (data not shown) (34).

The loss of $Fe^{II}P/TiO_2$ (or bis(pyr)$Fe^{II}P/TiO_2$) and the concurrent formation of $Fe^{III}P/TiO_2$ (or (pyr)$Fe^{III}P/TiO_2$) were found to be exponential (Figure 6-4c). The surface concentrations were calculated spectroscopically by standard addition of the ferrous and ferric forms absorbance spectra at each observation time. Observed rate constants, k_{obs}, were abstracted from the absorption changes for the disappearance of ferrous and the appearance of ferric forms. Second-order rate constants were determined from plots of k_{obs} vs. [RX] for each organohalides (Figure 6-4d) at the same

heme surface coverage, 4 x 10^{-9} mole/cm^2. At this surface coverage, the reactions were found to be first-order in heme and organohalides in our previous studies (34). Second-order rate constants increased in order of CCl_4 > $CHBr_3$ > $CHCl_2Br$ > $CHCl_3$ for both $Fe^{II}P/TiO_2$ and bis(pyr)$Fe^{II}P/TiO_2$ heme complexes (Table 6-2). The reactions were faster with $Fe^{II}P/TiO_2$ compared to bis(pyr)$Fe^{II}P/TiO_2$ for the halogenated methanes investigated in this study.

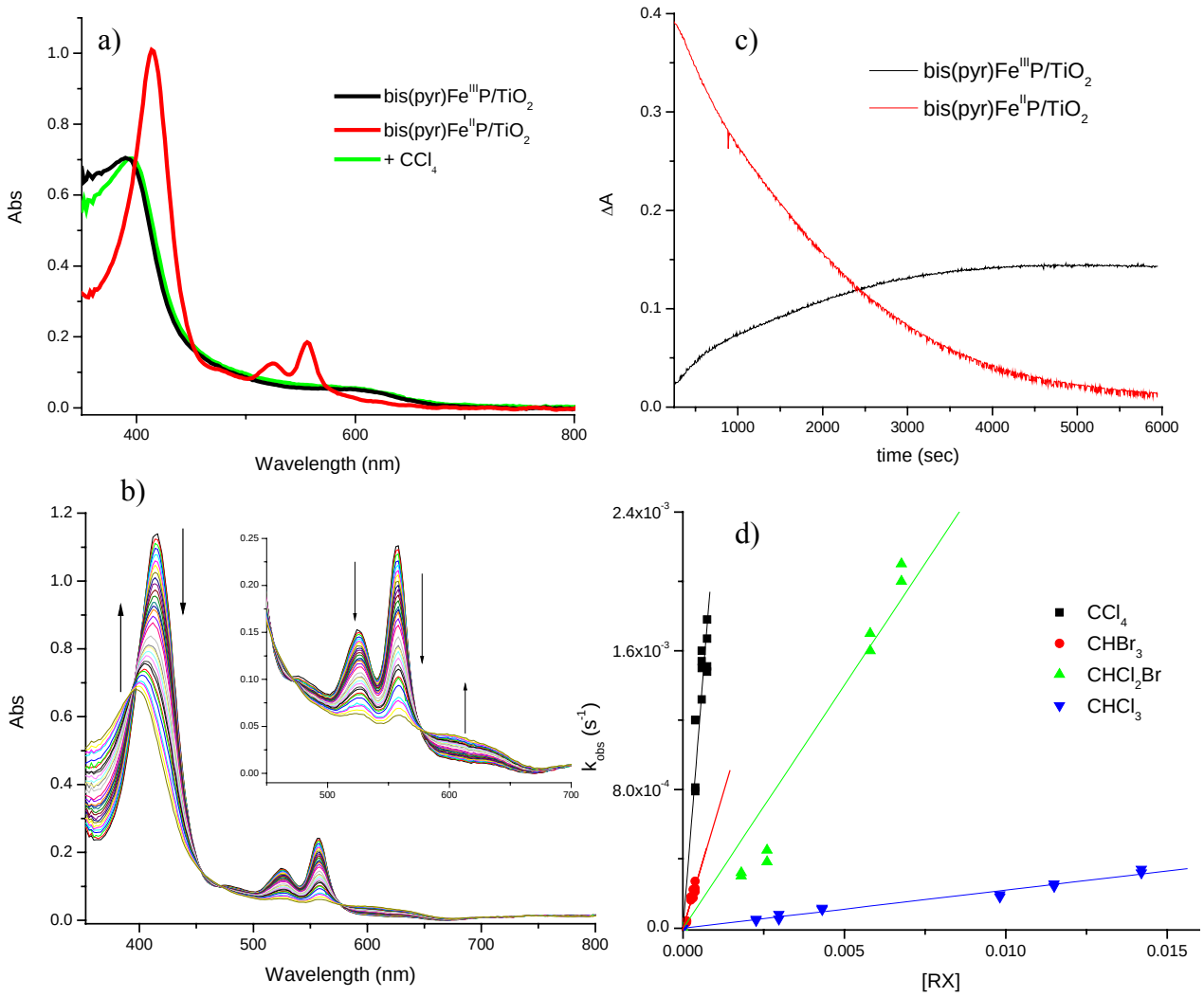

Figure 6-4. The RX reactions of bis(pyr)Fe^{II}P/TiO$_2$ in pH 4 acetic acid solution. a) UV-visible absorbance spectra of (pyr)Fe^{III}P/TiO$_2$ (—), bis(pyr)Fe^{II}P/TiO$_2$ (—), and the final product after addition of 5.83 x 10^{-4} M CCl_4 (—). b) The spectral changes observed after addition of 5.83 x 10^{-4} M CCl_4 to bis(pyr)Fe^{II}P/TiO$_2$ in pH 4. The arrows show the direction of absorption change after the addition. c) The plot of (pyr)Fe^{III}P/TiO$_2$ (—) and bis(pyr)Fe^{II}P/TiO$_2$ (—) monitored by the Soret bands at 398 nm and 414 nm. d) Plots of the observed rate constants vs. the indicated RX concentration in pH 4.

Table 6-2. Second-order rate constants and ΔG for bis(pyr)$Fe^{II}P/TiO_2$ and$Fe^{II}P/TiO_2$ reactions with halomethanes.

	E ($RX^{0/-}$)[a] (V *vs.* NHE)	ΔG[b] (V *vs.* NHE)	bis(pyr)$Fe^{II}P/TiO_2$ k (M^{-1} s^{-1})	ΔG[b] (V *vs.* NHE)	$Fe^{II}P/TiO_2$ k (M^{-1} s^{-1})
CCl_4	+0.085	-0.206	2.3 ± 0.1	+0.535	14.1 ± 0.7
$CHBr_3$	+0.035	-0.156	0.63 ± 0.03	+0.585	13.0 ± 1.0
$CHCl_2Br$	-0.066	-0.055	0.28 ± 0.02	+0.686	2.9 ± 0.2
$CHCl_3$	-0.145	+0.024	0.022 ±0.001	+0.765	0.63 ± 0.03

[a] taken from the reference (54)

[b]ΔG was calculated by the potential difference: $\Delta G = E° (Fe^{III/II}) - E° (RX^{0/-})$

Multi-electron transfer (MET) of bis(pyr)$Fe^{II}P/TiO_2(e^-)$ with CCl_4 in MeOH. Heme-carbene formation at nanocrystalline TiO_2 interfaces after the reaction of $Fe^{II}P/TiO_2(e^-)$ with CCl_4 in MeOH was recently reported (56). In this study, MET of bis(pyr)$Fe^{II}P/TiO_2(e^-)$ with CCl_4 was also investigated. The concentration of $TiO_2(e^-)$ was varied while the surface coverage of bis(pyr)$Fe^{II}P$ was kept the same. In all cases, the final spectrum after the addition of CCl_4/MeOH was (pyr)$Fe^{III}P/TiO_2$ (Figure 6-5a). There was no spectroscopic evidence of carbene formation (Figure 6-5b) during the reactions (55).

Product analysis by GC/MS. The products of CCl_4 reduction by heme/$TiO_2(e^-)$ in aqueous pH 4 solution were analyzed by GC/MS. Electrocatalysis was initially performed at an applied potential of -1.0 V (*vs*. Ag/AgCl). This potential reduced all hemin to heme and established a $TiO_2(e^-)$ concentration of 1.9 x 10^{-5} M. The excess CCl_4 was then added to the external electrolyte and the potential was applied for 4 hours. Control experiments performed with FTO electrodes without heme or TiO_2 showed no dechlorinated products. The aqueous solutions were extracted with pentane as described in the experimental section.

CCl_4 (m/z-Cl 117; Retention time 4.1 min): The major product of electrocatalysis was $CHCl_3$ (*m/z* 118) at RT = 3.5 min. Identification was confirmed by independent analysis of $CHCl_3$/pentane. A minor amount of a product was observed at RT = 8.3 min. The mass spectrum of this product was identical to that of tetrachloroethylene, $Cl_2C{=}CCl_2$ (*m/z* 164).

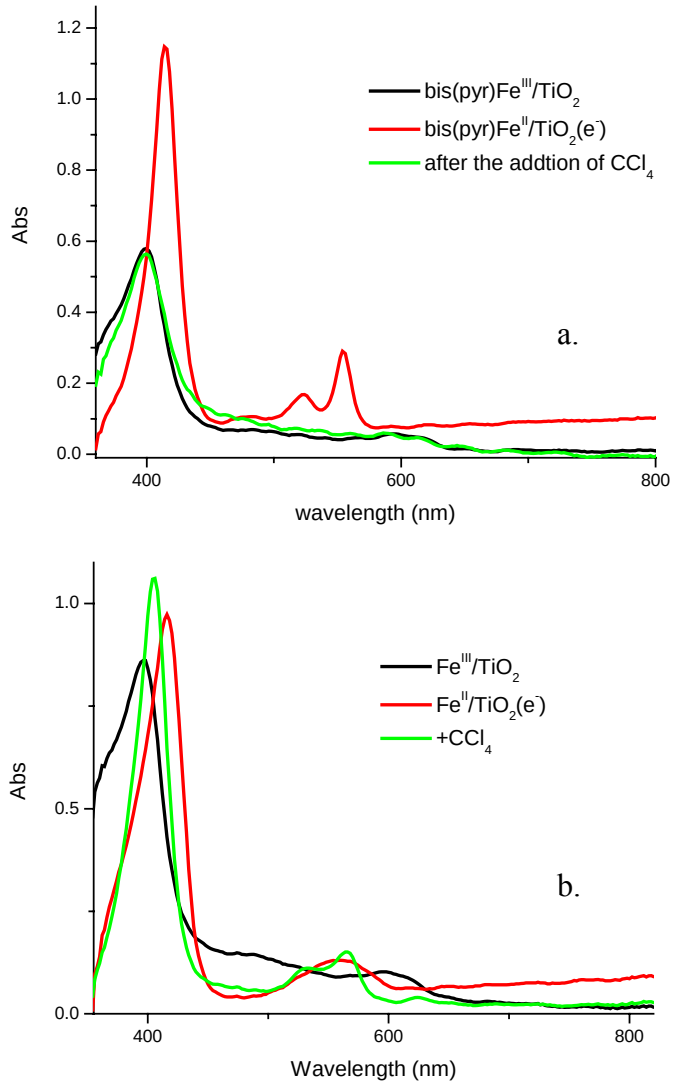

Figure 6-5. The UV-vis absorption specta of a) (pyr)$Fe^{III}P/TiO_2$ (—), bis(pyr)$Fe^{II}P/TiO_2(e^-)$(—) after ultra band gap illumination, and the final spectrum after addition of CCl_4 assigned to (pyr)$Fe^{III}P/TiO_2$ (—) in MeOH, and b) $Fe^{III}P/TiO_2$ (—), $Fe^{II}P/TiO_2(e^-)$(—) after ultra band gap illumination, and the final spectrum after addition of assigned to carbene adduct, $(CCl_2)Fe^{II}P/TiO_2$ (—) in MeOH.

Linear free energy relationship. Correlation between thermodynamics of the reactions (ΔG) and the second-order rate constants was investigated. The reactions without the excess electrons in TiO_2 were assumed to occur in single electron transfer steps by one electron transfer from an electron donor (heme complex) to an electron acceptor (halogenated methane). The observed rate constants of such reactions were thought to be related to the free energy of the reactions (56-60). Therefore, in this study, the overall free energy of the reactions was assumed to be proportional to the formal reduction potentials of the catalysts (E°). ΔG was calculated by the difference between E° of the catalysts and one electron reduction of halogenated methanes as expressed in Equation 6j.

$$\Delta G \propto E^\circ (Fe^{III/II}) - E^\circ(RX^{0/-}) \qquad (6j)$$

The ΔG calculations using the measured formal reduction potentials of $Fe^{III/II}P/TiO_2$ (-340 mV vs. Ag/AgCl) (34) and (pyr)$Fe^{III/II}P/TiO_2$ (+400 mV vs. Ag/AgCl) and the calculated one-electron reduction potentials (E_1) of RX in aqueous solution (54) were summarized in Table 6-2. The plots of the second-order rate constants vs. the estimated overall free energy (ΔG) showed the trend that the reactions were faster when ΔGs were more negative (Figure 6-6). The correlation coefficient (R^2) for $Fe^{III/II}P/TiO_2$ and (pyr)$Fe^{III/II}P/TiO_2$ reactions were 0.97 (Figure 6-6) and 0.85 (Figure 6-6a), respectively.

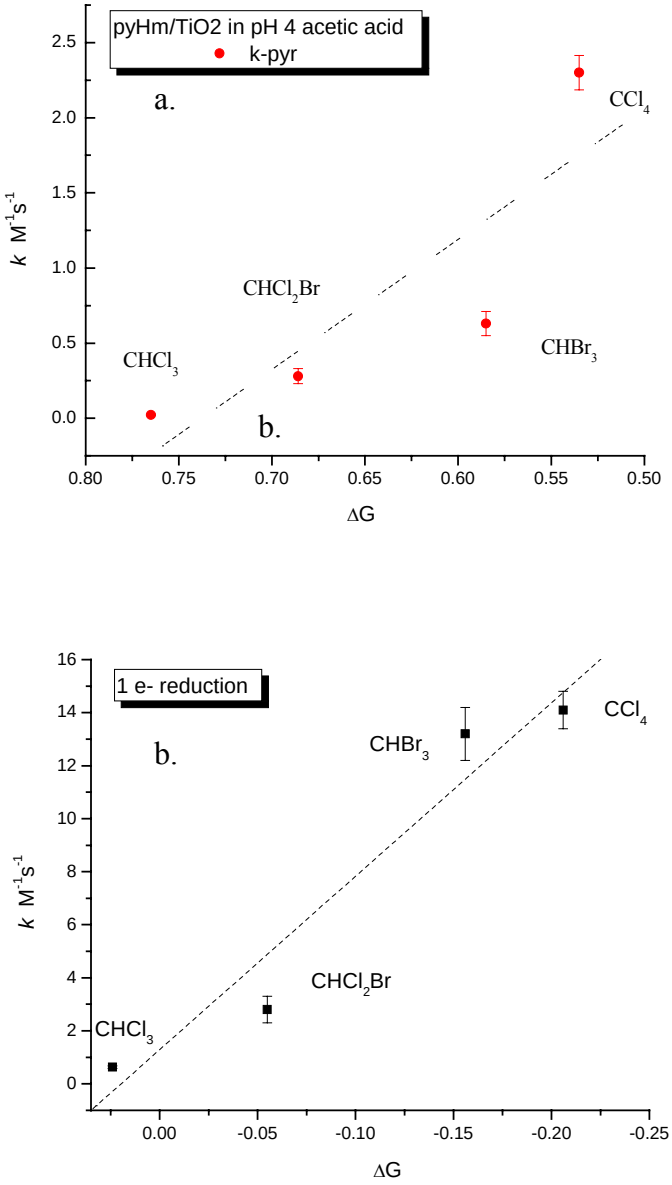

Figure 6-6. Thermondynamic correlation of second-order reaction constants vs. ΔG calculated from the difference between $Fe^{III/II}$ formal reduction potentials and one-electron reduction potentials of halomethanes. The reactions for a) bis(pyr)$Fe^{II}P/TiO_2$, $R^2 = 0.85$, and b) $Fe^{II}P/TiO_2$, $R^2 = 0.97$, in pH 4 acetic acid aqueous solution.

6.4 Discussion

Hemoproteins are a great interest for many researchers because of their important role in biology as electron carriers. Understanding the relationship between structures and functions that associates with 5th and 6th coordination sites and the functional role of the axial ligands are essential (46, 61). The substituted pyridines are the most widely used natural axial ligands (62). Pyridine has been known to bind to the heme iron and cause properties of heme reactivity (37, 38). For example, Fujii and co-workers reported the effect of ligand on heme environment and the activity (37), where pyridine induced a structural modification in cytochrome b_{558} and decreased the O_2^- generation activity.

Autoreduction of iron(III) porphyrins has been known to occur in the presence of some ligands such as cyanide, pyridine and its derivatives (39-46). The iron-ligand bond making and breaking processes and the mechanisms of these reactions are also important for the intramolecular electron transfer in biological systems. Autoreduction mechanisms at room temperature remain unclear due to the fast autoreduction rate (39), however, some possibilities were suggested (39, 42-43, 46, 50, 61, 63-65). For example, some researchers proposed the base-catalyzed intramolecular electron transfer via hemolytic cleavage of Fe-L bond as a general mechanism for the autoredution of Fe^{III} porphyrins in the presence of coordinating bases (39, 63). Others suggested an electron migration through the axial ligands involving radicals (64). The overall autoreduction of $Fe^{III}P/TiO_2$ in pyridine solution can be written as:

$$XFe^{III}P/TiO_2 + 2\ \text{pyridine} \rightarrow \text{bis(pyr)}Fe^{II}P/TiO_2 + X\bullet \qquad (6k)$$

Fe^{III} iron with an axial Cl ligand has been assigned to be high spin (S=5/2) (42). When hemin (Cl-Fe^{III}P or Cl-$Fe^{III}P/TiO_2$) was dissolved in pyridine solution, autoreduction of iron may occur due to the stable low spin (S=0) six-coordinate bis(pyr)Fe^{II}P (50, 61, 65). It is also suggested that the ease of autoreduction of Fe^{III}P is a result of their increased Lewis acidity (42, 43). In this work, the possible pathway for autoreduction from $Fe^{III}P/TiO_2$ by pyridine to form bis(pyr)$Fe^{II}P/TiO_2$ complexes, can be a formation of six-coordinated iron complex first followed by the reduction through intramolecular electron transfer by free ligands (39):

$$\text{i) Cl-Fe}^{III}\text{P/TiO}_2 + 2 \text{ pyridine} \rightleftharpoons [\text{bis(pyr)Fe}^{III}\text{P/TiO}_2]^+ + \text{Cl}^- \quad (6l)$$

$$\text{ii) } [\text{bis(pyr)Fe}^{III}\text{P/TiO}_2]^+ \rightleftharpoons \text{bis(pyr)Fe}^{II}\text{P/TiO}_2 + \bullet\text{pyr} \quad (6m)$$

$$\text{iii) bis(pyr)Fe}^{II}\text{P/TiO}_2 + \text{pyr} \rightleftharpoons \text{bis(pyr)Fe}^{II}\text{P/TiO}_2 \quad (6n)$$

where the steps of autoreduction are i) the formation of low spin iron(III) complexes (Equation 6l), ii) the autoreduction (Equation 6m), and iii) the intramolecular electron transfer by the free pyridine ligand (Equation 6n). Kadish and Bottomley (46) reported the observation of $[L_2Fe^{III}P]^+Cl^-$ because the pyridine ligands were strongly complexed with Fe^{III}. Cyclic voltammograms of pyridines in the range of $3.0 < pKa < 5.4$ yielded two reduction waves but only one oxidation wave. They concluded that both Fe^{III}PCl and $[L_2Fe^{III}P]^+Cl^-$ were present when pKa of a lignad was in this range and both reactants may be reduced to form $L_2Fe^{II}P$ (46). Since pKa of pyridine lays in this region, Equation 6l can be the suggestive first step. The observation of isosbestic

points for the reaction A can be explained the rapid reaction of Equation 6n (39). The half-wave potential for $(TPP)Fe(pyr)_2^+/(TPP)Fe(pyr)_2$ was reported to be + 0.06 V vs. SCE (46), indicating that the reduction of $Fe^{III}P$ to bis(pyr)$Fe^{II}P$ is thermodynamically favorable once $Fe^{III}P$ forms bis(pyr)$Fe^{III}P$.

The spectra of bis(pyr)$Fe^{II}P$ in pyridine solution and bis(pyr)$Fe^{II}P/TiO_2$ in pH 4 solution were the same within the experimental error (Figure 6-1a). This indicates that the two pyridine ligands stay bound to iron center of heme porphyrins and form stable 6-coordinate bis(pyr)FeP. In fact, when (pyr)FeP/TiO_2 was reduced and oxidized repeatedly by TiO_2 band gap excitation (λ > 370 nm) in pH 4, the spectra of bis(pyr)$Fe^{II}P/TiO_2$ were the same, λ_{max} = 414, 526, 556 nm. The bis(pyr)$Fe^{II}P/TiO_2$ was stable over 3 days in anaerobic condition. The literature has shown the stability of Fe^{II} porphyrin when pyridines were bound to iron (50, 61). Although the spin state of Fe^{II} porphyrins can vary with axial ligands, it is known that pyridine gives a diamagnetic state (S = 0). (66). The stability can be explained with electron withdrawal at the periphery of the Fe^{II} porphyrin system that facilitates sigma or pi acceptance by Fe^{II} and stabilizes the low spin dipyridine species (50). This is associated with the fully filled t_2g orbitals in the low spin d^6 electronic configuration. The red shift of Soret band and blue shift of Q-band area due to pyridine ligation has reported previously in the literature (37).

The binding constant of pyridine ligation to $Fe^{II}P/TiO_2$ measured here, β_2 = 9.3 ± 0.4 x10^{-4} M^{-2}, was expected (Figure 6-2). Compared to the literature value (40), e.g. 1.3 ± 0.2 x10^{-8} M^{-2}, our binding constant seems to be small. This could be due to the fact that the measurements were carried out on TiO_2 surface. There might be a

diffusion limit at TiO_2 interfaces that heme catalysts were not freely solvated by pyridine solution. The appearance of Soret band at 414 nm, and Q-band region at 526 nm and 556 nm shows the evidence of pyridine binding to iron to form bis(pyr)$Fe^{II}P/TiO_2$. The isosbestic points at λ_{iso} = 392, 456, and 570 nm indicate that there were only two detectable complexes, $Fe^{II}P/TiO_2$ and bis(pyr)$Fe^{II}P/TiO_2$, present. This result confirms that the second equilibrium constant, K_2, is much larger than K_1 and mono(pyr)$Fe^{II}P$ is difficult to observe spectroscopically.

The mechanisms of pyridine binding was not investigated in detail in this study, however, it is proposed that, in biology, enzymes interact with ligands by π-bonding (67). The affinity of iron porphyrin for ligands partly explained in terms of π-back bounding occurring by back-donation of electrons from the metal atom to the π system of ligands. K_2 is typically larger than K_1 that can be understood in terms of the ligand field stabilization energy for the t_2g low spin six-coordinate species.

The reduction of halogenated methanes with $Fe^{II}P/TiO_2$ and bis(pyr)$Fe^{II}P/TiO_2$ in pH 4 aqueous solution was determined under the condition that the reactions were first-order in heme and in organohalides concentration (34). The second-order rate constants for both $Fe^{II}P/TiO_2$ and bis(pyr)$Fe^{II}P/TiO_2$ increased in the order of CCl_4 > $CHBr_3$ > $CHCl_2Br$ > $CHCl_3$. This trend is expected based on the one electron reduction potentials of organohalides in water as indicated in Table 6-2 (54). The reactions of $Fe^{II}P/TiO_2$ were consistently faster compared to bis(pyr)$Fe^{II}P/TiO_2$ for all organohalides investigated in this study. This indicates that axial ligands are critical variables on heme reactivity. The ligand changes the arrangement of orbitals and can affect the environment of heme porphyrins. As a result, the reactivity of heme

complexes can be influenced. The larger reactivity with $Fe^{II}P/TiO_2$ can be partially explained with the heme $Fe^{III/II}$ formal reduction potentials, e.g. E° ($Fe^{III/II}P/TiO_2$) = -900 mV and E° ((pyr)$Fe^{III/II}P/TiO_2$) = -160 mV vs. $Fc^{+/0}$ (32, 34). Effects of axial ligands on reduction potentials have been reported in the literature (63, 68). This shows that heme reactivity is influenced by axial ligands that can change the redox potentials of catalysts.

The inner and outer sphere electron transfer mechanisms are of interests for phorphyrins and metalloporphyrins (62). In this study, the multi-electron transfer reactions of bis(pyr)$Fe^{II}P/TiO_2(e^-)$ with CCl_4 in MeOH showed no evidence of carbene formation (Figure 6-5). In outer sphere redox reactions, electrons are transferred between the species (reductant $\rightarrow$ oxidant) without changes in their coordination spheres and ligands are ideally unable to bridge and are π-acceptors. The MET reactions of bis(pyr)$Fe^{II}P/TiO_2(e^-)$ complexes is consistent with this predictions. From the results, we can conclude that the mechanism for the reduction of halomethanes by bis(pyr)$Fe^{II}P/TiO_2(e^-)$ as well as bis(pyr)$Fe^{II}P/TiO_2$ is outer sphere electron transfer. It is interesting to note that pyridine ligands have capable to change the mechanisms to outer sphere electron transfer.

The observation of tetrachloroethylene product by GC/MS analysis after the CCl_4 reduction indicated a net two-electron transfer process that produced dichlorocarbene intermediate during the reaction. The dimerization of this intermediate resulted in tetrachloroethylene has been reported previously (69). Whether the electron transfer mechanism for the formation of dichlorocarbene was a two-electron reduction or two single-electron transfers was not clear. Since the main product was $CHCl_3$, the electron

transfer mechanism for this reaction may be assumed to be two single electron transfer processes (Equation 1-g and –h).

i) First electron transfer $CCl_4 + e^- \rightarrow {}^{\bullet}CCl_3 + Cl^-$ (6o)

ii) Second electron transfer ${}^{\bullet}CCl_3 + e^- + H^+ \rightarrow HCCl_3$ (6p)

or ${}^{\bullet}CCl_3 + e^- \rightarrow :CCl_2 + Cl^-$ (6q)

In fact, the estimated reduction potentials of Equations 6q was more positive than Equation 6p (14). If the formation carbene was predominant, the main product would be expected to be dichloroethylene rather than chloroform. Therefore, we can conclude that the reaction of $Fe^{II}P/TiO_2(e^-)$ with CCl_4 in aqueous solution was more like to be dissociative electron transfer mechanism.

Understanding the relationship between reaction rate constants of organohalides pollutants and reduction potentials of organohalides and catalysts can be a useful tool to predict the dehalogenation processes in the environment. Some researchers have shown the strong correlations between thermondynamic values of the first electron transfer process and the degradation rate (56, 70). In our previous study, we have shown that the main product of the $Fe^{II}P/TiO_2$ reaction with CCl_4 in aqueous solution was $CHCl_3$ (34). This result indicates that dehalogenation of organohalides with $Fe^{II}P$ can also undergo hydrogenolysis at nanocrystalline TiO_2 surface. Hydrogenolysis of organohalides in water is proposed to be one-electron transfer and is assumed to be initiated by dissociative electron transfer, Equatio 6r (14, 56). Bylaska and co-workers showed that, of four possible pathways for the first one-electron reductive steps, the

dissociative electron transfer to from Cl^- was thermodynamically the most favorable pathway (59). Costentin and others also reported the more negative reduction potentials for the stepwise pathway ($RX/RX^{\bullet -}$) compared to the concerted pathway (60).

$$RX_a + 1\ e^- \rightarrow \bullet RX_{a-1} + X^- \qquad (6r)$$

We assumed that this was the case in our system. For the reactions of $Fe^{II}P/TiO_2$ and bis(pyr)$Fe^{II}P/TiO_2$, without excess electrons in the conduction band of TiO_2, undergo the pathway Equation 6r. Accordingly, to determine the relationship between the reaction rate constants and ΔG, one-electron reduction potentials of organohalides (54) and $Fe^{III/II}P/TiO_2$ formal reduction potentials (table 6-2) were used.

$$\Delta G \propto E^\circ (Fe^{III/II}) - E^\circ (RX^{0/-}) \qquad (6s)$$

The second-order rate constants decrease as ΔG for the complex increases. The correlation coefficients, R^2, between the reaction rate constants and ΔG for $Fe^{III/II}P/TiO_2$ and (pyr)$Fe^{III/II}P/TiO_2$ were reasonably high, 0.97 and 0.85. The similar correlation coefficients has been reported previously with zero-valent iron (56, 57). This suggest that the reaction rate of halogenated methanes investigated here are relatively associated with $Fe^{III/II}$ formal reduction potentials and one-electron reductions of organohalides. This study demonstrates that thermodynamics of reactions, ΔG , can be used to predict reduction rates of organohalides in aqueous solution.

6.5 Conclusions

This study described the influence of axial pyridine ligands on the redox properties and RX reactivity of heme catalysts. Axial ligation of pyridine to heme caused the +740 mV shifts in the $Fe^{III/II}P/TiO_2$ formal reduction potentials in pH 4 aqueous solution. Probably for this reason, the second order rate constans for RX reduction with bis(pyr)$Fe^{II}P/TiO_2$ were less than that measured in the absence of pyridine ligands. Multi electron transfer reaction of bis(pyr)$Fe^{II}P/TiO_2(e^-)$ with CCl_4 demonstrated that pyridine ligands can alter the reaction products. This study may contribute to understanding and predicting the redox reaction processes that involve electron transfer. In addition, molecular catalysts bound to mesoporous nanocrystalline TiO_2 thin films eliminate many of the difficulties encountered with colloidal solutions.

6.6 References

1. U. S. Environmental Protection Agency. Federal Register, www.epa.gov/safewater.

2. a) Groundwater Remediation Technology Analysis Center (GWRTAC) www.gwrtac.org. b) Remtech Engineers http://www.remtech-eng.com. c) Biological Remediation and Environmental Remediation for Hydrocarbon Contaminants. http://naturalenviro.com. d) Development in Innovative Groundwater Treatment. http://www.clu-in.org/products/newsltrs/gwc/view.cfm?issue=gwc1201.htm.

3. Obare, S. O., Meyer, G. J. Nanostructured materials for environmental remediation of organic contaminants in water. *J. Environ. Sci. Health A* **2004**, *39*, 2549-2582.

4. Brault, D., Neta, P. Reactions of iron porphyrins with trifluoromethyl, trifluoromethylperoxy, and tribromomethylperoxy radicals. *J. Phys. Chem* **1987**; *91,* 4156-4160.

5. Costentin, C., Robert, M., Saveant, J.-M. Successive removal of chloride ions from organic polychloride pollutants. Mechanisms of reductive electrochemical elimination

in aliphatic gem-polychlorides, α,β-Ppolychloroalkenes, and α,β-polychloroalkanes in mildly protic medium. *J. Am. Chem. Soc.* **2003**, *125*, 10729-10739.

6. Assaf-Anid, N., Hayes, K. F., Vogel, T. M. Reduction dechlorination of carbon tetrachloride by cobalamin(II) in the presence of dithiothreitol: mechanistic study, effect of redox potential and pH. *Environ. Sci. Technol.* **1994**, *28*, 246-252.

7. Perlinger, J. A., Buschmann, J., Angst, W., Schwarzenbach, R. P. Iron porphyrin and mercaptojuglone mediated reduction of polyhalogenated methanes and ethanes in homogeneous aqueous solution. *Environ. Sci. Technol.* **1998**, *32*, 2431-2437.

8. Ollis, D. F. Contaminant degradation in water. *Environ. Sci. Technol.* **1985,** *19*, 480-484.

9. Matheson, L. J., Tratnyek, P. G. Reductive Dehalogenation of chlorinated methanes by iron metal. *Environ. Sci. Technol.* **1994**, *28,* 2045-2053.

10. Loch, A. R., Lippa, K. A., Carlson, D. L., Chin, Y. P., Traina, S. J., Roberts, A. L**.** Nucleophilic aliphatic substitution reactions of propachlor, alachlor, and metolachlor with bisulfide (HS^-) and polysulfides (S_n^{2-}). *Environ. Sci. Technol.* **2002,** *36*, 4065-4073.

11. Roberts, A. L., Totten, L. A., Arnold, W. A., Burris, D. R., Campbell, T. J. Reductive elimination of chlorinated ethylenes by zero-valent metals. *Environ. Sci. Technol.* **1996,** *30*, 2654-2659.

12. Pearson, C. R., Hozalski, R. M., Arnold, W. A. Degradation of chloropicrin in the presence of zero-valent iron. *Environ.l Toxicol. Chem.* **2005**, *24*, 3037-3042.
13. Wade, R. S., Castro, C. E. Oixidation of heme proteins by alkyl halides. *J. Am. Chem. Soc.* **1973**, *95*, 231-234.

14. Balko, B. A., Tratnyek, P. G. Photoeffects on the reduction of carbon tetrachloride by zero-valent iron. *J. Phys. Chem. B.* **1998**, *102*, 1459-1465.

15. Calhoun, R. L., Winkelmann, K., Mills, G. Chain photoreduction of CCl_3F induced by TiO_2 particles. *J. Phys. Chem. B.* **2001**, *105*, 9739-9746.

16. Bahnemann, D. W., Moenig, J., Chapman, R. Efficient photocatalysis of the irreversible one-electron and two-electron reduction of halothane on platinized colloidal titanium dioxide in aqueous suspension. *J. Phys. Chem.* **1987**, *91*, 3782-3788.

17. Choi, W., Hoffmann, M. R. Kinetics and mechanism of CCl_4 photoreductive degradation on TiO_2: The role of trichloromethyl radical and dichlorocarbene. *J. Phys. Chem.,* **1996**, *100*, 2161-2169.

18. Fritsch, J. M., McNeill, K. Aqueous reductive dechlorination of chlorinated ethylenes with tetrakis(4-carboxyphenyl)porphyrin cobalt. *Inorg. Chem*. **2005**, *44*, 4852-4861.

19. Lewis, T. A., Morra, M. J., Brown, P. D. Comparative Product Analysis of Carbon Tetrachloride Dehalogenation Catalyzed by Cobalt Corrins in the Presence of Thiol or Titanium (III) Reducing Agents. *Environ. Sci. Technol.* **1996**, 30, 292-300.

20. Das, D. K., Medhi, O. K. The role of heme protionate in controlling the redox potential of heme: Square wave voltammetry of protoporphyrinate IX iron (III) in aqueous surfactant micelles. *J. Inorg. Biochem*. **1998**, *70*, 83-90.

21. Brault, D. Model studies in cytochrome P-450-mediated toxicity of halogenated compounds: radical processes involving iron porphyrins. *Environ. Health Perspectives* **1985,** *64*, 53-60.

22. Criddle, C. S., McCarty, P. L. Electrolytic model system for reductive dehalogenation in aqueous environments. *Environ. Sci. Technol.,* **1991**, *25*, 973-978.

23. Castro, C. E., Wade, R. S., Belser, N. O. Biodehalogenation: reactions of cytochrome P-450 with polyhalomethanes. *Biochemistry* **1985**, *24*, 204-210.

24. Nassar, A. F., Bobbitt, J. M., Stuart, J. D., and Rusling, J. F. Catalytic reduction of organohalides pollutants by Myoglobin in a biomembrane-like surfactant film. *J. Am. Chem. Soc.* **1995**, *117*, 10986-10993.

25. Semprini, L., Hopkins, G. D., McCarty, P. L., Roberts, P. V. In-situ transformation of carbon tetrachloride and other halogenated compounds resulting from biostimulation under anoxic conditions. *Environ. Sci. Technol.* **1992,** *26*, 2454-2461.

26. He, J., Sung, Y., Dollhopf, M. E., Fathepure, B. Z., Tiedje, J. M., Loffler, F. E. Acetate versus hydrogen as direct electron donors to stimulate the microbial reductive dechlorination process at chloroethene-contaminated sites**.** *Environ. Sci. Technol.* **2002**, *36*, 3945-3952.

27. Vogel, T., M., Criddle, C. S., McCarty, P. L. Transformations of halogenated aliphatic compounds. *Environ. Sci. Technol.* **1987,** *21*; 722-736.

28. Li, S., Wackett, L. P. Reductive dehalogenation by cytochrome P450CAM: Substrate binding and catalysis. *Biochemistry* **1993**, *32*, 9355-9361.

29. Ahr, H J., King, L. J., Nastainczyk, W., Ullrich, V. The mechanism of reductive dehalogenation of halothane by liver cytochrome P450. *Inter. Congr. Ser*. **1981**, *538*, 409-412.

30. Nastainczyk, W., Ullrich, V., Sies, H. Effect of oxygen concentration on the reaction of halothane with cytochrome P450 in liver microsomes and isolated perfused rat liver. *Biochem. Pharm*. **1978**, *27,* 387-92.

31. Obare, S. O., Ito, T., Balfour, M. H., Meyer, G. J. Ferrous hemin oxidation by organic halides at nanocrystalline TiO_2 interfaces. *Nano Lett*.**2003**, 3, 1151-1153.

32. Obare, S. O., Ito, T., Meyer, G. J. Controlling reduction potentials of semiconductor-supported molecular catalysts for environmental remediation of organohalide pollutants. *Environ. Sci. Technol*. **2005**, *39*, 6266-6272.

33. Obare, S. O., Ito, T., Meyer, G. J. Multi-electron transfer from heme-functionalized nanocrystalline TiO_2 to organohalide pollutants. *J. Am. Chem. Soc.* **2006**, *128*, 712-713.

34. Ito, T., Meyer, J. G. Heme mediated reduction of organohalide pollutants at nanocrystalline TiO_2 thin film interfaces. *Environ. Eng. Sci*. **2007**, *24/1*, in press.

35. Satterlee, J. D., La Mar, G. N., Bold, T. J. Dynamics and thermodynamics of axial ligation in metalloporphyrins. 6. Axial lability of nitrogenous bases in low-spin ferric complexes and the role of five-coordinate transient species. *J. Am. Chem. Soc.* **1977**, *99,* 1088-1093.

36. Stanford, M. A., Swartz, J. C., Phillips, T. E., Hoffman, B. M. Electronic control of ferroporphyrin ligand-binding kinetics. *J. Am. Chem. Soc.* **1980**, *102*, 4492-4499.

37. Fujii, H., Yonetoni, T., Miki, T., Kakinuma, K. Modulation of the heme environment of neutrophil cytochrome b_{558} to a "cytochrome P450-like" structure by pyridine. *J. Biol. Chem*. **1995**, *270*, 3193.

38. Iizuka, T., Kanegasaki, S., Makino, R., Tanaaka, T., Ishimura Y. Pyridine and imidazole reversibly inhibit the respiratory burst in porcine and human neutrophils: evidence for the involvement of cytochrome b_{558} in the reaction. *Biochem. Biophys. Res. Comm*. **1985**, *130*, 621-626.

39. Gaudio, J. D., La Mar, G. N. Magnetic resonance investigation of the autoreduction of tetraphenylporphinatoiron(III) chloride in the presence of piperidine. *J. Am. Chem. Soc.* **1978**, *100*, 1112-1119.

40. Brault, D., Rougee, M. Ferrous porphyrins in organic solvents. I. Preparation and coordinating properties. *Biochemistry* **1974**, *13*, 4591-4597.

41. Walker, F. A., Lo, M., Ree, M. T**.** Electronic effects in transition metal porphyrins. The reactions of imidazoles and pyridines with a series of para-substituted tetraphenylporphyrin complexes of chloroiron(III). *J. Am. Chem. Soc.* **1976**, *98*, 5552-5560.

42. Balch, A. L., Noll, Bruce C., Olmstead, M. M., Phillips, S. L. Structural and spectroscopic characterization of iron(III) dioxoporphodimethene complexes and their autoreduction to an iron(II) complex in pyridine. *Inorg. Chem*. **1996**, *35*, 6495-6506.

43. Hayashi, T., Nakashima, Y., Ito, K., Ikegami, T.,; Aritome, I., Aoyagi, K., Ando, T., Hisaeda, Y. Synthesis, characterization, and autoreduction of a highly electron-eeficient porphycenatoiron(III) with trifluoromethyl substituents. *Inorg. Chem*. **2003**, *42*, 7345-7347.

44. Sano, S., Sano, T., Morishima, I., Shiro, Y., Maeda, Y. On the mechanism of the chemical and enzymic oxygenations of alpha-oxyprotohemin IX to Fe.biliverdin IX alpha. *Proc. National Academy Sci. USA* **1986**, *83*, 531-5.

45. Walsh, T. A., Johnson, M. K., Barber, D., Thomson, A. J., Greenwood, C. Studies on heme d1 extracted from Pseudomonas aeruginosa nitrite reductase. *J. Inorg. Biochem*. **1981**, *14*, 15-31.

46. Kadish, K. M., Bottomley, L. A**.** Influence of substituted pyridines on the redox reactions of iron porphyrins. *Inorg. Chem.* **1980**, *19*, 832-836.

47. Heimer, T. A., D'Arcangelis, S. T., Farzad, F., Stipkala, J. M., Meyer, G. J. An acetylacetonate-based semiconductor-sensitizer linkage. *Inorg. Chem*. **1996**, *35*, 5319-5324.

48. Momenteau, M. The physical chemistry of hemes and hemopeptides I. Physicochemical properties and reduction of chlorodeuterohemin in organic solvent. Biochim. Biophys. Acta 1973, 304, 814-827.

49. Pond, A. E., Roach, M. P., Sono, M., Run, A. H., Franzen, S., Hu, R., Thomas, M. R., Wilks, A., Dou, Y., Ikeda, M., Ortiz de Montellano, P. R., Woodruff, W. H., Boxer, S. G., Dawson, J. H. Assignment of the heme axial ligand(s) for the ferric myoglobin (H93G) and heme oxygenase (H25A) cavity mutants as oxygen donors using magnetic circular dichroism. *Biochemistry* **1999**, *38*, 7601-7608.

50. Alben, J. O., Fuchsman, W. H., Beaudreau, C. A., Caughey, W. S. Substituted deuteroporphyrins. III. Iron(II) derivatives. Reactions with oxygen and preparations from chloro- and methoxohemins. *Biochemistry* **1968**, *7*, 624-635.

51. Shimizu, T., Nozawa, T., Hatano, M. Deuterium nuclear magnetic resonance spectroscopy of deuterated pyridine-iron(III) porphyrin complexes. Locations and relaxation times of bound deuterated pyridine resonances. *J. Biochem*. 1982, *91*, 1951-1958.

52. Cole, S. J. Curthoys, G. C., Magnusson, E. A. Ligand binding by metalloporphyrins. I. Thermodynamic functions of porphyriniron(II)-pyridine complexes. *J. Am. Chem. Soc.* **1970**, *92*, 2991-2996.

53 Coyle, C. L., Rafson, P. A., Abbott, E. H. Equilibria of imidazole with iron(III) tetraphenylporphine. *Inorg. Chem*. **1973**, *12*, 2007-2010.

54. Totten, L. A., Roberts, A. L. Calculated one- and two-electron reduction potentials and related molecular descriptors for reduction of alkyl and vinyl halides in water. *Crit. Rev*. *Environ. Sci. Technol*. **2001**, *31*, 175-221.

55. Stromberg, J. R., Wnuk, J. D., Pinlac, R. A. F., Meyer, G. J. Multielectron Transfer at Heme-Functionalized Nanocrystalline TiO_2: Reductive Dechlorination of DDT and CCl_4 Forms Stable Carbene Compounds. *Nano Lett.* **2006**, *6*, 1284-1286.

56. Scherer, M. M., Balko, B. A., Gallagher, D. A., Tratnyek, P. G. Correlation analysis of rate constants for dechlorination by zero-valent iron. *Environ. Sci. Technol.* **1998**, *32*, 3026-3033.

57. Song, H., Carraway, E. R. Reduction of chlorinated ethanes by nanosized zero-valent iton: kinetics, pathways, and effects of reaction conditions. *Environ. Sci. Technol*. **2005**, *39*,6237-6245.

58.Perlinger, J. A., Venkatapathy, R., Harrison, J. F. Linear free energy relationships for polyhalogenated alkane transformation by electron-transfer mediators in model aqueous systems. *J. Phys. Chem. A* **2000**, *104*, 2752-2763.

59. Bylaska, E. J., Dixon, D. A., Felmy, A. R., Tratnyek, P. G. One-electron reduction of substituted chlorinated methanes as determined from ab initio electronic structure theory. *J. Phys. Chem. A* **2002**, *106*, 11581-11593.

60. Constentin, C., Robert, M., Saveant, J. M. a) Successive removal of chloride ions from organic polychloride pollutants. Mechanisms of reductive electrochemical elimination in aliphatic gem-polychlorides, α,β-polychloroalkenes, and α,β-polychloroalkanes in mildly protic medium. *J. Am. Chem. Soc*. **2003**, *125*, 10729-10739. b) Does catalysis of reductive dechlorination of tetra- and trichloroethylenes by vitamin B12 and corrinoid-based dehalogenases follow an electron transfer mechanism? *J. Am. Chem. Soc*. **2005**, *127*, 12154-12155

61. Munro, O. Q., Madlala, P. S., Warby, R. A. F., Seda, T. B., Hearne, G. Structural, conformational, and spectroscopic studies of primary amine complexes of iron(II) porphyrins. *Inorg. Chem.* **1999**, *38*, 4724-4736.

62. Falk, J. E., Smith, K. M. Porphyrins and metalloporphyrins; Elesevier: New York, New York, 1975.

63. Crawford, P. W., Ryan, M. D. Electrochemistry and spectroscopy of sulfate and thiosulfate complexes of iron porphyrins**.** *Inorg. Chim. Acta* **2002**, *328*, 13-22.

64. Nakano, T., Kitamura, Y. A new system of autoreduction of hemin with isocyanide. *Chem. Lett*. **1989**, *7*, 1207-1210.

65. Collman, J. P., Reed, C. A. Syntheses of ferrous-porphyrin complexes. Hypothetical model for deoxymyoglobin. *J. Am. Chem. Soc.* **1973**, *95*, 2048-2049.

66. Kobayashi, H., Yanagawa, Y. Electronic spectra and electronic structure of iron(II) tetraphenylporphines. *Bull. Chem. Soc. Jp*. **1972**, *45*, 450-456.

67. Tsutsumi, M., Velapoldi, R. A., Hoffman, L., Suzuki, K., Ferrari, A. Unusual metalloporphyrins. III. Induced oxidation of cobalt(II) and iron(II) porphyrins by unsaturated hydrocarbons. *J. Am. Chem. Soc.* **1969**, *91*, 3337-3341.

68. Arguello, J. E., Costentin, C., Griveau, S., Saveant, J.M. Role of protonation and of axial ligands in the reductive dechlorination of alkyl chlorides by vitamin B_{12} complexes. Reductive cleavage of chloroacetonitrile by Co(I) cobalamins and cobinamides. *J. Am. Chem. Soc.* **2005,** *127*, 5049-5055.

69. Choi, W., Hoffmann, M. R. Photoreductive mechanism of CCl_4 degradation on TiO_2 particles and effects of electron donors. *Environ. Sci. Technol*. **1995**, *29*, 1646-1654.

70. Rusling, J. F., Miaw, C. L. Kinetic estimation of standard reduction potentials of polyhalogenated biphenyls. *Environ. Sci. Technol.* **1989**, *23*, 476-479.

Appendix 1: Mass Spectra Methods and Data for Organohalides and Products in Water

A1.1 Analytical method

The products formed by electrocatalysis and photocatalysis in aqueous solutions were analyzed by a Shimadzu GC17A/QP5050A GC/MS (Shimadzu Columbia, MD). The products were extracted from the aqueous solution with pentane. Typically a ~2 mL aliquot of pentane was added to ~ 10 mL of RX reaction mixture. The pentane reaction mixture was injected into the autosampler of the GC/MS. The injector temperature was 220 °C and the transfer interface was at 280 °C. An EI quadrupole based mass spectrometer served as the detector with an ionizing electron energy of 70 eV.

A1.2 GC/MS spectra of substrate: Propachlor and CCl_4

For CCl_4, the oven temperature was ramped from 40 °C, held for 10 min, to 80 °C at a rate of 7.2 °C/min. The pressure program was 1.0 kPa, ramp 2.7 kPa/min to 16 kPa, and held for 5 min. For propachlor, the oven temperature was ramped from 40 °C, held for 2 min, to 170 °C at a rate of 7.3 °C/min. The pressure program was 48.9 kPa, ramp 3 kPa/min to 99 kPa, and held for 5 min.

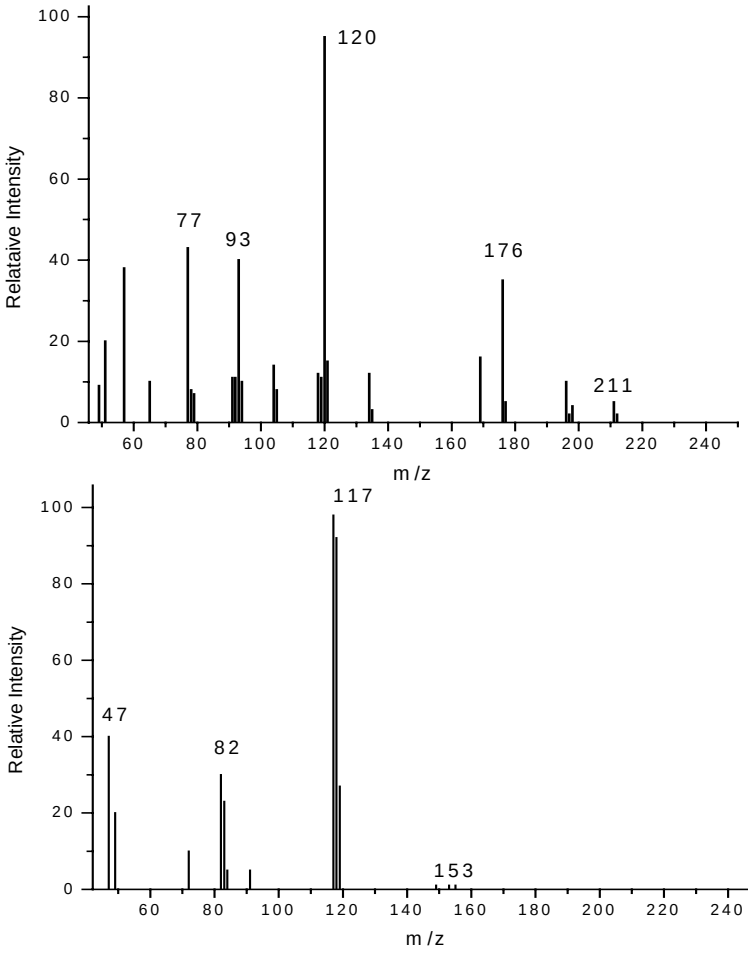

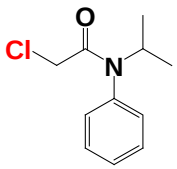

Propachlor
m/z = 211
R.T. = 20.4 min

CCl_4
m/z = 152
R.T. = 4.0 min

Figure A1-1. Mass spectrum of propachlor and CCl_4 in pentane. The retention time for propachlor and CCl_4 were R.T. = 20.4 and 4.0 min.

A1.3 Products observed from the reactions of Propahlor and CCl_4

The products of CCl_4 and propachlor reduction by heme/$TiO_2(e^-)$ in aqueous pH 8 solution were analyzed by GC/MS. Electrocatalysis was initially performed at an applied potential of -1.0 V (*vs*. Ag/AgCl). This potential reduced all hemin to heme and established a $TiO_2(e^-)$ concentration of 1.9×10^{-5} M. The CCl_4 (or propachlor) was added to the external electrolyte and the potential was maintained for an additional 4 hours. Control experiments performed with FTO electrodes without heme or TiO_2 showed no dechlorinated products. Products observed from photocatalytic reactions were also analyzed. In all cases, the aqueous solutions were extracted with pentane.

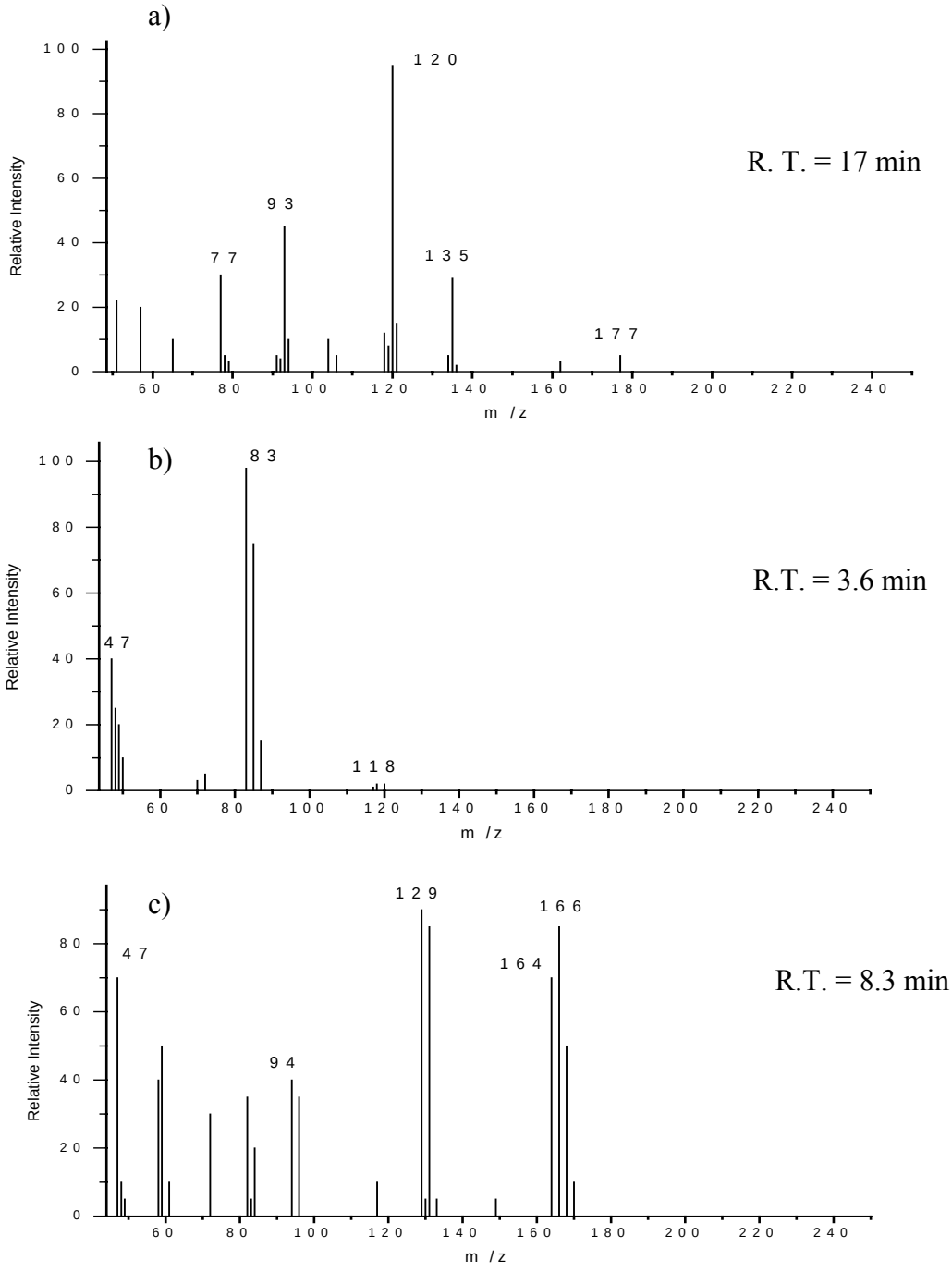

Figure A.1-2. GC/MS spectra of the products formed after the reactions of heme/$TiO_2(e^-)$ by electrocatalysis in pH 8 aqueous solution. a) shows the product observed from the reactions with propachlor, assigned to be deschloropropachlor (mz = 177, R.T. = 17 min). This product was also detected in the photocatalytic reactions. b) shows the main product observed from the reactions with CCl_4, assigned to be chloroform (m/z = 118, R.T. = 3.6). This product was also observed from the photocatalytic reactions. C) shows the product observed from the reactions with CCl_4, assigned to be tetrachloroethylene (m/z = 164, R.T. = 8.3). This product was not detected in the photocatalytic reactions.

Appendix 2: Cyclic Voltametry of Molecular Catalysts, TiO_2 Thin Films, and Heme-Functionarized TiO_2

A2.1 Experimental potocol

Cyclic voltammetry was used to estimate formal reduction potentials of the molecular catalysts in fluid solutions as well as on nanocrystallin TiO_2 thin films. Typically, tetrabutylammonium hexafluorophosphate (TBAH) was used in organic electrolytes and the conecntration was 0.1 M. A BAS model CV-50 W potentiostat was used in a standard three-electrode arrangement consisting of a Glassy carbon working electrode, a Pt gauze counter electrode, and Ag/AgCl reference electrode. For TiO_2 surface studies, the TiO_2 pastes were cast as mesoporous thin (~10μm) films onto transparent fluorine-doped tin oxide (FTO) and used as a working electrode.

The $M^{III/II}$ redox chemistry showed equivalent anodic and cathodic peak currents, $i_{pa}/i_{pc} \sim 1$, and a peak-to-peak separation of ~100 mV in fluid solution, Figure A.2-1. Plots of the square root of the peak current versus scan rate were linear as expected for a diffusional process.

The cyclic voltammetry of the catalysts bound to TiO_2 was also measured. In most cases, at potentials more negative than –1 V vs. Ag/AgCl, a background current due to the reduction of TiO_2 was superimposed on a peaks attributable to $Fe^{III\rightarrow II}/TiO_2$ reduction of the heme catalyst, Fig A.2-2. The corresponding

oxidation of $Fe^{II\rightarrow III}/TiO_2$ was not observed, which may be due to the oxidation of TiO_2 ($Ti^{III\rightarrow IV}$) background. The formal reduction potentials of $(pyr)Fe^{III/II}$ were more positive and therefore, equivalent cathodic and anodic peak currents were observed, Figure A.2-3.

Table A.2.1. Redox properties of catalysts in solution and on TiO_2 thin films.

	Electrolyte	E° (mV) *vs.* $Fc^{+/0}$
$Fe^{III/II}$	DMSO	-727
$Fe^{III/II}/TiO_2$	DMSO	-1063
$(pyr)Fe^{III/II}$	Pyridine	-463
$(pyr)Fe^{III/II}/TiO_2$	Pyridine	-403

A2.2 Cyclic voltammetry of catalysts

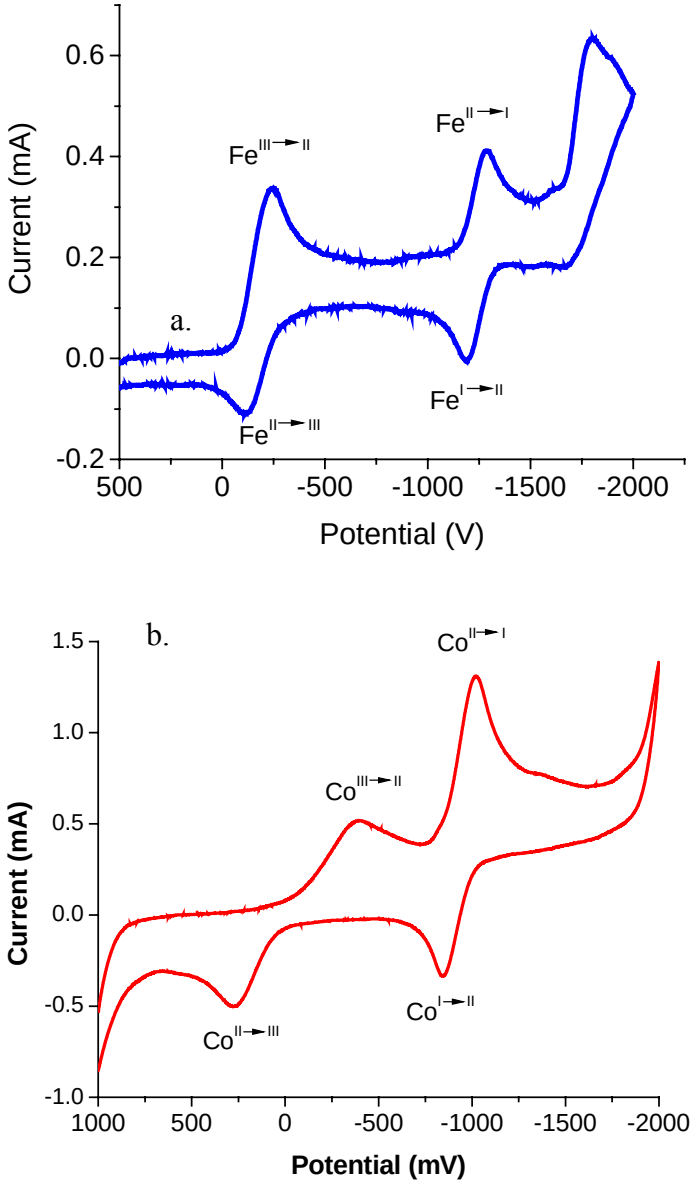

Figure A.2-1. Cyclic voltammetry of a) hemin and b) CoTCP in 0.1 M TBAH/DMSO electrolyte vs. Ag/AgCl. The concentration of molecular catalysts was 0.01 M and the scan rate was 100 mV/sec.

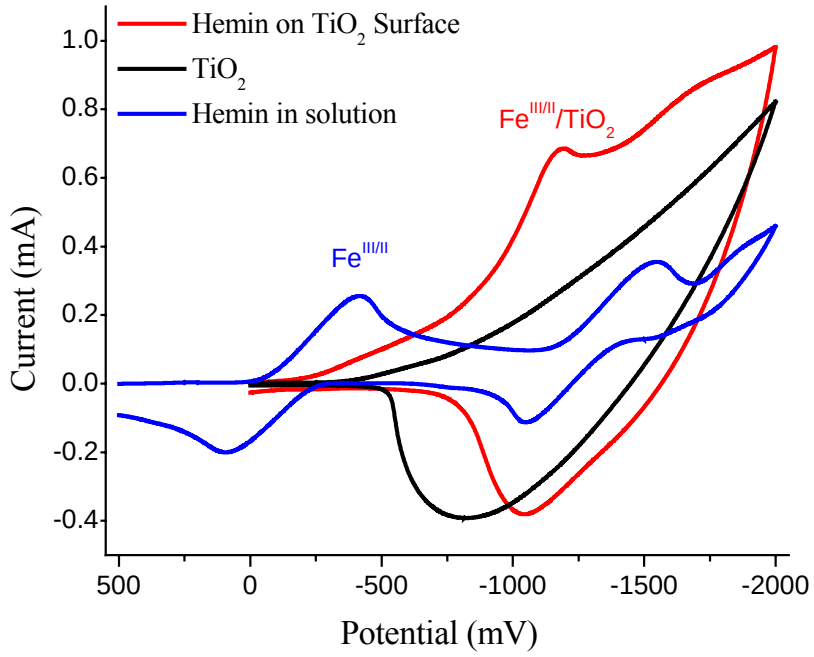

Figure A.2-2. Cyclic voltammetry of hemin (—), TiO_2 (—), and hemin/TiO_2 (—) in 0.1 M TBAH/DMSO electrolyte vs. Ag/AgCl. The scan rate was 100 mV/sec.

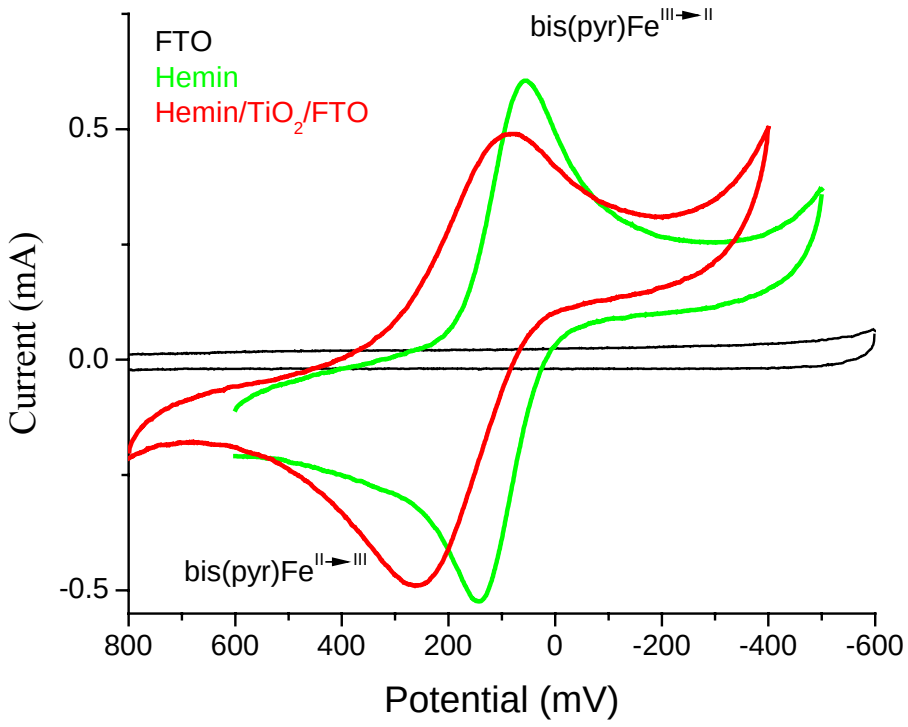

Figure A.2-3. Cyclic voltammetry of FTO (—), (pyr)$Fe^{III/II}$ (—),and (pyr)$Fe^{II/II}/TiO_2$ (—) in 0.1 M TBAH/Pyridine electrolyte vs. Ag/AgCl. The scan rate was 100 mV/sec.

Curriculum Vita

Tamae Ito was born in Kanagawa, Japan on September 7th, 1969. She received a Bachelors of Art in Chemistry from Case Western Reserve University in Cleveland, OH. She worked with Dr. Malcolm E. Kenney as a research assistant after receiving BA. In September, 2002, she began her graduate work in the Department of Chemistry at the Johns Hopkins University in Baltimore, MD. She pursued her doctoral degree under the guidance of Professor Gerald J. Meyer. Her primary aim is to research organohalide contaminants in groundwater and establish an efficient method to clean contaminated water. She completed her Ph.D work in October, 2006.